Developing molecular tools for the study of the STAT3 pathway

Ricardo Letra-Vilela

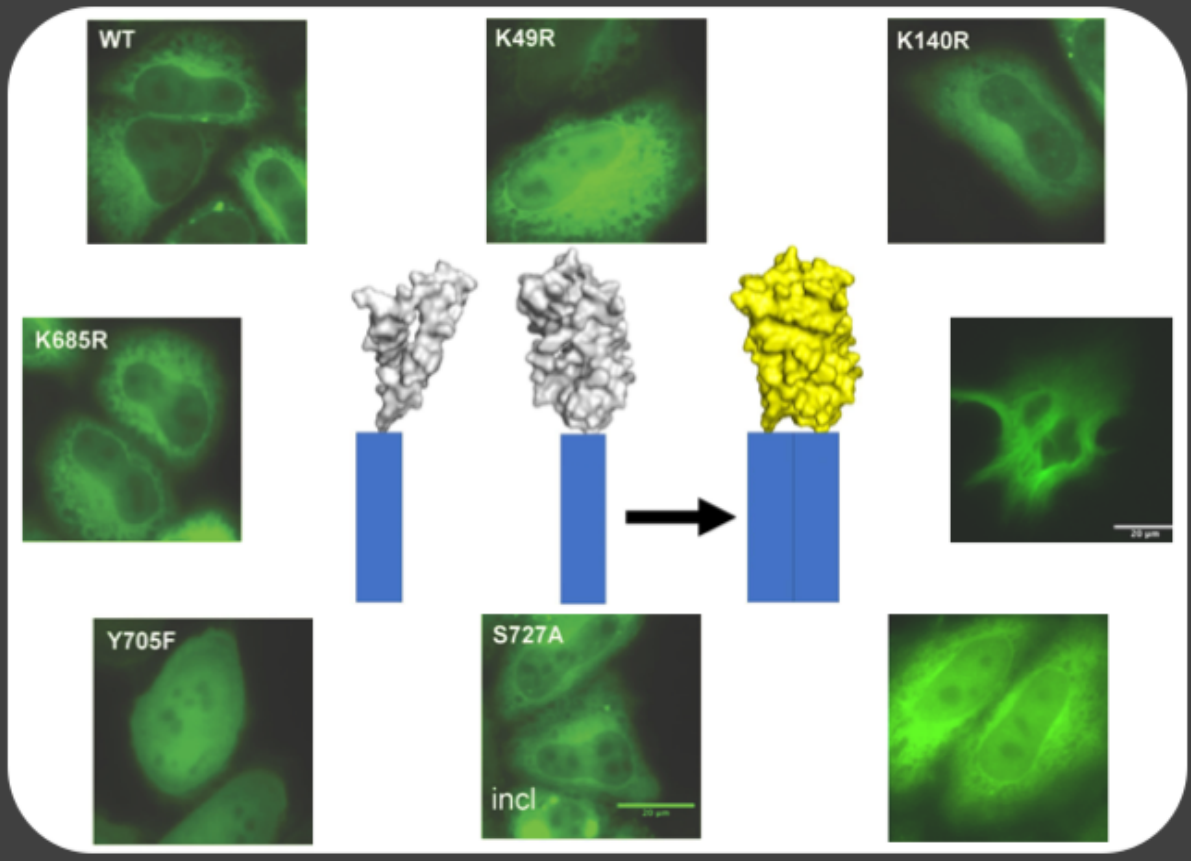

Dissertation presented to obtain the Ph.D degree in Molecular Biosciences

Instituto de Tecnologia Química e Biológica António Xavier | Universidade Nova de Lisboa

Oeiras,
May, 2022

UNIVERSIDADE NOVA DE LISBOA

Developing molecular tools for the study of the STAT3 pathway

Ricardo Letra-Vilela

Dissertation presented to obtain the Ph.D degree in Molecular Biosciences

Instituto de Tecnologia Química e Biológica António Xavier | Universidade Nova de Lisboa

Oeiras, May, 2022

Supervisors:

Dr. Federico Herrera, Faculdade de Ciências, Universidade de Lisboa

Dr. João Pedro Conde, Instituto Superior Técnico, Universidade de Lisboa

Summary

The STAT family of transcription factors plays key roles in the physiology of the immune system and during development. Among them, STAT3 is particularly relevant, as its deletion leads to early embryonic lethality. STAT3 is stimulated by a wide spectrum of cytokines and extracellular factors, regulating the transcription of genes related with survival/ apoptosis, proliferation and differentiation. STAT3 is overactivated in 70% of solid tumors, and activating mutations are related to cancer and some benign hyperproliferative disorders, such as Inflammatory Hepatocellular Adenome. STAT3 is considered an interesting target for cancer treatment, as it is also partially responsible for radio- and chemo resistance, and various direct or indirect inhibitors have been proposed as possible therapies. STAT3 activation is also found in a wide variety of Central Nervous System (CNS) disorders, especially in acute injury models, being often observed in circumstances involving astroglial reactivity, growth, proliferation and glial scar formation. This astrogliosis involves higher expression of the glial intermediate filament (GFAP), a common marker for neuroinflammation and CNS injury, and this response is also mediated by STAT3. In turn, inactivating mutations are associated to Hyper-immunoglobulin E syndrome. The structural changes and mechanisms underlying STAT3 activation or inactivation by post-translational modifications remain barely understood, with the exception of the Y705 phosphorylation, which has been extensively characterized.

In this thesis, we have developed a series of molecular tools that allow the study and characterization of different aspects of the JAK/STAT3/GFAP axis that is so relevant for astrogliogenesis during development and in pathological conditions. The central model for the analysis of STAT3 dynamics and protein-protein interactions in living cells

was based on bimolecular fluorescence complementation (BiFC) assays. Briefly, STAT3 was fused to two non-fluorescent halves of the Venus yellow fluorescent protein. When STAT3 dimerizes, the Venus halves get back together and reconstitute the fluorophore. Fluorescence is therefore proportional to the amount of STAT3 homodimers. We characterized the behavior of this system in living cells, and its potential to study STAT3 dynamics in living cells. We then created a high number of post-translational modification-inactivating mutations to analyze their effect in STAT3 homodimerization. We combined STAT3 mutant pairs so that post-translational modifications could not occur on one (asymmetric) or both STAT3 monomers (symmetric). We observed that asymmetric STAT3 post-translational modifications induced striking changes in the intracellular distribution of STAT3 homodimers, with biological consequences at the level of cell proliferation. Asymmetric post-translational modifications could therefore constitute a new level of regulation of STAT3 function.

Our model allowed us to observe the subcellular distribution of STAT3 dimers in living cells, and confirm their presence in the mitochondria. It was previously described that STAT3 can heterodimerize with the mitochondrial protein GRIM19, a protein connected to the mitochondrial respiration chain. Using the same approach described before, we developed a BiFC system to study the interaction between STAT3 and GRIM19. We observed that the heterodimerization with GRIM19 is dependent on cytokine stimuli and specific STAT3 Post-translational modifications and, knowing the role of GRIM19 on the Electron Transport Chain, we analyzed the levels of ATP after transfection of cells with WT and PTM-inactivating STAT3 mutants in the presence or absence of Leukemia Inhibitory Factor (LIF). We observed that specific PTM-inactivating mutations induced a decrease in ATP levels under LIF stimulation.

In order to refine our observations, we developed a STAT3-knockout HeLa cell line, as well as other STAT3-related tools to reveal STAT3 distribution with a better resolution (e.g. STAT3-miniSOG construct) that are currently being characterized in our lab. In order to take advantage of BiFC characteristic with Venus, we also started the development of a BiFC system using the fluorescent protein MiniSOG as reporter. When transfected in cells, plasmids containing specific halves of MiniSOG protein presented fluorescent signals. These results reveal the capacity of MiniSOG protein to recover the fluorescent function when, after interaction of both halves, reconstitutes the full protein. Additionally, we developed and optimized a series of constructs for normal and disease-associated GFAP versions that allowed their visualization in living cells. This is relevant for the field, because tagged versions of GFAP most frequently fail to produce filament networks. With our constructs, normal GFAP led to the formation of a functional GFAP intermediate filament network, and the mutant forms produced protein aggregates, as expected.

In summary, we produced a number of potentially useful tools to study the STAT3/GFAP axis that have been made publicly available, and our results indicate new venues for fine control of STAT3 behavior and function, study in vivo of GFAP oligomerization and possible BiFC systems, using MiniSOG for Electron Microscopy.

Key words: STAT3; GFAP; heterodimerization; asymmetric; BiFC system; astrogliogenesis

Sumário

A família de fatores de transcrição STAT desempenha papéis fundamentais na fisiologia do sistema imunológico e durante o desenvolvimento. Entre eles, o STAT3 é particularmente relevante, pois a sua deleção leva à letalidade embrionária precoce. O STAT3 é estimulado por um amplo espectro de citocinas e fatores extracelulares, regulando a transcrição de genes relacionados à sobrevivência/apoptose, proliferação e diferenciação. O STAT3 está superativado em 70% dos tumores sólidos, e as mutações ativadoras estão relacionadas ao cancro e alguns distúrbios híper-proliferativos benignos, como o adenoma hepatocelular inflamatório. O STAT3 é considerado um alvo interessante para o tratamento do cancro, pois é parcialmente responsável pela resistência à rádio e à quimioterapia, levando a que vários inibidores diretos ou indiretos têm vido a ser propostos como possíveis terapias. A ativação de STAT3 também é encontrada em uma ampla variedade de distúrbios do Sistema Nervoso Central (SNC), especialmente em modelos de lesão aguda, sendo frequentemente observada em circunstâncias que envolvem reatividade astroglial, crescimento, proliferação e formação de cicatriz glial. Essa astrogliose envolve maior expressão do filamento intermédio glial GFAP, um marcador comum de neuroinflamação e lesão do SNC, e essa resposta é também mediada por STAT3. Por sua vez, mutações inativadoras estão associadas à síndrome de hiperimunoglobulina E. As mudanças estruturais e os mecanismos subjacentes à ativação ou inativação de STAT3 por modificações pós-translacionais permanecem pouco compreendidos, com exceção da fosforilação Y705, que foi amplamente caracterizada.

Nesta tese, desenvolvemos uma série de ferramentas moleculares que permitem o estudo e caracterização de diferentes aspetos do eixo JAK/STAT3/GFAP que é de extrema importância para a

astrogliogénese durante o desenvolvimento e em condições patológicas. O modelo central para a análise da dinâmica de STAT3 e interações proteína-proteína em células vivas foi baseado em ensaios de complementação de fluorescência bimolecular (BiFC). Resumidamente, STAT3 foi fundido a duas metades não fluorescentes da proteína fluorescente amarela Vénus. Quando o STAT3 dimeriza, as metades de Vénus juntam-se novamente e reconstituem o fluoróforo. A fluorescência é, portanto, proporcional à quantidade de homodímeros de STAT3. Caracterizámos o comportamento deste sistema em células vivas e o seu potencial para estudar a dinâmica de STAT3 em células vivas. Em seguida, criámos um grande número de mutações inativadoras de modificações pós-translacionais para analisar o seu efeito na homodimerização de STAT3. Combinámos pares de mutantes de STAT3 para que modificações pós-translacionais não pudessem ocorrer em um (assimétrico) ou em ambos os monómeros de STAT3 (simétrico). Observámos que modificações pós-translacionais de STAT3 assimétricas induziram mudanças marcantes na distribuição intracelular de homodímeros de STAT3, com consequências biológicas ao nível da proliferação celular. Modificações pós-translacionais assimétricas poderiam, portanto, constituir um novo nível de regulação da função de STAT3.

O nosso modelo permitiu-nos observar a distribuição sub-celular de dímeros de STAT3 em células vivas e confirmar a sua presença nas mitocôndrias. Foi descrito anteriormente que STAT3 pode heterodimerizar com a proteína mitocondrial GRIM19, uma proteína ligada à cadeia de respiração mitocondrial. Usando a mesma abordagem descrita anteriormente, desenvolvemos um sistema BiFC para estudar a interação entre STAT3 e GRIM19. Observámos que a heterodimerização com GRIM19 é dependente de estímulos de citocinas e de modificações pós-translacionais especificas de STAT3, conhecendo o papel do GRIM

19 na Cadeia de Transporte de Eletrões, analisámos os níveis de ATP após a transfecção de células com STAT3 WT e mutantes inativadores de modificações pós-translacionais na presença ou ausência do Fator Inibitório de Leucemia (LIF). Observámos que mutações específicas inativadoras de modificações pós-translacionais induziram uma diminuição nos níveis de ATP sob estimulação com LIF.

Com o objetivo de refinar as nossas observações, desenvolvemos uma linha de células HeLa STAT3-knockout, bem como outras ferramentas relacionadas com STAT3 de modo a revelar a distribuição de STAT3 com uma melhor resolução (por exemplo, construção STAT3-miniSOG) que estão a ser caracterizadas no nosso laboratório. Para aproveitar as características do BiFC com o Vénus, também iniciámos o desenvolvimento de um sistema BiFC usando a proteína fluorescente MiniSOG como repórter. Quando transfectados em células, os plasmídeos contendo partições específicas da proteína MiniSOG apresentaram sinais fluorescentes. Esses resultados revelam a capacidade da proteína MiniSOG em recuperar a função fluorescente quando, após interação de ambas as metades, reconstitui a proteína completa. Além disso, desenvolvemos e otimizámos uma série de construções para versões de GFAP normais e associadas a doenças que permitiram a sua visualização em células vivas. Isto é relevante para o campo, porque as versões marcadas do GFAP geralmente falham em produzir redes de filamentos. Com os nossos plasmídeos, o GFAP WT levou à formação de uma rede de filamentos intermédios de GFAP funcional, e as formas mutantes produziram agregados de proteínas, como esperado.

Em resumo, produzimos uma série de ferramentas potencialmente úteis para estudar o eixo STAT3/GFAP que foram disponibilizadas publicamente, e os nossos resultados indicam novos locais para controle fino do comportamento e função de STAT3, estudo

in vivo de oligomerização de GFAP e possíveis sistemas BiFC, usando MiniSOG para Microscopia Eletrónica.

Palavras-Chave: STAT3; GFAP; heterodimerização; assimétrico; Sistema BiFC; astrogliogénese

Acknowledgements

I would like to mention all the people that made the development of this thesis possible, both personally and academically:

To my supervisor Dr. Federico Herrera, for the opportunity to work in his laboratory. I know that looking to all these years, it was harder than what is supposed to be, but specially for that I need to thank you for all the patience and all the dedicated time during the past 6 years. Also thank you for all the transmission of knowledge and the good advice that allowed me to grow personally and scientifically. I will always be grateful.

To my co-supervisor Dr. João Pedro Conde for his support throughout this thesis. Thank you for all the time dispended to promptly answer all my questions. Also, thanks for the continuous preoccupation.

I would like to give special thanks to Dr. Mariana Santa-Marta for all the help during my thesis, supporting me and believing in me. Also, thanks for the scientific discussions and personal talks.

To all the persons that gave me technical support at ITQB, in microscopy and flow cytometry facilities at IGC, IMM, FCUL and SALK.

To all the people that receive me at The SALK institute, specially António Currais, António Pinto Duarte, Joshua and Gamze. I would also to give a big thank you to Holiday. Thanks to you I had a place to stay at San Diego.

To all the colleagues that I have the pleasure to have during all these years, specially Joana Branco, Fernanda, Beatriz, Ricardo Quiteres, Mickael, Andreia and Cristina. All of you make me feel at home in the lab.

To my parents, Luisa Letra and José Vilela, my grandmothers, Maria Clara and Anita, my girlfriend, Inês, my friends Paulo Grazina, Gonçalo Toste, Rafael, João, André Cardoso and others, thank you for your support and for keeping me motivated and focused during all the

year. Thank you for believing in me and for helping me in all the stages of my live.

I would like to acknowledge two persons that were important in different ways and unfortunately, they are not here anymore. To professor Solange, who showed me Molecular Biology during my bachelor and gave me the first opportunity to work in a lab; and to Dr. Dave Schubert, who accepted me in his lab at SALK.

There is space for one more person, Filipe. You were more than a colleague of faculty and more than a colleague of year. You were a brother for the last years. Thanks to you I was able to be always happy, I will never forget our time together.

If I can dedicate all this work to someone I would like to be my sister. Rita you were more than a sister, and for that you deserve to be the last one. I will always love you.

Ricardo José Letra Vilela Ribeiro PhD work was supported by an individual FCT fellowship (Ref. PD/BD/128163/2016), and by the following grants: Centre grants from Fundação para a Ciência e Tecnologia (FCT) to the BioISI Research Unit (Refs. UIDB/04046/2020 and UIDP/04046/2020) and the Microscopy facility at FCUL (as a node of the Portuguese Platform of BioImaging, reference PPBI-POCI-01-0145-FEDER-022122); Project LISBOA-01-0145-FEDER-007660 (Cellular Structural and Molecular Microbiology) funded by FEDER funds through COMPETE2020—Programa Operacional Competitividade e Internacionalização (POCI); by individual grants to Dr. Federico Herrera through FCT (Refs. IF/00094/2013/CP1173/CT0005, PTDC/MED-NEU/31417/2017 and PTDC/FIS-MAC/2741/2021).

General Contents

Summary ***I***

Sumário ***IV***

Acknowledgements ***VIII***

List of Abbreviations ***XVIII***

Chapter 1 ***1***

Introduction ***1***

1. Signal Transducer and Activator of Transcription 3 (STAT3) is an essential transcription factor **2**

1.1. STAT3 functions in health and disease 2

1.2. *STAT3* structure and domain organization 5

1.3. Canonical and non-canonical *STAT3* Pathways 9

1.3.1. The canonical *STAT3* pathway 9

1.3.2. Non-Canonical *STAT*3 pathways 11

1.4. Regulation of *STAT3* by post-translational modifications 14

1.4.1. Understudied phosphorylation events 16

1.4.2. Lysine modifications 17

1.4.3. Other *STAT3* post-translational modifications 19

2. Downstream the canonical *JAK/STAT3* pathway: the glial fibrillary acidic protein and CNS pathologies **20**

2.1. *GFAP*: the protein 22

2.2. *GFAP* mutations cause Alexander disease 24

3. Methods for the study of protein-protein interactions **27**

3.1. Co-immunoprecipitation 28

3.2. Fluorescence Resonance Energy Transfer (FRET)/ Bioluminescence Resonance Energy Transfer (BRET) 29

3.3. Fluoppi and Dimerization-dependent fluorescent proteins 31
3.4. Protein Complementation Assays (PCAs) 33
3.4.1. Bimolecular fluorescence complementation (BiFC) assays for the study of protein-protein interactions 35

4. Aims 39

Chapter 2 40

Materials + Methods 40

1. Reagents 41

2. General Cloning Procedures 42
2.1. DNA Purification 42
2.2. Ligation 43
2.3. Bacterial Transformation and growth 43
2.4. Confirmation of clones by restriction reaction and sequencing 44

3. Templates 45
3.1. Venus - *STAT3* BiFC system 45
3.2. Human GFAP plasmid 46

4. Transposase Reaction 47

5. Site-Directed Mutagenesis 50

6. Generation of *STAT3 MiniSOG* BiFC constructs 52
6.1. Insert/Vector preparation 52

7. Generation of *GFAP* BiFC constructs 54
7.1. *Venus-GFAP/GFAP-Venus* regular BiFC constructs 54
7.2. Insert/Vector preparation 54

8. Mammalian cell cultures 56

9. Flow cytometry 56

10. Diaminobenzidine (DAB) reaction 57

11. Microscopy 58

12. Immunoblotting 60

12.1. Total protein extraction 60

12.2. Nuclear and cytoplasmic protein extraction 60

12.3. Immunoblotting 61

13. Cell proliferation/viability Assay 62

14. ATP determination 63

15. *STAT3* CRISPR/Cas9 Knockout 63

16. Statistical analysis 64

17. List of Plasmids 65

Chapter 3 67

Results (Part I) 67

Asymmetric PTMs change the subcellular distribution of STAT3 homodimers 67

Specific symmetric PTM-resistant mutations cause changes in the intracellular localization of resting STAT3 dimers 75

Relative contribution of specific residues to STAT3 dimerization, intracellular location, and cell proliferation 79

Generation of a HeLa cell line knocked out for endogenous STAT3 88

Development of new BiFC constructs for the study of underexplored STAT3 PTM sites 90

Polo-like kinase (PLK)-1 inhibitors reduce spontaneous **STAT3** *dimerization* **91**

Discussion **95**

Results (Part II) ***98***

STAT3 PTMs regulate its interaction with GRIM-19 and consequent function ***98***

Generation of a BiFC system for STAT3 - GRIM19 interaction **101**

Dimerization between GRIM19 and STAT3 is induced by cytokines and affected by specific PTMs **103**

STAT3-GRIM19 dimers control intracellular ATP levels **105**

Development of a new system for STAT3 visualization **106**

Complementary MiniSOG fragments are able to recover fluorescence **109**

Chapter 3 ***114***

Results (Part III) ***114***

New tools for the visualization of STAT3- regulated genes ***114***

First attempts to generate a BiFC system for the visualization of GFAP dimerization and oligomerization **119**

Generation of a transposon tag for GFAP **122**

Generation of new tagged versions of human and mouse GFAP **124**

The Alexander disease-associated R239C mutation led to GFAP aggregation in U251 cells **126**

Chapter 4 ***134***

General Discussion and Conclusions ***134***

References ***141***

Figure 1 - Schematic representation of STAT3.....5
Figure 2 - *STAT3* structure and domain organization 8
Figure 3 - Post Translational modifications on *STAT3*.....15
Figure 4 - Schematic representation of *GFAP*.....22
Figure 5 - Scheme of IF assembly.....24
Figure 6 - Distribution of Alexander Disease Mutations 26
Figure 7 - Co-immunoprecipitation (Co-IP).....29
Figure 8 - FRET and BRET 31
Figure 9 - Fluoppi system.....32
Figure 10 - ddFP technology 33
Figure 11 - Bimolecular fluorescence complementation (BiFC) assays for the visualization of protein-protein interactions in living cells.....36
Figure 12 - Venus - *STAT3* BiFC plasmid map.....46
Figure 13 - Human GFAP plasmid map.....47
Figure 14 - EGFP transposon 48
Figure 15 - Transposition reaction with EGFP 49
Figure 16 - Workflow of the colony screening.....49
Figure 17 - Representative fluorescence microscopy pictures of the qualitative classification of *STAT3* distribution in HeLa cells 59
Figure 18 - Bimolecular Fluorescence Complementation (BiFC) system for *STAT3* 70
Figure 19 - Resting *STAT3* dimers are mainly cytoplasmic, but accumulate in the nucleus upon cytokine stimulation 72
Figure 20 - The disease-associated L78R mutation inhibits *STAT3* dimerization, and promotes its aggregation and nuclear translocation ..73
Figure 21 - Schematic representation of *STAT3*.....76
Figure 22 - The Y705F phosphoresistant mutation led to an increase in nucleocytoplasmic distribution. 78
Figure 23 - Examples of cells showing mitochondrial localization of *STAT3* dimers versus *STAT3* inclusions".....79

Figure 24 - Inactivating mutations in key lysine residues only regulate unstimulated *STAT3* dimerization in pairs containing a mutation in residues K49 and S727 81
Figure 25 - Genetic blockage of key phosphorylatable residues only regulate unstimulated *STAT3* dimerization in pairs containing mutation in residue S727 and K49 82
Figure 26 - Double PTM mutations containing S727A or K49R in a dimer containing also S727A or K49R increase homodimerization of unstimulated *STAT3* 83
Figure 27 - Asymmetric signal transducer and activator of transcription 3 (*STAT3*) post-translational modifications regulate intracellular distribution of *STAT3* homodimers 84
Figure 28- Asymmetric dimers lead to higher differences in *STAT3* dimer localization 86
Figure 29 - Post-translational modifications regulate cell proliferation after unstimulated *STAT3* dimerization 87
Figure 30 - *STAT3* levels of HeLa knockout cells 88
Figure 31 - Expression and phosphorylation of *STAT3* in HeLa WT and *STAT3* KO cells 89
Figure 32 - PTM-mutants of underexplored phosphorylatable sites at *STAT3* 91
Figure 33 - Screening with a library of kinase inhibitors 93
Figure 34 - Kinase inhibitor 28 is autofluorescent 94
Figure 35 - Unstimulated cells do not present interaction between *GRIM19* and *STAT3* 102
Figure 36 - *STAT3-GRIM19* dimers localize to the mitochondria 103
Figure 37 - Genetic blockage of PTMs at the residues K49, K140 and S727 led to potentiation of the interaction with *GRIM19* after LIF stimulation 104

Figure 38 - Inhibitory mutations of PTMs of the residues K49 and K140 led to a decrease of ATP levels after LIF stimulation.....106
Figure 39 - Schematic representation of MiniSOG-STAT3 construct..107
Figure 40 - *MiniSOG* properties 108
Figure 41 - A split-*MiniSOG* system to visualize protein-protein interactions by CLEM.....110
Figure 42 - *STAT3* BiFC system is able to bind to *GFAP* promotor and regulate trascription 118
Figure 43 - BiFC pairs show very low fluorescence levels. 120
Figure 44 - *GFAP* expression is not compromised by the addition of a Tag 122
Figure 45 - Sites of *EGFP* insertion in *GFAP* 123
Figure 46 - *EGFP-hGFAP* incorporates to IF network. 124
Figure 47 - Tagged versions of *GFAP* - *mGFAP*. 125
Figure 48 - Pattern of distribution of WT and Mutant *GFAP*.....126
Figure 49 - *GFAP* tag does not compromise distribution in living cells127
Figure 50 - CNB-001 decrease *GFAP* aggregation. 129

Table I - Primers for Site-Directed Mutagenesis 51
Table II - Primers for PCR amplification of MiniSOG halves 53
Table III - List of plasmids generated.....65

List of Abbreviations

AG-tag	Azami-Green fluorescent protein tag
ALK	Anaplastic Lymphoma Kinase
Ape	A Plasmid Editor
AxD	Alexander Disease
BiFC	Bimolecular fluorescence complementation
BMX	Bone Marrow X-linked
BRET	Bioluminescence resonance energy transfer
CCD	Coiled-Coil domain
CLEM	Correlated light and electron microscopy
CNS	Central Nervous System
DBD	DNA binding domain
ddFPs	Dimerization-dependent fluorescent proteins
Dha	Ha epitope tag
DHFR	Dihydrofolate reductase
DMEM	Dulbecco's Modified Eagle Medium
DMSO	Dimethyl Sulfoxide
EGF	Epidermal-growth factor
EM	Electron Microscopy
ER	Endoplasmic reticulum
FACS	Fluorescence-assisted cell sorting
FBS	Fetal Bovine Serum
FGF	Fibroblast-growth factor
FGFR	Fibroblast growth factor receptor
FKPB12	FK506-binding protein
FLIM	Fluorescence lifetime imaging
Fluoppi	Fluorescent protein-protein interaction visualization
FRAP	*FKBP*-rapamycin-associated protein
FRET	Fluorescence resonance energy transfer
G/S	Glutamine/Serine
GAS	Interferon-Gamma Activated Sequences
GFAP	Glial fibrillary acidic protein
GFP	Green fluorescent protein
GRIM19	Gene associated with retinoid-IFN-induced mortality 19
hGFAP	human GFAP
HIES	Hyper-IgE syndrome
IF	Intermediate Filament
IFNs	Interferons
IgE	Immunoglobulin E
IHCA	Inflammatory hepatocellular adenomas
IL	Interleukins
IP3R3	Inositol trisphosphate receptor 3

ISRE	Interferon-Stimulated Response Elements
KO	Knockout
LD	Linker domain
LIF	Leukemia inhibitory factor
LM	Light Microscopy
MAMs	Mitochondria-associated ER membranes
mGFAP	mouse GFAP
MiniSOG	Mini Singlet Oxygen Generator
MTT	3-(4,5-dimethylthiazol-2-yl)-2,5-diphenyltetrazolium bromide
NMR	Nuclear magnetic resonance
NMR	Nuclear magnetic resonance
PB1-tag	Bem1p tag
PBS	Phosphate buffer saline
PCAs	Protein complementation assays
pCMV	cytomegalovirus promoter
Pen-Strep	Penicillin-streptomycin commercial antibiotic mixture
PKM	Pyruvate Kinase
PLK	Polo-like kinase
PPIs	Protein-protein interactions
PTMs	Post-translational modifications
RFs	Rosenthal fibers
RT	Room temperature
SCs	Schwann cells
SH2	Src homology region 2
STAT	Signal Transducer and Activator of Transcription
SUMO	Small Ubiquitin-like Modifier
TAD	C-terminal transactivation domain
TAE	Tris Acetate EDTA
TGF-Beta	Transforming-growth factor beta
ULFs	Unit length filaments

Chapter 1
Introduction

1. Signal Transducer and Activator of Transcription 3 (STAT3) is an essential transcription factor

1.1. STAT3 functions in health and disease

The STAT family of transcription factors is formed by 7 members (STAT1, 2, 3, 4, 5a, 5b and 6) originally identified during investigations on gene expression induced by interferons (IFNs) in the immune system. In subsequent years, they were characterized as key transducers for a much wider spectrum of extracellular cytokine stimuli, and related to multiple biological functions beyond immunity (Yu, Lee, Herrmann, Buettner, & Jove, 2014).

Deletion of STAT proteins in mice revealed key roles in the physiology of the immune system and during development. Mice lacking STAT1 or STAT2 are viable, but they are more sensitive to viral infections and other pathologies. *STAT1* knockout (KO) mice present signaling defects in the response to Type-I and Type-II IFNs, where the expression of proteins induced by IFN-α- and IFN-γ is absent or decreased (Durbin, Hackenmiller, Simon, & Levy, 1996; Meraz et al., 1996). *STAT2* knockout mice also show reduced STAT1 phosphorylation and activation (Park, Li, Cha, & Schindler, 2000). In *STAT4* knockout mice, B cells are not able to switch class and produce Immunoglobulin E (IgE). *STAT4* KO mice are viable and fertile, but cannot mediate the response to IL-12, impairing the production of IFN-γ, cellular proliferation, enhancement of natural killer cell cytotoxicity and Th1 cell differentiation (Kaplan, Sun, Hoey, & Grusby, 1996; Thierfelder et al., 1996), while the differentiation of Th2 cells is lost in *STAT6* knockout mice. *STAT5a* knockout leads to loss of prolactin-dependent mammary gland development, and knockout of both *STAT5a* and *STAT5b* leads to the loss of other prolactin functions such as the development of the corpus luteum and female fertility (Ihle, 2001). STAT3

gained special importance because it is the only STAT protein which deletion leads to early embryonic lethality(Takeda et al., 1997).

STAT3 is important for the modulation of the innate and adaptive immune responses by the stimulation of cytokines such as IFNs, IL-2, IL-6, IL-7, IL-10, IL-12, IL-15, IL-21, IL-23 and IL-27 (Harris et al., 2007) and is involved in the regulation of transcription of genes related with apoptosis, proliferation and differentiation (Villarino, Kanno, Ferdinand, & O'Shea, 2015). STAT3 is found overactivated in 70 % of solid tumors, where it is often essential for cancer cell survival and proliferation (M. Wu et al., 2019). This made STAT3 a putative target for cancer treatment and various direct or indirect inhibitors have been proposed as possible future cancer therapies. For example, in rhabdomyosarcoma, *Fibroblast growth factor receptor* (*FGFR*) inhibition with Ponatinib decreases STAT3 phosphorylation and tumor growth *in vivo* (Furtek, Backos, Matheson, & Reigan, 2016). Inhibitors of STAT3 dimerization such as short peptides derived from the helices of N-terminal domain of *STAT3* have also proved to inhibit transcriptional activity and act as a potential approach for cancer treatment (Dimri, Sukanya, & De, 2017). Nitidine chloride was found to suppress tumor growth and induce apoptosis by regulating STAT3 signaling in human oral cancer (L.-H. Kim et al., 2017). *STAT3* mRNA can be a target of antisense oligonucleotides such as AZD9150, which is in clinical trials in a non-Hodgkin's lymphoma population, primarily consisting of patients with diffuse large B-cell lymphoma (Reilley et al., 2018).

STAT3 activation is also found in a wide variety of Central Nervous System (CNS) disorders, especially in acute injury models. It is often observed in circumstances involving reactive astrocytes and glial scar formation, such as excitotoxicity, neonatal white matter injury, neuropathic pain, epilepsy, glaucoma or ischemia (Acarin, González, & Castellano,

2000; Nobuta et al., 2012; Tsuda et al., 2011; Xu et al., 2011; S. Zhang et al., 2013).

Deletion of *STAT3* specifically in astrocytes showed attenuated expression of *glial fibrillary acidic protein* in these cells after spinal cord injury in comparison to wild type mice. These knockout mice also showed impairment of astrocyte hypertrophy and a pronounced disruption of astroglial scar formation after spinal cord injury (J. E. Herrmann et al., 2008). STAT3 function in spinal cord injury was also analyzed with the use of STAT3 inhibitor S31-201 in rats. Animals treated with the inhibitor presented a reduction in tissue damage and a promotion of neural stem cell differentiation after spinal cord injury (Cui et al., 2016).

STAT3 mutations are associated with cancer, Inflammatory hepatocellular adenomas (IHCA) or Hyper-IgE syndrome (HIES). These mutations induce structural changes that can lead to either inactive or constitutively activated STAT3. For example, some HIES-related mutations (i.e. R382W, R382Q, V463del, and V637M) are found in mutation hotspots and lead to STAT3 deficiency (Chandesris et al., 2012). On the other hand, IHCA-related mutations (i.e. L78R, E166Q, D502Y, Y640F, Y657_M660dup, G656_Y657insF and K658Y) lead to STAT3 constitutive nuclear translocation and activation of transcription even in the absence of cytokine stimuli (Pilati, Amessou, Bihl, Balabaud, Van Nhieu, et al., 2011a). The COSMIC database registered a high number of cancer-related *STAT3* mutations, being the residues Y640 and D661 the more frequently mutated. Most of these activating mutations are heterozygous, acting in a dominant manner. The structural changes and mechanisms underlying STAT3 activation or inactivation by these mutations remain barely characterized, but a clear picture of STAT3 domain organization and overall structure could help to understand these disorders.

1.2. STAT3 structure and domain organization

STAT3 structure is common to all proteins of the STAT family, and it is characterized by six domains (Fig. 1): an N-terminal domain (NTD), a Coiled-Coil domain (CCD), a DNA binding domain (DBD), a linker domain (LD), a Src homology region 2 (SH2) domain and a C-terminal transactivation domain (TAD) (Becker, Groner, & Müller, 1998; Nkansah et al., 2013b; Ren et al., 2008). The STAT family is the only family of transcription factors carrying an SH2 domain, very common and relevant in other signaling proteins. The SH2 domain allows STAT3 to bind phosphotyrosine residues in other proteins, such as membrane receptors and other STAT molecules (B. A. Liu, Engelmann, & Nash, 2012).

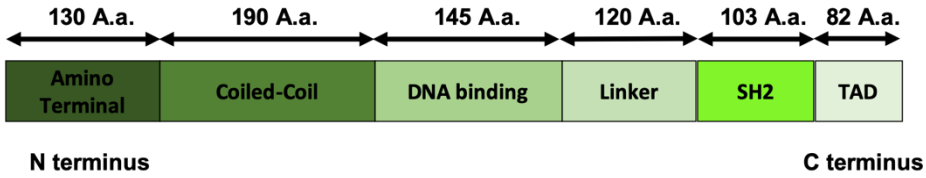

Figure 1 - Schematic representation of STAT3 - STAT3 has 770 Amino acids (A.a) and is divided in six domains, the N-Terminal domain (1-130 Aa), the Coiled-coil domain (130-320 Aa), the DNA binding domain (320-465 Aa), the linker domain (465-585 Aa), the SH2 domain (585-688 Aa) and the TAD (688-770 Aa).

*STAT*s are naturally found as latent homo- or heterodimers and can form higher order oligomers in response to stimuli. The rate-limiting phosphorylation step in the canonical STAT3 pathway occurs on tyrosine 705 (Y705), located in the TAD, and this phosphotyrosine is recognized by the SH2 domain of other STAT3 molecules. Thus, the SH2 and TAD domains are generally considered to be largely responsible for STAT3 homodimerization and tetramerization (Droescher & Vinkemeier, 2012; Lim & Cao, 2006). However, *STAT3* does not really need to be Y705-

phosphorylated to homodimerize, and the NTD was more recently identified as an essential domain for STAT3 homodimerization (Braunstein, Brutsaert, Olson, & Schindler, 2003; Vogt et al., 2011). STAT3 lacking the NTD is capable of being phosphorylated, although it does not accumulate in the nucleus. Deletion of the NTD of STAT3 also abrogated dimer formation prior to STAT3 phosphorylation (Vogt et al., 2011). Together with the CCD, the NTD also plays a key role in the interactions with other proteins. The two domains responsible for DNA interaction are the DBD and LD. They enable the transcription of specific target genes by binding to a specific response element in the DNA, the Interferon-Gamma Activated Sequences (GAS).

The TAD is strongly affected by STAT3 alternative splicing, originating two main isoforms of *STAT3* (α and β) (Maritano et al., 2004; Raaijmakers et al., 2017). Alternative splicing in STAT3 leads to a frameshift that exchanges the last 55 amino acids of the TAD domain by 7 new amino acids and a stop codon, producing a shorter protein of 722aa that lacks the relevant S727 residue, which is required for the STAT-GRIM19 interaction, among others (Aigner, Just, & Stoiber, 2019). The STAT3 beta proteoform has much lower abundance than STAT3 alpha, and mice lacking this proteoform are viable and fertile (Maritano et al., 2004). However, STAT3 beta can partially compensate for STAT3 functions during development, as mice lacking only *STAT3* alpha died just after birth and not during development (Maritano et al., 2004). Interestingly, a switch between the levels of alpha and beta proteoforms leads to tumor regression more effectively than total depletion of *STAT3* (Zammarchi et al., 2011; Zheng et al., 2016). *STAT3* can also have two more isoforms originated from the absence of the three nucleotides encoding for S701 in either *STAT3α* or *STAT3β*: *STAT3ΔS- α* (769 AA) and *STAT3ΔS-β* (721 AA) (Hiller et al., 2006; Schaefer, Sanders, & Nathans, 1995; Turton, Annis, Rui, Esnault, & Mosher, 2015). The roles

of these variants in health and disease are largely unknown, but S701 is a target for phosphorylation, and this post-translational modification could be relevant for specific *STAT3* functions (Zheng et al., 2016).

The functions of all *STAT3* domains cannot be reduced to these generic roles and in fact there are studies pointing to crosstalk between different domains. An example of this crosstalk is the I568F mutation in the LD associated to Hyper-IgE syndrome, that leads to conformational changes in SH2, DBD and CCD and the reduction of SH2 binding affinity to phosphotyrosine peptides (Namanja, Wang, Buettner, Colson, & Chen, 2016). Also, Hyper-IgE syndrome patients carrying the V637M mutation in the SH2 domain show no Y705 phosphorylation at the TAD after cytokine stimulation, preventing STAT3 transcriptional activity (Renner et al., 2008). In contrast, IHCA or cancer patients presenting mutation in Y640 enhance *STAT3* activation (Pilati, Amessou, Bihl, Balabaud, Nhieu, et al., 2011). One possible explanation of this crosstalk between domains can be the intramolecular interactions in the tertiary, 3-dimensional structure of STAT3.

Until now, it has not been possible to obtain the full structure of any member of the STAT family. The STAT1 structure is the most complete to date, including the NTD but lacking a large part of the TAD (Protein Database Ref. 1YVL). The existing STAT3 and STAT5 structures do not include the NTD and a large portion of the TAD (Protein Database Ref. 6QHD for STAT3 and Ref. 1YU1 for STAT5), although in the case of STAT3 the NTD structure has been solved separately (Protein Database Ref. 4ZIA). The tendency of STAT*s* to form aggregates and problems with protein expression and purification are some of the reasons that lead to this lack of structure (Sgrignani et al., 2018). Fig. 2 shows a reconstruction of the STAT3 dimer using the available structures solved from STAT3 fragments (the TAD is not included from residue T714).

In addition to structural changes, STAT3 functions are determined by other signaling currencies, such as post-translational modifications, protein-protein interactions and subcellular localization. STAT3 pathways are surprisingly diverse and could explain the highly pleiotropic nature of this transcription factor.

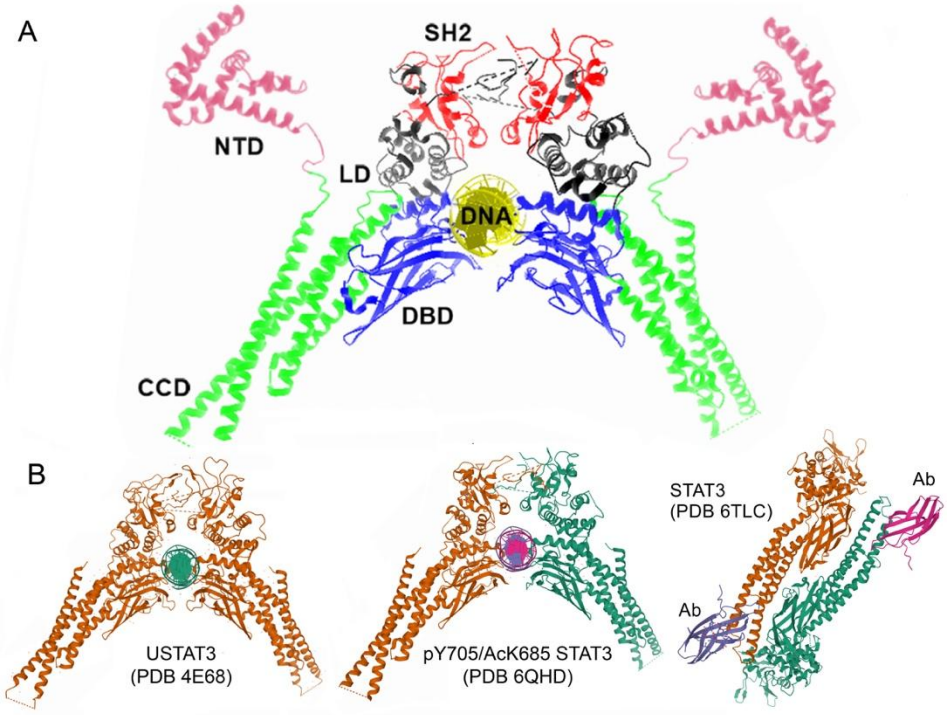

Figure 2 - STAT3 structure and domain organization - A, reconstruction of the structure of *STAT*3 dimers bound to DNA, from Protein Database references 4ZIA (N-terminal domain, NTD, in pink) and 6QHD (DNA-bound STAT3 without the N-terminus and no TAD after residue 715). The actual position of the NTD when STAT3 dimers are bound to DNA or as inactive dimers remains unknown. The color code corresponds to the different domains, indicated in the figure and the main text. B, three structures of STAT3 dimers, bound to DNA (PDB 4E68 and PDB 6QHD) or inactive (PDB 6TLC). Phosphorylated and unphosphorylated forms of STAT3 dimers are virtually superimposable, at least when they are bound to DNA. It is unknown how and when STAT3 dimers shift conformation from the antiparallel orientation to the scissor-like conformation of DNA-bound dimers. Adapted from (Diallo & Herrera, 2021).

1.3. Canonical and non-canonical STAT3 Pathways

1.3.1. The canonical STAT3 pathway

The canonical STAT3 pathway is characterized by the phosphorylation of STAT3 at Y705 and its translocation to the nucleus, where it induces the transcription of specific target genes. This pathway can be triggered by a wide spectrum of extracellular factors. These include cytokines of the Interleukin-6 family, such as interleukins (IL) 6, 11, 27 and 31, Oncostatin M, leukemia inhibitory factor (LIF), ciliary neurotrophic factor, cardiotrophin-1, cardiotrophin-like cytokine and neuropoietin (Derouet et al., 2004; Jones & Jenkins, 2018), but also epidermal-growth factor (EGF), fibroblast-growth factor (FGF), transforming-growth factor beta (TGF-Beta) or retinoic acid, among others (Boeuf, Hauss, De Graeve, Baran, & Kedinger, 1997; Decker & Kovarik, 2000; Herrera, Chen, & Schubert, 2010a; Niwa, Burdon, Chambers, & Smith, 1998; J. J. Zhang et al., 1998).

These external stimuli bind and activate their corresponding membrane receptors, such as EGFR, PDGFR, Her2, FGFR, VEGFR, GFR, LIFR, gp130 and HGFR. Upon activation of membrane receptors, latent cytoplasmic STAT3 is recruited to the inner side of the cell membrane and activated by phosphorylation at Y705 (Cimica, Chen, Iyer, & Reich, 2011). STAT3-activating receptors can be divided in two classes: those with intrinsic tyrosine kinase activity that can phosphorylate STAT3 at Y705 directly; and those that lack intrinsic tyrosine kinase activity, and therefore need to recruit cytoplasmic kinases to phosphorylate STAT3, such as the JAK family (JAK1, JAK2, JAK3 and TYK2) (Johnston & Grandis, 2011; Pilati, Amessou, Bihl, Balabaud, Van Nhieu, et al., 2011b;

Sgrignani et al., 2018; Xiong, Yang, Shen, Zhou, & Shen, 2014). Additionally, there are also cytoplasmic kinases that can activate STAT3 signaling apart from cytokines and receptors, such as the Src kinase family, Pyruvate Kinase (PKM), Anaplastic Lymphoma Kinase (ALK), the Bone Marrow X-linked (BMX) kinase, the Bcr-Abl fusion protein or Oncogenic RET/PTC (Rearranged in Transformation/Papillary Thyroid Carcinoma) Tyrosine Kinase (Gao, Wang, Yang, Liu, & Liu, 2012; Guryanova et al., 2011; Johnston & Grandis, 2011; Xiong et al., 2014; Zamo et al., 2002).

It was originally thought that Y705 phosphorylation was necessary and sufficient for STAT3 homodimerization through the reciprocal interactions between SH2 domains and pY705 residues in the TAD domain. However, the NTD is also involved in STAT3 dimerization (Braunstein et al., 2003; Vogt et al., 2011), and several reports indicate that STAT3 reservoirs are mostly latent, unphosphorylated STAT3 dimers (Braunstein et al., 2003; Haan et al., 2000; Vogt et al., 2011). The canonical view of the pathway also argues that phosphorylation at Y705 leads to translocation of STAT3 dimers from the cytoplasm to the nucleus after cytokine stimulation (Bhattacharya & Schindler, 2003). However, some authors observed that there is a constant shuttling of unphosphorylated STAT3 between the cytoplasm and the nucleus, and pSTAT3 dimers are simply retained in the nucleus after cytokine stimulation (A. Herrmann et al., 2007; Meyer & Vinkemeier, 2004; Pranada, Metz, Herrmann, Heinrich, & Müller-Newen, 2004).

Once in the nucleus, phosphorylated STAT3 binds to its GAS response elements and induces the expression of genes related to cell survival, proliferation and differentiation, such as Bcl-2, Mcl-1, Bcl-xL Survivin or Hsp70. Constitutive activation of STAT3 in cancer can therefore promote the survival and proliferation of tumoural cells, but also their metastasis through the upregulation of genes such as *Fascin*,

Vimentin, *RhoU*, *AKT*, *PIM-1* and *TNF-R2* (Carpenter & Lo, 2014; B.-H. Kim, Yi, & Ye, 2016). In spinal cord injury, stroke and neurodegenerative disorders, STAT3 regulates directly the expression of the intermediate filament GFAP during the reactive gliosis observed in these pathologies (J. E. Herrmann et al., 2008; Hol & Pekny, 2015)

Although Y705 phosphorylation is the critical step in the canonical pathway, there are other post-translational modifications (PTMs) that can influence this pathway. For example, phosphorylation at S727 can enhance or prevent STAT3 maximal activation, being its actual role still a matter of discussion (Schuringa, Schepers, Vellenga, & Kruijer, 2001; J. Yang et al., 2010). STAT3 has more than 80 identified PTMs, but the vast majority of reports (>90% in phosphositeplus.org) focuses only on Y705 and S727 phosphorylation events, and the roles of the rest of PTMs on the canonical *STAT3* pathway remain poorly characterized.

1.3.2. Non-Canonical *STAT*3 pathways

Non-canonical STAT3 pathways are a series of unexpected STAT3 behaviors and functions independent of Y705 phosphorylation. Contrary to what was initially thought, unphosphorylated STAT3 (USTAT3) is also able to dimerize, translocate to the nucleus and regulate the transcription of a different set of genes, such as *Cyclin B1*, *E2F1*, *M-Ras* and *Met* (Braunstein et al., 2003; Nkansah et al., 2013b; J. Yang et al., 2005). Higher nuclear levels of USTAT3 are positively correlated with the malignancy of glioblastoma (Rodrigues et al., 2016). The effect of higher levels of unphosphorylated STAT3 in the nucleus is also observed in the development of cardiac hypertrophy, where it is responsible for the expression of the angiotensin II receptor 1 (H. Yue, Li, Desnoyer, & Karnik, 2010).

In agreement with current standards in the field, we call USTAT3 to STAT3 that is not phosphorylated at Y705, but this does not mean that it is not phosphorylated at other residues. STAT3 has 41 phosphorylatable residues and 40 additional PTMs that could regulate USTAT3 function. Most surprisingly, USTAT3 functions do not necessarily occur in the nucleus, but also at mitochondria and the endoplasmic reticulum (ER) (Avalle & Poli, 2018; Srivastava & DiGiovanni, 2016; Stark & Darnell, 2012).

Phosphorylation at Serine 727 is key to many non-canonical STAT3 functions and, although it is not the only PTM involved, it is definitely the most studied. This residue, also located in the C-terminal transactivation domain region of STAT3, is very conserved among the members of the STAT family, with exception of STAT2 and the beta isoforms of STAT3 (Verhoeven et al., 2020; Wen & Darnell, 1997). In melanoma and chronic lymphocytic leukemia, the STAT3 pathway was frequently found activated with phosphorylation at S727 but without phosphorylation at Y705 (Hazan-Halevy et al., 2010a; Sakaguchi, Oka, Iwasaki, Fukami, & Nishigori, 2012). In glioblastoma, this phosphorylation alone was related with cancer progression and tumor cell survival (G.-S. Lin et al., 2014). It was also observed a different role for the phosphorylation of these two residues in mouse embryonic stem cells, being S727 phosphorylation associated with the transition of mouse embryonic stem cells from pluripotent state to neuronal differentiation, while Y705 phosphorylation leads to self-renewal of mouse embryonic stem cells (Guanyi Huang, Yan, Ye, Tong, & Ying, 2014).

The role of S727 phosphorylation is not only related to nuclear functions of STAT3, but also to its mysterious mitochondrial functions. Mitochondrial STAT3 is responsible for the transcriptional regulation of mitochondrial genes related to the electron transport chain, an interesting but not particularly surprising function of STAT3 (R. Yang & Rincon, 2016).

What is most surprising is that mitochondrial STAT3 also binds directly and increases the activity of components of the electron transport chain, such as succinate oxidoreductase (complex II), ATP synthase (complex V) and lactate dehydrogenase (Wegrzyn, Potla, Chwae, Sepuri, Zhang, et al., 2009). Mitochondrial STAT3 promotes tumor growth and metastasis in breast cancer (Q. Zhang et al., 2013). While phosphorylation at Y705 has been observed in mitochondrial STAT3, only S727 phosphorylation is essential for STAT3 mitochondrial functions (Gough et al., 2009; Wegrzyn, Potla, Chwae, Sepuri, Koeck, et al., 2009).

How *STAT3* enters mitochondria remains a matter of discussion. No mitochondrial localization signal has been identified in the STAT3 amino acid sequence, although the C-terminus is clearly necessary for mitochondrial localization (Tammineni et al., 2013). Some authors described the interaction of STAT3 with *Gene associated with retinoid-IFN-induced mortality 19* (*GRIM19*) as a key step for mitochondrial translocation (Jon E. Angell, Lindner, Shapiro, Hofmann, & Kalvakolanu, 2000; Guochang Huang et al., 2004; Su et al., 2020; Tammineni et al., 2013; J. Zhang et al., 2003), although more recent studies casted some doubts on this interaction (Su et al., 2020). GRIM19 was originally described as a novel cell death regulatory molecule in response to IFN and retinoic acid toxicity (Jon E. Angell et al., 2000; Deiss & Kimchi, 1991; Nallar & Kalvakolanu, 2017), and later largely studied as a tumor suppressor (W. Zhang et al., 2015). The human *GRIM19* gene is located on chromosome 19p12.3 (Zheng et al., 2016), and encodes for a small mitochondrial protein (16 kDa) that can be also found in the nucleus and cytoplasm (J E Angell, Lindner, Shapiro, Hofmann, & Kalvakolanu, 2000; Fearnley et al., 2001). GRIM19 suppresses canonical STAT3 transcriptional activity by interacting and relocating the transcription factor to mitochondria, and this interaction was increased after treatment with interferons and retinoic acid (Kalakonda, Nallar, Lindner, et al., 2007; J.

Zhang et al., 2003). GRIM19 targets the TAD in STAT3, being the phosphorylation of Serine 727 essential for their interaction (J. Zhang et al., 2003). This interaction raised the hypothesis that the anti-oncogenic function of GRIM19 is mediated by inhibiting STAT3 function (Kalakonda, Nallar, Lindner, et al., 2007; Lufei et al., 2003).

Besides nucleus, cytoplasm and mitochondria, STAT3 has been also found in endoplasmic reticulum at the mitochondria-associated ER membranes (MAMs) (Avalle et al., 2019; Su et al., 2020). This localization leads to the interaction of STAT3 with *inositol trisphosphate receptor 3* (IP3R3), the responsible for calcium release from ER. This interaction leads to the degradation of IP3R3, reducing calcium flux and preventing apoptosis (Avalle et al., 2019).

1.4. Regulation of STAT3 by post-translational modifications

As stated above, Y705 and S727 phosphorylation are the two-best characterized PTMs in STAT3. While the role of Y705 phosphorylation is unequivocally linked to the canonical activation of STAT3-mediated transcription, phosphorylation at S727 has contradictory effects. Some authors observed that S727 was required for full transcriptional activation mediated by STAT3 (Wen, Zhong, & Darnell, 1995), while others found that S727 phosphorylation was a negative regulator of Y705 phosphorylation and canonical STAT3 transcriptional activity (Chung, Uchida, Grammer, & Blenis, 1997). RhoA leads to activation of STAT3 transcriptional activity by the phosphorylation at both Y705 and S727, and this interaction was demonstrated to be important for oncogenic transformation (Aznar et al., 2001). In chronic lymphocytic leukemia, constitutive phosphorylation of S727 without tyrosine phosphorylation still leads to STAT3 nuclear translocation, DNA binding and regulation of a specific set of genes such as *Bcl2*, *Pim1*, *Bcl-XL*, *Cyclin D1*, *p21* (*Waf1*),

and *c-Myc* (Hazan-Halevy et al., 2010b). As we mentioned above, phosphorylation of serine 727 is strongly associated with mitochondrial STAT3 functions (Boengler, Hilfiker-Kleiner, Heusch, & Schulz, 2010; Gough et al., 2009; Wegrzyn, Potla, Chwae, Sepuri, Zhang, et al., 2009).

However, STAT3 functions can be also regulated by many PTMs beyond Y705 and S727 phosphorylation (Srivastava & DiGiovanni, 2016; J. Yang & Stark, 2008). According to the Phosphosite Plus database (https://www.phosphosite.org/homeAction), STAT3 can be subjected to approximately 80 different PTMs, including phosphorylation (on tyrosines, serines and threonines), methylation (on arginines and lysines), acetylation (on lysines) and ubiquitination/sumoylation (on lysines). Further PTMs have been reported in the literature, such as oxidation (on cysteines), proteolytic cleavage or O-linked β-N-acetylglucosamination, among others. The potential roles of these PTMs in STAT3 behavior and function are barely understood.

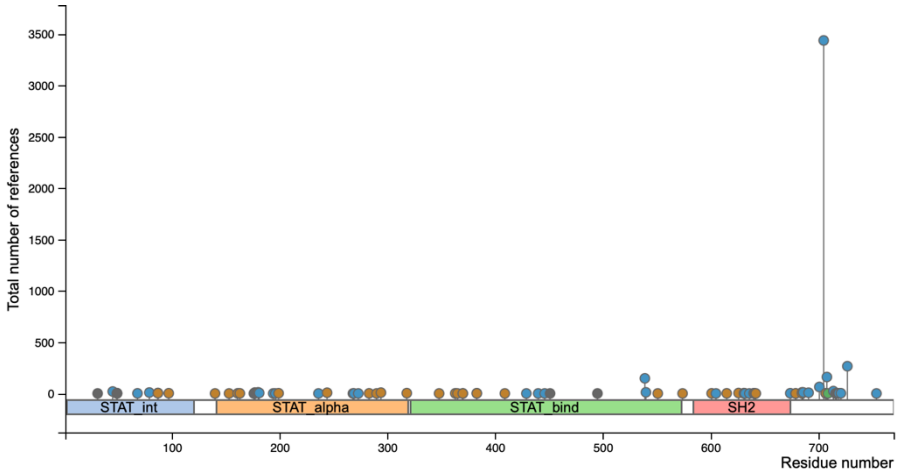

Figure 3 - Post Translational modifications on STAT3 – Different PTMs distributed accordingly with the residue where they occur and the number of references of each one. Phosphorylation on the Residue 705 and 727 are the ones more studied. Adapted from Phosphosite Plus database (https://www.phosphosite.org/homeAction)

1.4.1. Understudied phosphorylation events

Phosphorylation is the most described PTM at STAT3, happening in 41 different residues (10 Tyrosines, 16 Serines and 15 Threonines). STAT3 phosphorylated at residues Y45 or Y68 is found in both cytoplasm and nucleus, but being enriched in the nucleus of breast cancer cells (C. Huang et al., 2018). Y45 phosphorylation is mediated by Src kinase, and it reverses NTD-mediated *STAT* dimerization (C. Huang et al., 2018).

Y640 phosphorylation (in the SH2 domain) limits STAT3 activity due to the phosphate group that will occupy the binding site for T708, a crucial binding site for STAT3-DNA complex formation (Mori et al., 2017). This residue is also related with cancer, where a Y640F mutation stabilizes activated STAT3 dimers in response to interferon and accelerates nuclear translocation (Mori et al., 2017). This mutation also increases Y705 phosphorylation in the context of IHCA mediated by the Src kinase (Pilati, Amessou, Bihl, Balabaud, Van Nhieu, et al., 2011a).

The T714 residue, present in the TAD, is co-phosphorylated with S727, and this double phosphorylation is important for STAT3-induced gene transcription of *Mcl-1*, a protein of the *Bcl2* family, promoting cell survival in renal tumors (Waitkus et al., 2014). Phosphorylation at S754 is associated with inhibition of canonical STAT3 transcriptional activity in the presence of cytosolic DNA after microbial infection (Hsia, Hutti, & Baldwin, 2017). T717 phosphorylation could also be relevant, as this PTM is mutually exclusive with O-GlcNAcylation by a Cullin-3-regulated O-GlcNAc transferase, which inhibits Y705 phosphorylation and STAT3 canonical transcriptional activity in macrophages (Alfaro et al., 2012; X. Li et al., 2017). To the best of our knowledge, no reports on the remaining phosphorylatable residues exist.

1.4.2. Lysine modifications

Lysine residues are a putative target for a high number of different PTMs, including ubiquitination, sumoylation, acetylation or methylation. Ubiquitination/sumoylation is the second most common PTM in STAT3. These PTMs are the addition of the proteins ubiquitin or Small Ubiquitin-like Modifier (SUMO) to lysine residues and share similar patterns of action (Deol, Lorenz, & Strieter, 2019). In the case of ubiquitination, proteins can be mono or polyubiquitinated, being the fate of the protein determined by the types of bond between ubiquitin molecules (Deol et al., 2019). The most common fate of ubiquitinated proteins is the degradation at the proteasome, but ubiquitination can also alter their cellular location, activity and protein interactions. In the case of sumoylation, the structural differences of the SUMO proteins will lead to a different fate of the sumoylated protein (Han, Feng, Gu, Li, & Chen, 2018). Together, they are responsible for modifications in 34 residues (31 ubiquitinated and 3 sumoylated), being the lysine 47 identified as a major mono-ubiquitination site for STAT3 (Ray et al., 2014). The importance of ubiquitination was proved in studies where it was showed that mono-ubiquitination enhanced STAT3 transcriptional activity for specific genes such as *SOCS3*, *BCL2*, *BCL2L1*, *APEX1*, *SOD1*, *CCND1* and *MYC* (Ray et al., 2014).

Acetylation is the second most common lysine PTM: at least 10 residues can undergo acetylation (K49, K87, K370, K383, K615, K631, K685, K679, K707 and K709) (Ma et al., 2017). Acetylation is less frequent than phosphorylation and ubiquitination, but its role in STAT3 function is still prominent. STAT3 can suffer acetylation in Lysine 685 in response to cytokines from the IL-6 family, enhancing Y705 phosphorylation and STAT3 dimerization (Ohbayashi et al., 2007; Wang, Cherukuri, & Luo, 2005; Yuan, Guan, Chatterjee, & Chin, 2005). Lysine 685 acetylation plays a major role in cancer, and Histone Deacetylase inhibitors that avoid

STAT3 acetylation and the consequent activation of transcription are currently considered as putative anti-cancer treatments (S.-C. Lee et al., 2019; Min et al., 2018). In keratinocytes treated with IL22, acetylation at Lysine 685 also occurs and possibly leads to psoriasis, and acetylation inhibitors have been suggested as a potential therapy (Sestito et al., 2011). Nuclear translocation of the CD44 protein (a cytokine receptor) can also lead to K685 acetylation and STAT3 activation (J. L. Lee, Wang, & Chen, 2009). In lymphoma, K685 acetylation by *p300/CBP* leads to nuclear export of STAT3 to cytoplasm (Gupta, Han, Stenson, Wellik, & Witzig, 2012).

Acetylation also occurs on the NTD of STAT3 in the Lysine 49 mediated by *p300/CBP* under IL6 stimulation (Hou, Ray, Lee, & Brasier, 2008; Ray, Boldogh, & Brasier, 2005a). When this acetylation is blocked, STAT3 still binds DNA, but it abrogates IL-6-induced angiotensinogen (hAGT) activation. This mechanism was observed in the hepatic acute-phase response (Ray et al., 2005a).

It was later discovered that Lysine 49 can also be dimethylated by the methyltransferase EZH2 after Y705 phosphorylation in response to IL-6. In the absence of this methylation, a set of IL-6 dependent genes are downregulated, such as *BCL3*, *SERPINA1*, *GADD45G*, and *SOCS3* (Dasgupta, Dermawan, Willard, & Stark, 2015). Like K49, K140 is also methylated after tyrosine phosphorylation induced by IL-6, methylation being mediated by SET9 and demethylation by LSD1 (J. Yang et al., 2010). This methylation is coupled with Serine 727 phosphorylation and happens at the nucleus (J. Yang et al., 2010). A third methylation event has been identified at K180. This methylation is mediated by *EZH2* and leads to increased Y705 phosphorylation, promoting STAT3 activity in glioblastoma stem cells. A K180A mutation prevents Y705 phosphorylation in STAT3 after cytokine stimulation (E. Kim et al., 2013; Stark, Wang, & Lu, 2011; J. Yang et al., 2010).

1.4.3. Other STAT3 post-translational modifications

STAT3 can suffer other types of PTMs such as cleavage or cysteine modifications. Limited cleavage can lead to different shorter variants of STAT3 besides the α and β splicing isoforms. A 72Kda C-terminal fragment was identified in 1998 and designated as *STAT3γ* (Chakraborty & Tweardy, 1998). Later on, more STAT3 fragments were described, such as STAT3δ (64 KDa) and an 83 KDa fragment, and they were suggested to have a regulatory role in specific cells such as white blood cells (Hevehan, Miller, & Papoutsakis, 2002; Oda, Wakao, & Fujita, 2002). In 2017, two more C-terminal fragments were described, STAT3ε (N-terminal, 50 KDa) and –ζ (C-terminal, 45 KDa) (Mehta et al., 2017). STAT3 proteolytic fragments are described to react differently to PTMs: STAT3-gamma (72KDa) is extremely resistant to Y705 phosphorylation, while the delta fragment (64 KDa) is normally phosphorylated (Hevehan et al., 2002).

The intracellular REDOX state can also interfere in STAT3 function (Simon, Rai, Fanburg, & Cochran, 1998; Waris, Huh, & Siddiqui, 2001). Cysteines are the main target of REDOX PTMs, and tend to form disulfide bonds with other cysteine residues within the same STAT3 molecule, in the other STAT3 molecule of a homodimer, or in other interacting proteins. STAT3 has 14 cysteine residues, some of them having therapeutic potential for cancer, such as C108, C259, C367, C468, C542 and C687, since they can be alkylated by natural and artificial compounds that inactivate the transcription factor, such as curcumin, Stattic or other antitumoral agents (Buettner et al., 2011; Hahn et al., 2018; Heidelberger et al., 2013; L. Li, Cheung, Evans, & Shaw, 2010). Triple cysteine-to-serine substitutions of residues C418, C426 and C468 significantly prevented the decrease in STAT3 DNA binding and transcriptional activity

in response to H_2O_2-induced oxidative stress, and a fourth substitution at C765 further enhanced this effect (L. Li et al., 2010).

2. Downstream the canonical JAK/STAT3 pathway: the glial fibrillary acidic protein and CNS pathologies

In the human brain, neurons are not the most abundant type of cells. Astrocytes, a type of glial cells, overcome the number of neurons by over fivefold outside the cerebellum (Azevedo et al., 2009). They were originally thought to have a rather passive, structural role in the CNS. Nowadays, astrocytes are described as an extremely active player in a variety of biological functions related to the maintenance of neuronal survival and function and beyond, from brain development and physiology to various CNS pathologies (Parpura et al., 2012). In pathological conditions, such as mild traumatic injuries or neurodegenerative disorders, astrocytes become reactive and hypertrophic and secrete molecules that contribute to neuroinflammation without invading the area covered by other astrocytes. When the pathology involves damage of the blood-brain barrier, of which the astrocytes are an integral part, astrocytes proliferate and close the wound, forming the glial scar that limits tissue damage (Burda & Sofroniew, 2014; Seifert, Schilling, & Steinhäuser, 2006).

There is evidence that activated phospho-STAT3 translocate to the nucleus and turns on the transcription of genes involved in glial differentiation (Levy & Darnell, 2002). *STAT3* is expressed during CNS development and mediates the cytokine-gp130 signaling axis that induces glial differentiation in the perinatal period (Bonni et al., 1997). *STAT3* was later proven to be both necessary and sufficient for astrocyte differentiation (Hong & Song, 2014). There is also substantial evidence that *STAT3* mediates astrogliosis in pathological conditions, being

involved in the scar formation after spinal cord injury and other types of neurotoxicity (J. E. Herrmann et al., 2008; O'Callaghan, Kelly, VanGilder, Sofroniew, & Miller, 2014). The relevance of STAT3 in the production of new astrocytes during embryonic development and in pathological conditions has been commonly elucidated using GFAP as the main astroglial marker (Ben Haim et al., 2015; J. E. Herrmann et al., 2008; O'Callaghan et al., 2014).

The glial fibrillary acidic protein is an intermediate filament described for the first time in 1971 as a major component of astrocytic cytoskeleton (Eng, Vanderhaeghen, Bignami, & Gerstl, 1971), soon becoming the principal marker for the identification of astrocytes (Sofroniew & Vinters, 2010). The GFAP promoter is also extensively used to target the expression of specific genes to astrocytes (Michael Brenner, Kisseberth, Su, Besnard, & Messing, 1994), and it contains response elements to STAT3 (Herrera, Chen, & Schubert, 2010b). However, GFAP expression can be also found in other cell types throughout the body: in adult neural precursor cells in the olfactory bulb, dentate gyrus in the hippocampus and subventricular zone (a D. R. Garcia, Doan, Imura, Bush, & Sofroniew, 2004; Seri, García-Verdugo, McEwen, & Alvarez-Buylla, 2001); in Schwann cells (Bianchini et al., 1992); in lymphocytes (Riol, Tardy, Rolland, Lévesque, & Murthy, 1997); in supporting cells of the enteric nervous system (Kato et al., 1990; Martucciello, 2008). Its up-regulation in these cells is linked to pathological conditions, such as certain demyelinating and axonal neuropathies (Bianchini et al., 1992) and in Hirschsprung's and Crohn´s diseases (Kato et al., 1990; Martucciello, 2008).

Upregulation of GFAP expression is a hallmark of reactive astrocytes and responsible for their hypertrophy (Hol & Pekny, 2015), although this increase can have different intensities in different regions of the CNS and populations of astrocytes (Jany, Hagemann, & Messing,

2013). However, *GFAP*-null mice show no overt phenotypes in their development, fertility, and gross CNS morphology and behavior (McCall et al., 1996). *GFAP*-null astrocytes also have a normal morphology and distribution without any detectable deficiency of neuronal development, and produce a normal blood-brain barrier (Gomi et al., 1995). The role of GFAP is probably compensated by other intermediate filaments, such as vimentin and/or nestin. However, *GFAP*-null mice are significantly more sensitive to pathological challenges, such as stroke-induced ischemia (De Pablo, Nilsson, Pekna, & Pekny, 2013; Nawashiro, Messing, Azzam, & Brenner, 1998).

2.1. GFAP: the protein

The human *GFAP* gene is localized in chromosome 17, band q21 and it contains nine exons and eight introns. The final protein has 432 amino acids and a molecular weight of 50 KDa (Bongcam-Rudloff et al., 1991; Isaacs, Baker, Wavrant-De Vrièze, & Hutton, 1998; Kumanishi et al., 1992). After alternative mRNA splicing, the GFAP gene originates at least nine isoforms, being *GFAP-α* the most predominant isoform in the CNS (Kamphuis et al., 2012; Middeldorp & Hol, 2011).

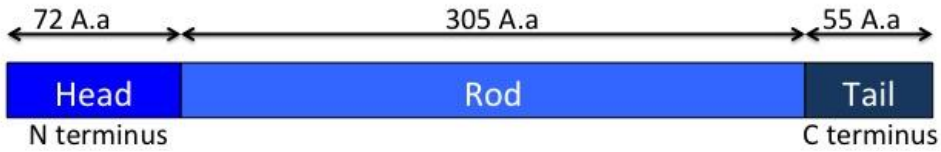

Figure 4 Schematic representation of *GFAP* - *GFAP* has 432 Amino acids (A.a) and is divided in three domains, the Head (1-72 Aa), the Rod (73-377 Aa) and the Tail (378-432 Aa).

GFAP has the domain organization typical of an intermediate filament (IF), with a head with 72 amino acids, a Rod domain with 305

amino acids and a non-alpha-helical tail with 55 amino acids that shares some phosphorylatable residues with vimentin, suggesting an important role of these sites for IF function (Geisler & Weber, 1983; Reeves, Helman, Allison, & Israel, 1989). The three-dimensional structure of GFAP remains undefined. This is due to the difficulty of crystallization of full-length IF proteins because of their intrinsic structural flexibility and tendency to self-assemble into filaments. To avoid this problem, attempts to reveal the structure were made by dividing IF proteins in smaller fragments (B. Kim, Kim, & Jin, 2018).

GFAP forms 10 nm diameter filaments through a process divided in several steps. The first stage in the assembly is the formation of a dimer originated from the interaction between two rod domains from polypeptide chains that wind around each other in a coiled-coil structure. Then, in order to form tetramers, these dimers associate in an anti-parallel manner originating the initial building blocks of all IFs. Then, these building blocks will associate through the nonhelical tail domains to form unit length filaments (ULFs) with 20 nm in diameter. The final stage is the association of these units longitudinally to form filaments with hundreds of nanometers in length (Fig. 4) (Chernyatina, Guzenko, & Strelkov, 2015; Etienne-Manneville, 2018).

PTMs also play a role in GFAP structural organization and filament assembly and disassembly (Inagaki et al., 1990, 1996; Sihag, Inagaki, Yamaguchi, Shea, & Pant, 2007). The most studied one is phosphorylation by various kinases such as *protein kinase A*, *calmodulin-dependent protein kinase II* and *protein kinase C*, which are responsible for the disassembly of the filaments by site-specific phosphorylation. These phosphorylation sites are mainly in the head domain (T7, S8, S13, S17 and S34) being one in the tail domain (S389) (Inagaki et al., 1990, 1996). The amino acids that suffer phosphorylation in the head domain are conserved among species and GFAP isoforms, indicating the high

importance of phosphorylation in the regulation of GFAP fibrillization (Middeldorp & Hol, 2011).

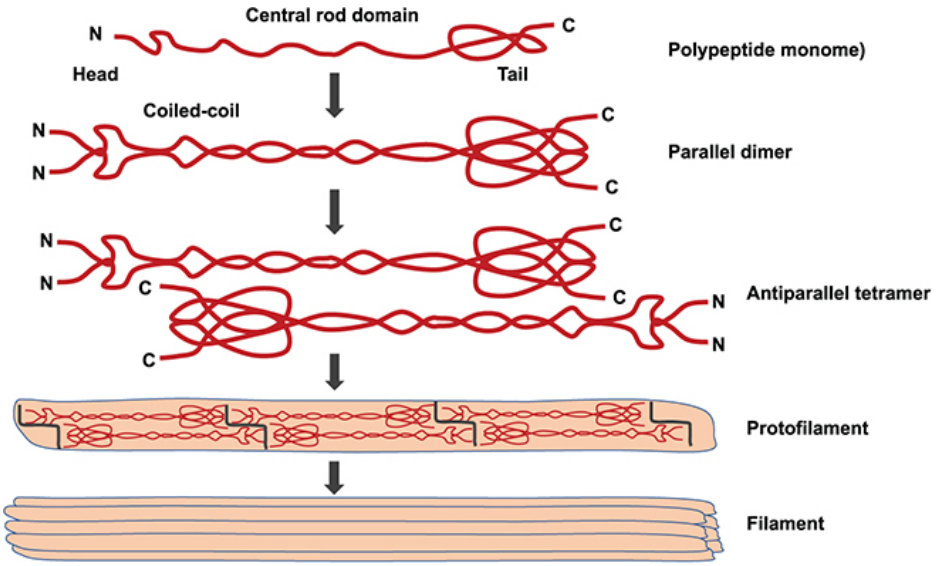

Figure 5 - Scheme of IF assembly – IF assembly occurs in four stages. It starts with the formation of a parallel dimer with two GFAP molecules, then these dimers form an antiparallel tetramer that interacts through the nonhelical tails domains forming unit length filaments (ULFs) with 20 nm in diameter. The final stage is the association of these units longitudinally to form filaments. Adapted from (Mierke, 2018)

2.2. *GFAP* mutations cause Alexander disease

Alexander Disease (AxD) was originally described by W. Stewart Alexander in 1947, as a case of mental retardation in an infant with hydrocephalus (Alexander, 1947). AxD was described as a rare, fatal and progressive neurodegenerative disorder in an infant that died at 16 months of age after severe developmental delays, regression in cognitive and motor skills, seizures and progressive macrocephaly and autosomal-dominant leukodystrophy (Alexander, 1949). In the histological examinations, large numbers of fuchsinophilic bodies were found in white matter and beneath both the ependyma and the pia, but sparing the

cortex. These bodies showed a characteristic perivascular predominance and were thought to be a product of fiber degeneration and cell bodies of the fibrillary neuroglia (Alexander, 1947).

AxD was later confirmed to be a rare disease with an incidence of approximately 1:2.7 million. However, the incidence is probably much higher, as it is frequently misdiagnosed due to the symptoms that are also common to other disorders and often difficult to identify without previous clinical experience with this disorder (Quinlan, Brenner, Goldman, & Messing, 2007). Ninety-five per cent of the cases show mutations in the *GFAP* gene, while the causes of the other 5% are not known (A. Messing, Brenner, Feany, Nedergaard, & Goldman, 2012b; Yoshida et al., 2011). AxD can be divided in three types: Infantile (0-2 years), Juvenile (2-12 years) and Adult (more than 12 years). Lifespan is generally related with the age of onset, early onset having a life expectancy of 14 years after onset and late onset having a survival expectancy of 25 years after onset (Prust et al., 2011; Russo, Aron, & Anderson, 1976).

The link between *GFAP* mutations and AxD was not discovered until 2001 (M Brenner et al., 2001). On this seminal article, the authors analyzed DNA samples from 11 patients diagnosed with Alexander Disease. When compared with 53 samples from control DNA samples and two non-Alexander disease leukodystrophy control DNAs, 10 of the DNA samples from AxD contained novel heterozygous mutations of *GFAP* predicting non-conservative amino acid changes, all involving arginines.

AxD-related *GFAP* mutations are heterozygous, being 90% of them a single amino acid change, although a few insertions and deletions have been also found (R. Li et al., 2005). Almost all the AxD cases are due to *GFAP* mutations that arise spontaneously, the parents not being carriers (R. Li et al., 2005). Mutations at residues R79 and R239 are the most frequent and correspond to 20% of all reported cases of AxD (R. Li, Messing, Goldman, & Brenner, 2002). AxD-related *GFAP* mutations act in

a gain-of-toxic-function manner, as *GFAP*-null mice display a phenotype that does not resemble AxD, while GFAP-overexpressing mice develop histopathological features of AxD (Gomi et al., 1995; McCall et al., 1996; Pekny et al., 1995).

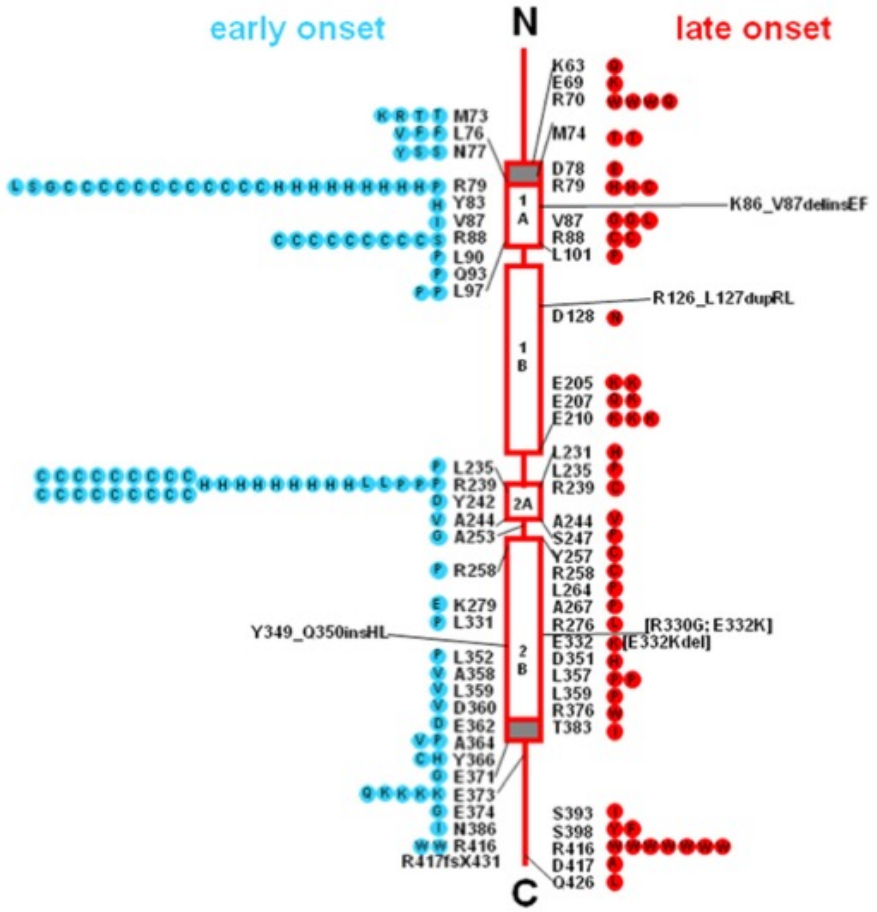

Figure 6 - Distribution of Alexander Disease Mutations - On the left we can observe early onset mutation, shown as blue circles and on the right late onset cases, shown as red circles. Mutations on aminoacids R79 and R239 account for approximately 20% of all AxD cases. Adapted from (A. Messing, Brenner, Feany, Nedergaard, & Goldman, 2012a).

Although there is a clear genetic link between *GFAP* mutations and AxD, the phenotypic variability between affected individuals suggests that genetic modifiers and environmental factors also play a role in the development of the disease. It is possible to find individuals carrying the same mutation displaying differences in the severity of the disease, individuals with disease-causing mutations who do not display symptoms and, in rare cases, individuals with all the pathological hallmarks of AxD but without *GFAP* mutations (Johnson, 2002).

Mutations in *GFAP* increase the protein levels beyond a toxic threshold which leads to the formation of eosinophilic protein inclusions referred as Rosenthal fibers (RFs). RFs are known to be constituted mainly by GFAP, vimentin, alpha-b-crystallin and the small heat shock protein (hsp27) (Ming Der Perng et al., 2006; Tomokane, Iwaki, Tateishi, Iwaki, & Goldman, 1991). RFs are a characteristic of AxD, although they can also be found in glial scars or pilocytic astrocytomas (Louis et al., 2016; Sun et al., 2008). However, the number and distribution of RFs are higher in AxD than the other pathologies (Johnson, 2002; Sosunov, Olabarria, & Goldman, 2018). Overexpression of wild type GFAP also leads to the formation of RFs that are indistinguishable to the ones present in AxD (a Messing et al., 1998). Lithium has been previously described to decrease GFAP aggregates in a model of AxD, by increasing the autophagy pathway for protein degradation and decreasing activation of *STAT3* which, as we described above, is a key regulator of GFAP transcription and astrogliogenesis (Daniels et al., 2015).

3. **Methods for the study of protein-protein interactions**

The human genome encodes for approximately 20000 genes, but the final diversity of proteins is much larger. Alternative splicing of messenger RNAs multiply gene products by 5, and post-translational modifications

increase even further the possible total number of proteoforms (Aebersold et al., 2019). Protein-protein interactions (PPIs) represent the final level of diversification at a cellular level, as the different proteoforms can associate with other proteins and biomolecules in multiple combinations. This increasing diversity of molecular mechanisms enables the versatility and adaptability that characterizes the interaction between living cells and their environment.

PPIs are indeed essential for signal transduction, metabolism, and maintenance of cell architecture, among many other fundamental phenomena (Nooren & Thornton, 2003; Wetie et al., 2013). In order to study PPIs in complex biological contexts, different approaches have been developed, such as co-immunoprecipitation (followed by immunoblotting, mass spectrometry, crystallography, or other protein identification methods), fluorescence resonance energy transfer (FRET), bioluminescence resonance energy transfer (BRET), and protein complementation assays (PCAs), among others (Braun et al., 2009; Coriano, Powell, & Xu, 2016; Kenworthy, 2001; J.-S. Lin & Lai, 2017; Pfleger & Eidne, 2005).

3.1. Co-immunoprecipitation

Co-immunoprecipitation allows to purify protein complexes in native conditions by means of specific antigen-antibody reactions, which can include post-translationally-modified proteoforms. This technique allows incomparable analytical power, as once proteins and complexes are purified, they can be analyzed by mass spectrometry, crystallographic studies or nuclear magnetic resonance (NMR), among others. On the other hand, it requires the lysis of cells, killing them and strongly limiting the type of dynamic studies that can be carried out. It also comprises a series of protein purification steps that can lead to loss of a great number

of PPIs, depending on the binding and elution conditions. Its sensitivity is variable and difficult to determine, often making it difficult to identify low-abundance and transient PPIs. Finally, its usefulness for quantification is limited, and depends on both the efficiency of immunoprecipitation procedures and the type of protein identification method used afterwards (Struk et al., 2019).

Microscopy-based methods to study PPIs have lower analytical power, but enable the monitorization of the interactions in living cells and provide higher spatial and temporal resolution.

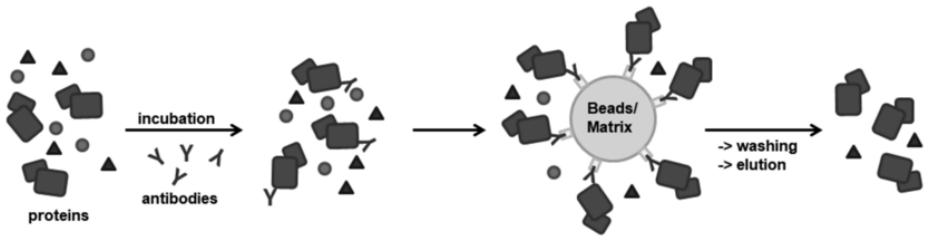

Figure 7 - Co-immunoprecipitation (Co-IP) - Proteins are incubated with specific antibodies against one of the proteins of interest and then captured by beads or a matrix. Adapted from (Schiedel et al., 2018).

3.2. Fluorescence Resonance Energy Transfer (FRET)/ Bioluminescence Resonance Energy Transfer (BRET)

FRET is based on the fusion of two different fluorophores to the proteins of interest that could interact (Kretzschmar, Dinger, Henze, Brocke-Heidrich, & Horn, 2004). These fluorophores are usually variants of the *green fluorescent protein* (*GFP*) and must have overlapping emission/excitation spectra for FRET to occur. Very briefly, when the donor fluorophore is excited with the corresponding wavelength, it transfers energy to the acceptor fluorophore, but only if it is close enough (<10 nm) and properly oriented (Kerppola, 2008b) (Leavesley & Rich,

2016). The acceptor fluorophore is then excited and emit its own fluorescence. Emitted fluorescence intensity from the acceptor is correlated with the level of interaction of proteins (Truong & Ikura, 2001). If the acceptor is photobleached, the donor´s fluorescence also becomes more intense, since the quenching by the acceptor is removed. Other variants of FRET, such as Fluorescence Lifetime Imaging (FLIM) use the shorter lifespan of the photons of the donor when it is interacting with the acceptor as a reporter of protein-protein interactions.

BRET shares some common characteristics with FRET. This approach is also based on the fusion of an energy donor (luciferase) and an energy acceptor, typically a fluorescent protein. For the energy transfer to happen, the emission spectrum of the donor must overlap with the excitation spectrum of the acceptor (P. Wu & Brand, 1994). Like in FRET, if the fusion proteins interact with each other in a distance lesser than 10nm, a resonance energy transfer occurs and an additional light signal is detected (Boute, Jockers, & Issad, 2002; Pfleger & Eidne, 2006). The main advantages of BRET versus FRET are the absence of an external light source to excite the energy donor, avoiding the possibility of cell autofluorescence and photobleaching of donor and acceptor; and a 10-fold higher sensitivity (Arai et al., 2001). However, BRET shares the main FRET disadvantages, like the reversibility of the complex, the need for very skilled researcher to use it and analyze data, or the difficulties to apply it to high-throughput setups which could be partially overcome by other methods.

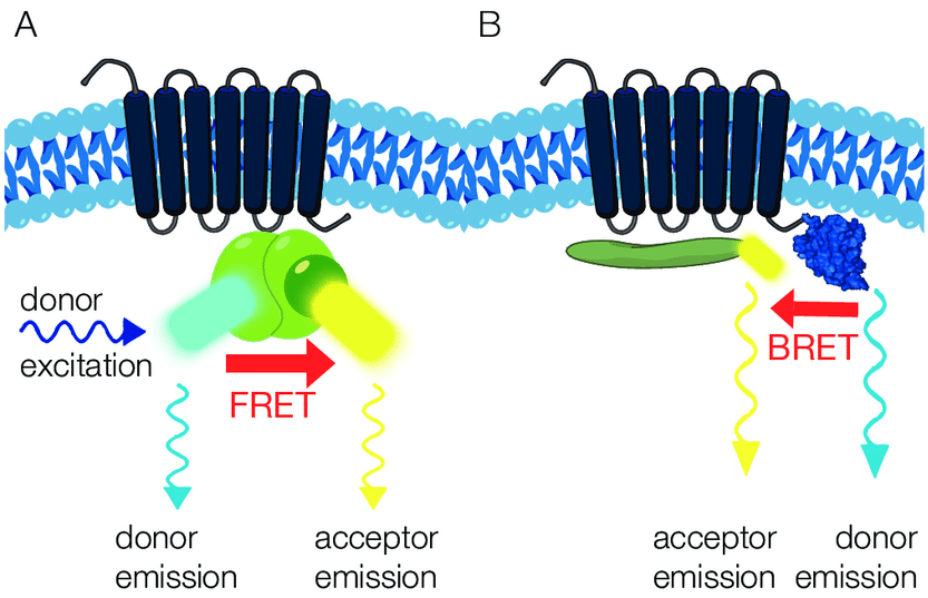

Figure 8 - FRET and BRET - A, FRET depends on the fusion of two different fluorophores (donor and acceptor) to the PI. When the donor is excited with the respective wavelength will transmit energy to the acceptor that will emit fluorescence. B, BRET share the same characteristics that FRET with the exception that there is no need of external light to the excitation of the donor fluorophore. Adapted from (Maria Goreti usboko, 2018).

3.3. Fluoppi and Dimerization-dependent fluorescent proteins

Some FRET/BRET disadvantages could be overcome by assays based on fluorescent protein-protein interaction visualization (Fluoppi) systems (Titeca, Lemmens, Tavernier, & Eyckerman, 2019). This system is based on the fusion of two tags, a Phox and Bem1p tag (PB1-tag) and a tetrameric *Azami-Green fluorescent protein* tag (AG-tag) to the proteins of interest. The interaction of these proteins leads to the formation of condensed phase-separated droplets (Watanabe et al., 2017). In the homoFluoppi variant both tags are fused together creating a construct of PB1 and mAG1 together with the protein of interest (Watanabe et al.,

2017). Comparing with FRET/BRET, this homofluoppi system allows the visualization of transient interactions due to the irreversibility of the binding. However, fluorescence is not necessarily proportional to the interaction of proteins, existing fluorescence signal even in the absence of interaction (Okada et al., 2018). Fluorescence just reorganizes in droplets, not changing the intensity, therefore restricting the detection of changes in protein dimerization to microscopy approaches that enable direct visualization of droplets.

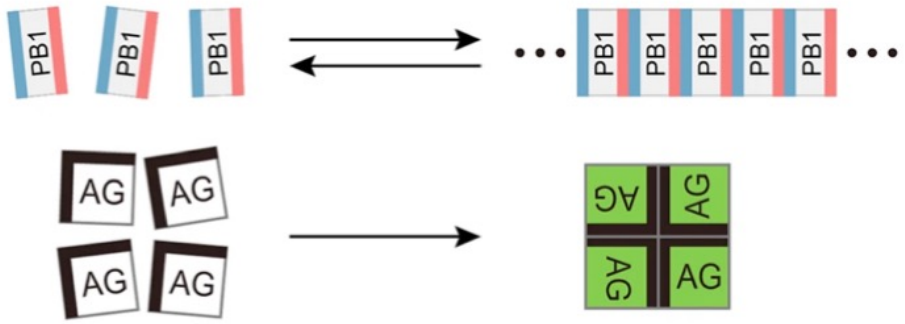

Figure 9 - Fluoppi system - Oligomerization of the p62 PB1 domain (top) and the fluorescent protein Azami-Green (bottom). Interaction of these proteins leads to the formation of condensed phase-separated droplets. On the homofluoppi system, both proteins are fused to the PI leading to the visualization of the interaction of the Proteins of Interest. Adapted from (Watanabe et al., 2017).

PPIs can also be analyzed by means of Dimerization-dependent fluorescent protein (ddFPs) systems (Alford, Ding, Simmen, & Campbell, 2012). ddFPs are composed of two tags fused to the proteins of interest and emit fluorescence at an intensity proportional to their interaction, just like FRET or BRET. However, in this case the tags are full-length *GFP* versions that have been engineered to produce fluorescence only when they form a dimer. Thus, when the proteins of interest do not interact, the

GFP versions remain as monomers, and their fluorescence is dim. When the proteins of interest interact, both ddFPs also dimerize and emit bright fluorescence. This system has a simpler setup than FRET, because it involves a single fluorophore, and is reversible like FRET, allowing to study both transient and stable protein-protein interactions. However, this reversibility can be a disadvantage to study very fast and/or low-abundance transient interactions (Alford et al., 2012).

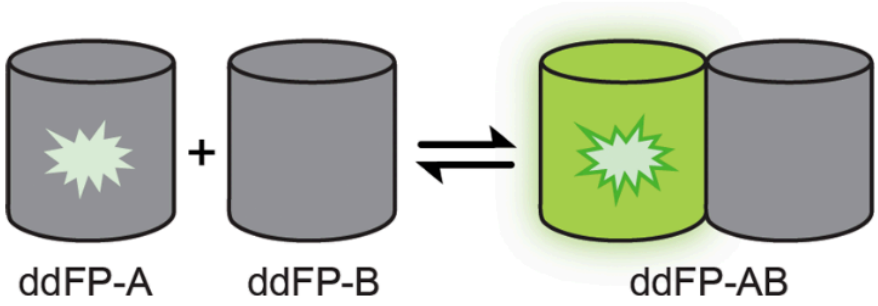

Figure 10 - ddFP technology – weak or non-fluorescent fluorophores emit fluorescence once they interact. Adapted from (Alford et al., 2012)

Finally, a different set of methods to visualize PPIs is based on a particular property of proteins known as protein complementation.

3.4. Protein Complementation Assays (PCAs)

Protein complementation (or transcomplementation) is a property of proteins discovered in 1958 by Richards. He digested a ribonuclease into several fragments that lost the original activity, but the activity was recovered when they were incubated back together. This property has aroused the interest of many researchers since then, and identified in virtually any protein where it has been tested. PCAs have been developed based on a plethora of proteins with technological value, such as beta-

galactosidase, ubiquitin, dihydrofolate reductase (DHFR), thymidine kinase, β-lactamase, TEV protease, the GFP family, and *luciferase*, among others (Galarneau, Primeau, Trudeau, & Michnick, 2002; Hu & Kerppola, 2003; Pelletier, Campbell-Valois, & Michnick, 1998; Villalobos, Naik, & Piwnica-Worms, 2007; Wehr, Reinecke, Botvinnik, & Rossner, 2008).

In 1994, a PCA was described to detect PPIs based on complementary ubiquitin fragments. Split-ubiquitin fragments were fused to interacting protein pairs, and they recovered the normal function of recruiting ubiquitination machinery when the proteins interacted. The authors fused the split-fragments to a *dihydrofolate reductase* with an ha epitope tag (Dha) reporter and to the leucine zipper homodimerization domain of the yeast Gcn4 protein (Johnsson & Varshavsky, 1994). Soon later, a PCA was reported using split fragments of beta-galactosidase fused to the *FKBP*-rapamycin-associated protein (FRAP) and the *FK506-binding protein* (*FKPB12*). These two proteins are described to interact in the presence of rapamycin, and beta-galactosidase recovered its function upon their interaction (Rossi, Charlton, & Blau, 1997). Since then, a wide variety of PCAs have been described (Kerppola, 2008a).

In PCAs, the recovery of the functional protein needs the close proximity or direct interaction of the two split fragments. The assembly of the full reporter protein is dependent on an increase in the interactions between the reporter fragments (due to PPI between the proteins of interest), the thermodynamic stability of the macromolecular complex and the concentration of the split-fragments in a confined space (Gegg, Bowers, & Matthews, 1997; Hu, Chinenov, & Kerppola, 2002; Kerppola, 2010; Robida, A. and Kerppola, 2009). Ideally, the inactive fragments should not produce signal in the absence of PPIs between the proteins of interest. However, very often the fragments have high affinity for each

other and engage into spontaneous binding, resulting in unspecific background signals (Michnick, 2003; Walter et al., 2004).

Like in other methods to study PPIs, in PCAs the fusion protein is expressed in a relevant intracellular context allowing the study of native PPIs, their dynamics and modifications in living cells (Remy & Michnick, 2007). PCA´s design frequently enables their use in most laboratories, as users only need very common laboratory equipment, and they can choose among a great variety of existing reporters suitable for each particular protein and biological context (McLachlan, Katzenellenbogen, & Zhao, 2011; Schlecht, Miranda, Suresh, Davis, & St Onge, 2012; L. Yue et al., 2017). A potentially limiting step can be the flexibility of the reporter fragments to associate. To overcome this issue, a flexible glutamine/serine (G/S)-rich linker can be introduced between the split-fragments and the proteins of interest (X. Chen, Zaro, & Shen, 2013). Some studies indicate that adding linkers in PCAs can improve the detection of the interactions between the proteins of interest (Chrétien et al., 2018).

In the particular case when the PCA is based on splitting fluorescent proteins, it is called bimolecular fluorescence complementation (BiFC) assay.

3.4.1. Bimolecular fluorescence complementation (BiFC) assays for the study of protein-protein interactions

The first attempt to apply protein complementation to the fluorescent protein *GFP* was for the study of PPIs in *Escherichia Coli*. The authors wanted to prove that *GFP* could be split in two non-fluorescent fragments that could reconstitute the fluorophore upon interaction. Complementary *GFP* fragments were fused to Leucine Zippers. The leucine zippers were previously described to interact forming non-covalent

ligations that lead the *GFP* fragments close to each other and reconstitute the fluorescence (Ghosh, Hamilton, Regan, V, & V, 2000). Two years later, it was applied for the same purpose in mammalian cells, where it was named BiFC assay (Fig. 11). In this case the authors used the *yellow fluorescent protein*, *YFP*, divided in two fragments and fused to two transcription factors, *bZIP* and *Rel* (Hu et al., 2002). This BiFC system enabled the monitorization of *bZIP/Rel* dimers at a subcellular level and the relationship between nuclear translocation and transcriptional activity of this complex. BiFC is currently widely used for direct visualization of protein interactions in living cells from all kingdoms, providing a powerful tool for genetic or pharmacological screenings (Gonçalves, Matos, & Outeiro, 2010; Herrera, Gonçalves, & Outeiro, 2012a; Morell, Espargaro, Aviles, & Ventura, 2008). This method allowed, for example, to visualize simultaneously dimers/oligomers and larger aggregates in living cells, thus enabling the study of the mechanisms of pathological aggregation in neurodegenerative disorders such as Parkinson´s, Alzheimer´s or Huntington´s diseases (Herrera & Fleming, 2011).

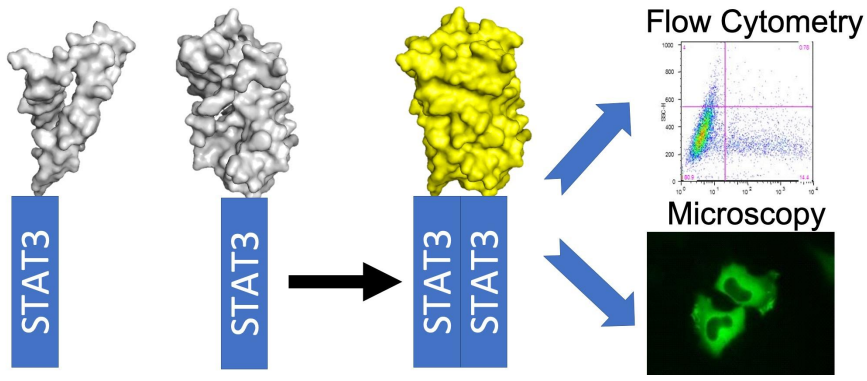

Figure 11 - Bimolecular fluorescence complementation (BiFC) assays for the visualization of protein-protein interactions in living cells - The proteins of interest are fused to two non-fluorescent fragments of a reporter protein. We used *Venus*, a third-generation yellow fluorescent protein that has been optimized for this type of assay. When the proteins of interest dimerize/oligomerize, the two *Venus* halves get together and reconstitute the functional fluorophore. Fluorescence can be measured by conventional

methods, such as flow cytometry, microscopy or fluorimetry, and is proportional to the number of dimers.

Until now, 15 fluorescent proteins have been used for complementation assays, all of them with distinct spectral and physical-chemical properties (Kodama & Hu, 2012). This also allowed to visualize several PPIs simultaneously, by means of a multicolor analysis using spectral variants from GFP. However, some variants do not fold back easily at 37 ºC or display poor brightness, creating difficulties for the study of PPIs in physiological conditions in mammals (Grinberg, Hu, & Kerppola, 2004; Hynes, Yost, Mervine, & Berlot, 2008; Kodama & Wada, 2009; Vidi, Chemel, Hu, & Watts, 2008; Waadt et al., 2008). The most common pair of reporters for multicolor BiFC is Venus/Cerulean (Yellow/Cyan), two third-generation fluorescent proteins (Miller et al., 2016).

Venus is also the most common fluorophore for single-color BiFC, as it is much brighter than other fluorescent proteins and has intrinsically improved folding efficiency at 37ºC, while most split fluorescent proteins need a preincubation at 30ºC (Herrera, Gonçalves, & Outeiro, 2012b). It also enables the use of weaker promoters to approximate the expression of the interactors to physiological levels. Some disadvantages of Venus-based BiFC systems include higher background and lower signal-to-noise ratios than the original proteins (GFP, YFP, EGFP, and EYFP) and saturated signals (Herrera et al., 2012b; Shyu, Liu, Deng, & Hu, 2006). In order to overcome these disadvantages, alternative split Venus halves have been intensively investigated, and some mutations and different split fragments have been found to reduce background and increase signal-to-noise ratio. For example, a Venus N-terminal part VN154 fragment carrying the T153M mutation was used to study protein interactions in *Xenopus* embryos (Saka, Hagemann, & Smith, 2008). A BiFC system for the study of c-Fos and c-Jun interaction used a VN155 and VC155 halves

with 3 different point mutations V150A, L201V, and L207V (Nakagawa, Inahata, Nishimura, & Sugimoto, 2011). Finally, splitting Venus at amino acid 210, instead of the most common 158 and 172 Aa split versions, leads to a striking decrease in background fluorescence and a significant increase in the signal-to-noise ratio (Gookin & Assmann, 2014; Ohashi, Kiuchi, Shoji, Sampei, & Mizuno, 2012). An additional recent measure to prevent background is the development of a tripartite split system, with two halves (20 amino acids long) attached to the proteins of interest and a third fragment free, interacting with the other split fragments once the proteins of interest interact (Cabantous et al., 2013).

More recently, a BiFC system based on the MiniSOG tag has been described (Boassa et al., 2019). MiniSOG stands for mini Singlet Oxygen Generator, and is a tag produced from the LOV (light, oxygen and voltage) 2 domain of a plant protein with less than half of the size of GFP. Its ability to generate singlet oxygen in response to light makes of MiniSOG a very versatile tag, enabling selective killing of target cells by oxidative stress or the detection of proteins of interest by Electron Microscopy (EM) (Shu, Lev-ram, et al., 2011). This is possible because singlet oxygen catalyzes the polymerization of diaminobenzidine into an osmiophilic reaction product visible by EM. However, MiniSOG is also a fluorescent flavoprotein that allows visualization by fluorescence microscopy, enabling correlated light and electron microscopy (CLEM) among other applications (Shu, Lev-Ram, et al., 2011). Therefore, MiniSOG BiFC systems could allow the visualization of PPIs by both fluorescent and electron microscopy, as was recently demonstrated (Boassa et al., 2019). The current system is based on a split version of MiniSOG with an N-terminus of 94 amino acids and a C-terminus of 46 amino acids, mSOG1-94 and mSOG-95-140, respectively. As a proof-of-concept, these fragments were successfully fused to the basic region-leucine zipper

domains of bFOS and bJun, two subunits of the AP-1 transcriptional complex.

4. **Aims**

The STAT3 pathway plays key roles in human health and disease, including CNS disorders involving astroglia. STAT3 dimerization and post-translational modifications are two rate-limiting events for both canonical and non-canonical functions. *GFAP* is a glial gene relevant to CNS disorders regulated by STAT3. The overall aim of the present work is the development of new tools for the analysis of the STAT3/*GFAP* signaling axis in living cells. We have focused specifically on the development of molecular tools that enable the visualization of STAT3 homo- and heterodimers and GFAP molecules in living cells. These tools could contribute to our understanding of the role of PTMs and disease-related mutations on the behavior and function of STAT3 and GFAP.

Chapter 2

Materials + Methods

1. **Reagents**

Restriction and Ligation enzymes were purchased from Thermo Scientific (Waltham, MA, USA). Alkaline Phosphatase, NZY5α Competent Cells and PCR/Gel DNA purification kits were acquired from NZYTech, (Lisbon, Portugal). Phusion DNA Polymerase were obtained from Thermo Scientific (Waltham, MA, USA) and PfuTurbo DNA polymerase from Agilent (Santa Clara, California, USA). ZR Plasmid Miniprep and ZR Plasmid Midiprep were purchased from Zymo Research (Irvine, California, USA). PCR primer synthesis and DNA sequencing were performed by Eurofins Genomic (Ebersberd, Germany) and StabVida (Caparica, Portugal). EZ-Tn5 in frame insertion Kit was acquired from Epicentre (Madison, Wisconsin, USA).

Cell culture media (Dulbecco's Modified Eagle Medium - DMEM - and Leibovitz's L-15 medium), Fetal Bovine Serum (FBS), penicillin-streptomycin commercial antibiotic mixture (Pen-Strep) (10,000 units/mL of penicillin and 10,000 µg/mL of streptomycin), L-glutamine (200mM), TrypLE Express dissociation reagent, Ca^{2+} - and Mg^{2+} -free phosphate buffer saline (PBS) 1X and Leukemia inhibitory factor (LIF) were obtained from Gibco (Thermo Scientific, Waltham, MA, USA). DAPI and Bradford were acquired from PanReac Appli-Chem (Barcelona, Spain). Stattic was purchased from Selleckchem (TX, USA). *STAT3* CRISPR Knockout/Cas9 plasmid pool was purchased from Santa Cruz Biotechnology (Dallas, Texas, USA). The LDH assay kit was purchased from Takara/Clontech (Tokyo, Japan). 3-4,(5-dimethylthiazol-2-yl)-2,5-diphenyltetrazolium bromide (MTT) was purchased from Calbiochem (San Diego, USA). The NE-PER™ Nuclear and Cytoplasm Extraction and ATP Determination (A22066) kits were purchased from Thermo Fisher Scientific (Waltham, MA USA). Chemiluminescent HRP substrate was purchased from Bio-Rad Laboratories (Hercules, CA, USA). CNB-001 and J147 drugs were a

kind gift from Dr. David Schubert (The Salk Institute for Biological Studies, La Jolla, CA, United States). Human glioblastoma U251 cells were obtained from Public Health England (reference 09063001, Salisbury, UK). HEK293 human embryonic kidney cells were obtained from ATCC (reference CRL-1573). HeLa human cervix adenocarcinoma cells (reference CRM-CLL-2) were a kind gift. The p53 – VC and Mdm2 – VC plasmids were a kind gift from Cecilia Rodrigues and Joana Amaral (University of Lisbon, Portugal) (Dias et al., 2013), and the VN-*STAT3* and VC-*STAT3* plasmids were synthetized by GeneArt services (Thermo Scientific, Waltham, MA, USA)(See maps in section 3.1 below).

2. General Cloning Procedures

2.1. DNA Purification

PCR products (digested or not) and digested vectors were run in agarose gels (1% in Tris-acetate-EDTA 1X) for 45 minutes to confirm their size and/or the digestion efficiency. Selected bands were purified from gels by means of the NZYGelpure kit, following manufacturer´s instructions. First, agarose was melted at 60ºC for 10 minutes in 300 µl of Binding Buffer per 100 mg of Agarose. Second, melted agarose was added to a column and centrifuged at 13000xg for 1 min at RT. Third, columns were washed with an ethanol-based washing buffer. Finally, DNA was eluted with 30 µl of MiliQ water and quantified by means of a Nanodrop 2000c (Thermo Fisher Scientific Inc., West Palm Beach, United States).

2.2. Ligation

Once vector and insert were digested and purified, they were ligated using T4 DNA ligase for 2 hours at room temperature. Four different molar proportions of vector:insert amounts were used to increase chances of a successful ligation: 1:0 (no insert), 1:3, 1:6 and 1:9. The 1:0 ligation was used as a control for non-specific vector religation. Ligations always contained 100 ng of vector and the amounts of insert were calculated according to the relative size between inserts and vectors.

2.3. Bacterial Transformation and growth

In order to amplify plasmids or select clones, thermocompetent *E. coli* bacteria were transformed with ligation reactions, site-directed mutagenesis products or full constructs. For conventional ligation reactions 10µl of the reaction were used, and 5µl for Site-Directed Mutagenesis. The reactions were mixed with competent bacteria and incubated on ice for 30 minutes. Bacteria were heat-shocked at 42ºC for 45 seconds and placed on ice for 2 minutes. Three-hundred µl of liquid Luria Broth (LB) medium [1% w/v Tryptone; 0.5% w/v Yeast extract; 171 mM NaCl] without antibiotics were added, and bacteria were incubated with agitation (150 rpm) at 37ºC for 1 hour. Bacteria suspensions were seeded on LB Agar 1X petri dishes containing the corresponding antibiotics to select transformant clones and incubated at 37ºC overnight. The antibiotics employed were ampicillin (100 µg/ml, for all pcDNA 3.1 constructs), kanamycin (50 µg/ml, for the GFP-mGFAP construct) or a mixture of both (for transposon strategies).

In some cases, such as ligation reactions or mini/midipreps, transformant clones were later grown in liquid LB medium containing the corresponding antibiotic at 37ºC and in agitation (150 rpm) overnight.

After that we need to extract and ligate and in order to do that the bacterial cultures containing the constructs, were pulled down by centrifugation, after reaching 600 nm of absorvance, at maximum speed for 20 sec at room temperature (RT), resuspended, and lysed by means of the ZR Plasmid Miniprep kit (Zymo Research, Irvine, California, USA), following manufacturer´s instructions. After gentle centrifugation (14000xg 2 min at RT) to remove cell debris, clean supernatants were applied to DNA purification columns. The columns were washed, and the DNA was eluted in 30 µl of MiliQ H_2O and quantified by means of a Nanodrop 2000c (Thermo Fisher Scientific Inc., West Palm Beach, United States).

2.4. Confirmation of clones by restriction reaction and sequencing

For conventional restriction digestion, clone confirmation was carried out by digesting 1-3 µg of DNA with the same restriction enzymes used for cloning. Digestion reactions were run in a Tris-Acetate-EDTA (TAE 1X) Agarose gel (1% w/v) for 40 minutes at 80 volts. The clones showing a DNA fragment at the right size were sequenced for further confirmation (GATC, Cologne, Germany). Site-Directed Mutagenesis confirmation was only done by sequencing. Sequencing results were analyzed by means of the A Plasmid Editor (Ape) freeware (http://biologylabs.utah.edu/jorgensen/wayned/ape/). Positive clones were stored at -80ºC as glycerol or Dimethyl Sulfoxide (DMSO) stocks. Glycerol stocks were done by adding 500 µl of glycerol to 500 µl of bacteria suspension in LB liquid medium and DMSO stocks were done by adding 35 µl of DMSO to 500 µl of bacteria suspension in LB liquid medium.

3. **Templates**

3.1. Venus - STAT3 BiFC system

VN- and VC-STAT3 BiFC constructs synthetized by GeneArt services (Fig. 12) were used as templates to produce various PTM and structural mutants by Site-Directed Mutagenesis. These constructs have the pcDNA 3.1 mammalian expression plasmid as a backbone, where the expression of Venus-STAT3 fusion proteins is under the control of a cytomegalovirus promoter (pCMV), which allows high levels of constitutive expression in mammalian cells. After the insert, the vector has a bovine growth hormone polyA tail for mammalian expression. Constructs have ampicillin and neomycin resistance sequences for selection in bacteria and mammalian cells, respectively. The VN Venus fragment is from amino acid 1 to 158 and the VC Venus fragment from amino acid 158 to 238, in both cases without a linker between them and the STAT3 sequence. Single cut restriction enzymes are represented in figure 11.

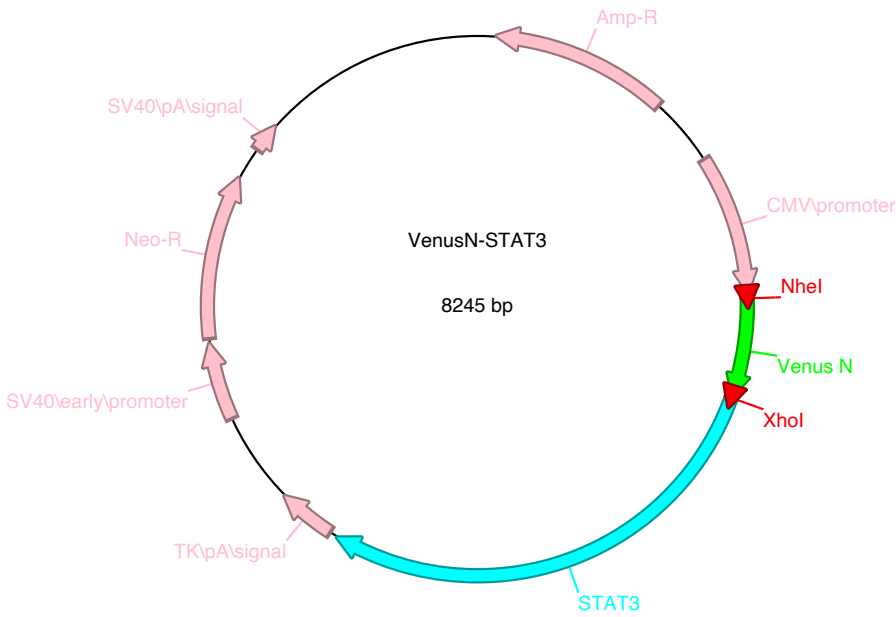

Figure 12 – Venus - STAT3 BiFC plasmid map- Template of Venus N (VN)– *STAT3* plasmid from the *STAT3* BiFC system. The Venus C (VC)- STAT3 plasmid has the same features, with the only difference of the Venus fragment.

3.2. Human GFAP plasmid

The template carrying the sequence of the wild type human GFAP alpha gene used for the transposition reaction was a kind gift from Professor Brenner (University of Alabama at Birmingham, USA) (Fig. 13). Similar to STAT3 plasmids, the backbone of this construct is the pcDNA 3.1+ plasmid, where the expression of fusion proteins was under the control of a pCMV. This promoter allows high levels of constitutive expression in mammalian cells. After the insert, the vector has a bovine growth hormone polyA tail for mammalian expression. Constructs have ampicillin and neomycin resistance sequences for selection in bacteria and mammalian cells, respectively.

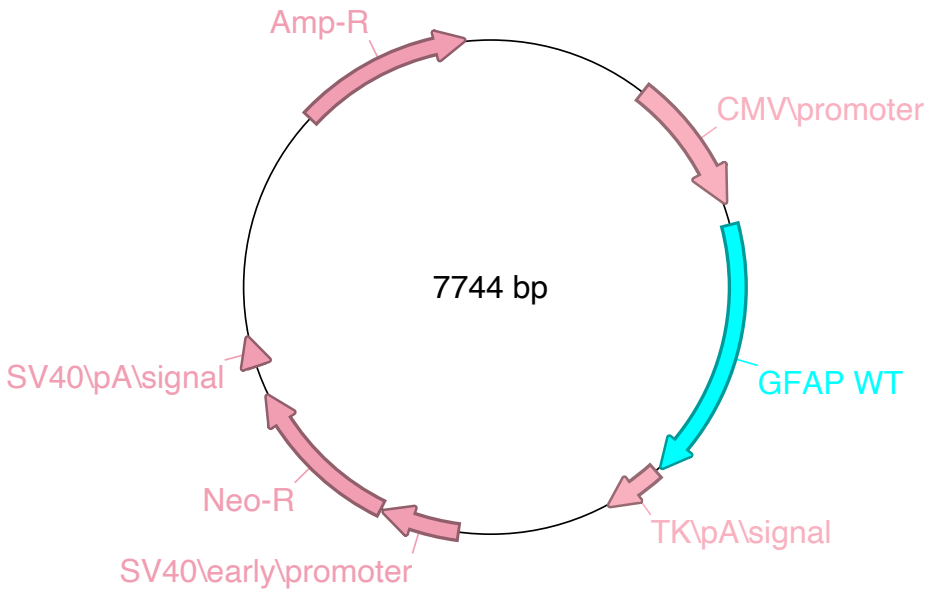

Figure 13 - Human GFAP plasmid map.

4. Transposase Reaction

A human-GFAP-EGFP construct was originated by transposase reaction of EGFP into a wild type human GFAP construct (Fig. 12) (see section 3.2). The protocol followed was the one provided by the EZ-Tn5 in frame insertion Kit. Briefly, the transposon insertion mixture was prepared by adding 1 µl of EZ-Tn5 Transposase to 0.2 µg of the pcDNA3.1-hGFAP plasmid and a molar equivalent of the EGFP Transposon kindly provided by Dr. Mika Ruonala (Fig. 14). The mixture was incubated for 2h at 37ºC and the reaction was stopped by adding 1µl of EZ-Tn5 Stop solution and incubating the reaction for 10 min at 70ºC. One µl of the reaction was transformed into bacteria (Section 2.3 above). The EGFP Transposon sequence contains a resistance to Kanamycin to select the clones with the insertion of the Transposon. However, it will be later removed by digestion with SrfI and religation. If the transposon lands

in an open reading frame and is in frame with the coding sequence, an EGFP- tagged protein will be produced.

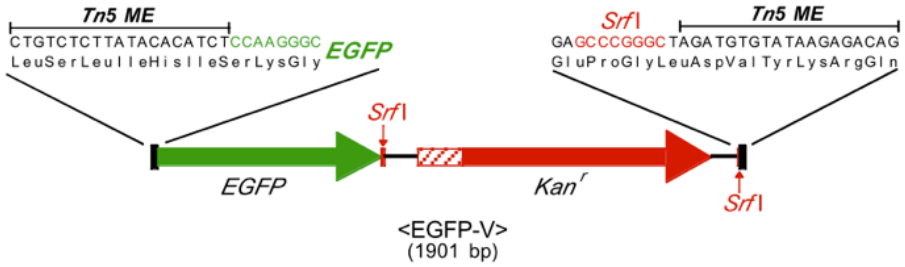

Figure 14 - EGFP transposon- The EGFP transposon has a region of 19 bp in both termini called Tn5 mosaic ends (MEs) that enables transposition. The transposon carries a Kanamycin resistance (Kan^r) sequence and a stop codon in the 5' end of the Kan^r cassette. The Kan^r is necessary to identify the colonies that have incorporated the transposon in the construct, but can be removed later by Srf1 digestion. Adapted from (Sheridan et al., 2002)

Insertion of the transposon inside of the GFAP sequence was confirmed by PCR. PCR was carried out using 20 ng of template DNA, 0.2 µM of primers (FWD 5' GCCGCTCGAGGAGAGGAGACGCATCACCTC 3' and REV 5' GCCGCTCGAGTCACATCCTTGTGCTCCTGC 3') and 250 µM of dNTPs in a total volume of 50 µl containing 2.5 units of Phusion DNA polymerase and the corresponding amplification buffer. The following thermocycling conditions were used: initial denaturation at 98ºC of 30s followed by 35 cycles of denaturation at 98ºC for 10s; annealing at 60ºC for 30 sec; and extension at 72ºC for 2 min. Clones containing the insertion were purified as described in Section 6.1 and digested with *Srf*I for 2 hours at 37ºC for the removal of the sequence code for Kanamycin resistance.

In order to confirm in-frame insertion of EGFP, mammalian cells were transfected with the candidate constructs and tested for the presence of fluorescent signal by Flow Cytometry (Section 9). Confirmation of the insertion position was made by sequencing.

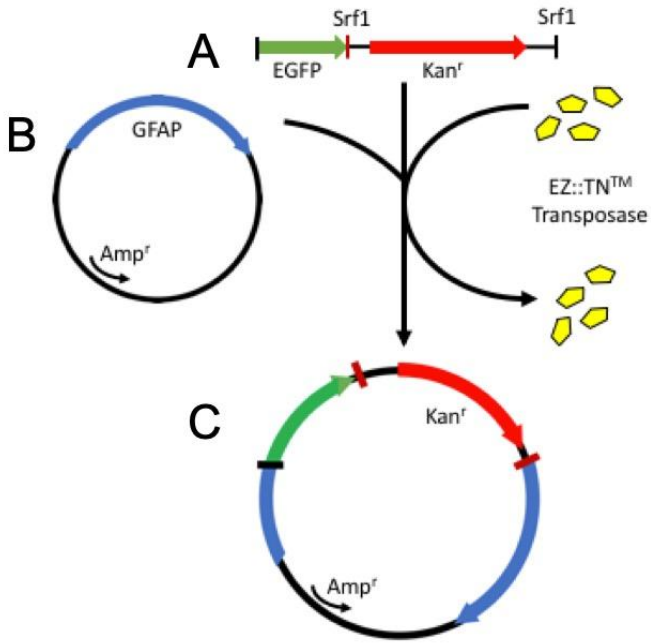

Figure 15 - Transposition reaction with EGFP – A, a transposon (1902 bp) containing the coding region for EGFP and Kan resistance (Kan^r), with restriction sites for Srf1 digestion to remove the Kanr. B, Target plasmid, pcDNA3.1/Amp with a coding region for the intermediate filament GFAP. C, Transposed plasmids carried both Amp^r (from the pcDNA) and Kan^r (from the transposon), allowing us to select specific colonies containing the insertion of the transposon.

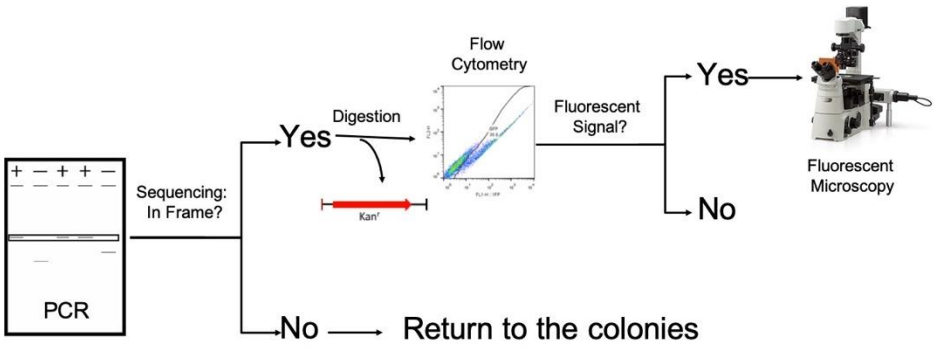

Figure 16 - Workflow of the colony screening - After the transposase reaction, bacteria were transformed with the reaction and grown in plates containing Ampicillin and

Kanamycin to select the positive clones. DNA was extracted from grown colonies, and a PCR with a Forward and Reverse primer for GFAP was done to reveal if the transposon is inside of our protein of interest. Bands with 3197 bp size contained GFAP (1296 bp) and the transposon (1902 bp). Positive colonies were digested with Srf1 and re-ligated to remove the coding region for Kan^r and the stop codon. Plasmids originated from the digestion were transfected into cells and tested for fluorescence by means of flow cytometry, and the ones presenting fluorescence were taken to fluorescent microscopy to see the pattern of GFAP distribution. The insertion site was confirmed by sequencing.

5. **Site-Directed Mutagenesis**

Single point mutations were inserted by site-directed mutagenesis into the VN-*STAT3* and VC-*STAT3* plasmids. The protocol followed was the one from QuikChange II Site-Directed Mutagenesis Kit. PCRs were carried out using 20 ng of template DNA, 0.2 µM of mutagenesis primers (Table I) and 250 µM of dNTPs in a total volume of 50 µl containing 2.5 units of Pfu turbo DNA polymerase (Agilent, Santa Clara, Califórnia, USA) and the corresponding amplification buffer. The following thermocycling conditions were used: denaturation at 95ºC followed by 12 cycles of 95ºC for 30s; annealing at 62ºC for 1 min; and extension at 68ºC for 8 min (1 min/kb, as specified by the manufacturer). In order to digest methylated parental plasmids, mutagenesis reactions were then incubated with *Dpn*I for 1 h at 37ºC. For the ligation, 5 µl from each reaction were used.

The Alexander disease-related R239C substitution was inserted by site-directed mutagenesis into the human-GFAP-EGFP plasmid. The protocol followed was the same for STAT3 mutants with the mutagenesis primers shown in Table I.

Table I - Primers for Site-Directed Mutagenesis

PTM Mutation	Primer Sequence (5' → 3')
Y45F	FWD CAAGATTGGGCATTTGCGGCCAGCAAAG
	REV CTTTGCTGGCCGCAAATGCCCAATCTTG
K49R	FWD CATATGCGGCCAGCAGAGAATCACATGCCAC
	REV GTGGCATGTGATTCTCTGCTGGCCGCATATG
Y68F	FWD GATTGACCAGCAGTTTAGCCGCTTCCTG
	REV CAGGAAGCGGCTAAACTGCTGGTCAATC
Y79F	FWV GAGTCGAATGTTCTCTTTCAGCACAATCTACG
	REV CGTAGATTGTGCTGAAAGAGAACATTCGACTC
K140R	FWD GTGGTGACGGAGAGACAGCAGATGCTG
	REV CAGCATCTGCTGTCTCTCCGTCACCAC
Y176F	FWD GGATGACTTTGATTTCAACTTCAAAACCCTCAAGAGTCAAGG
	REV CCTTGACTCTTGAGGGTTTTGAAGTTGAAATCAAAGTCATCC
S181A	FWD CTATAAAACCCTCAAGGCTCAAGGAGACATGCAAG
	REV CTTGCATGTCTCCTTGAGCCTTGAGGGTTTTATAG
C418S	FWD GAGGGAGCAGAGAAGTGGGAATGGGG
	REV CCCCATTCCCACTTCTCTGCTCCCTC
C426S	FWD GGCCGAGCCAATAGTGATGCTTCCC
	REV GGGAAGCATCACTATTGGCTCGGCC
Y539F	FWD GACCTGGTGTGAATTTTTCAGGGTGTCAGATC
	REV GATCTGACACCCTGAAAAATTCACACCAGGTC
Y640F	FWD GTCCGTGGAACCATTCACAAAGCAGCAG
	REV CTGCTGCTTTGTGAATGGTTCCACGGAC
K685R	FWD GAGGCATTCGGAAGGTATTGTCGGCC
	REV GGCCGACAATACCTTCCGAATGCCTC
S691A	FWD GTATTGTCGGCCAGAGGCCCAGGAGCATCCTGAAG
	REV CTTCAGGATGCTCCTGGGCCTCTGGCCGACAATAC
Y705F	FWD CAGGTAGCGCTGCCCCATTCCTGAAGACCAAGTTTATC
	REV GATAAACTTGGTCTTCAGGAATGGGGCAGCGCTACCTG
T708D	FWD CTGCCCCATACCTGAAGGACAAGTTTATCTGTGTG
	REV CACACAGATAAACTTGTCCTTCAGGTATGGGGCAG
S727A	FWD CATTGACCTGCCGATGGCACCCCGCACTTTAGATTC
	REV GAATCTAAAGTGCGGGGTGCCATCGGCAGGTCAATG

hGFAP-EGFP-R239C	FWD CTGAAAGAGATCTGCACGCAGTATG
	REV CATACTGCGTGCAGATCTCTTTCAG

6. Generation of STAT3 MiniSOG BiFC constructs

Nine different BiFC MiniSOG-STAT3 plasmids were generated by PCR amplification and restriction digestion, with STAT3 fused to nine different non-fluorescent fragments of the *MiniSOG* protein: MiniSOG 1, amino acids 1-138; MiniSOG 2, amino acids 1-183; MiniSOG 3, amino acids 1-216; MiniSOG 4, amino acids 1-276; MiniSOG 5, amino acids 1-192; MiniSOG 6, amino acids 138-321; MiniSOG 7, amino acids 183-321; *MiniSOG* 8, amino acids 216-321; MiniSOG 9, amino acids 276-321. Fusion proteins with MiniSOG fragments inserted in the N-terminus of STAT3 were cloned in a pcDNA 3.1 backbone. A full length STAT3-MiniSOG construct was synthesized to serve as a positive control.

6.1. Insert/Vector preparation

The *MiniSOG-STAT3* BiFC plasmids were made using two cloning steps. First, *MiniSOG* halves were inserted in the pcDNA 3.1 vector. The *MiniSOG* inserts were obtained by PCR using a previously synthesized full-length *MiniSOG* gene as a template. PCRs were carried out using 20 ng of template DNA, 0.2 μM of primers (Table II) and 250 μM of dNTPs in a total volume of 50 μl containing 2.5 units of Phusion DNA polymerase and the corresponding amplification buffer. The following thermocycling conditions were used: initial denaturation at 98ºC of 30s followed by 35 cycles of denaturation at 98ºC for 10s; annealing at 60ºC for 30 sec; and extension at 72ºC for 30 sec (30 s/kb, as specified by the manufacturer). PCR products were purified as described in Section 2.1 above.

Purified PCR products and the pcDNA 3.1 vector were digested with *BamH*I for 2 hours at 37 ºC, and the vector was further incubated with alkaline phosphatase for 1 hour at 37 ºC to prevent unspecific religation. Insert and vector were then purified (Section 2.1 above) and ligated (Section 2.2 above).

Table II - Primers for PCR amplification of MiniSOG halves

Construct	Primer Sequence (5' → 3')
Minisog 1	FWD ATTCGCGGATCCACCATGGAAAAAAGCTTTGTGATTACCGA
1-138 (bp)	REV ATTCGCGGATCCTTACGGGCCCTGCAGAAAGC
Minisog 2	FWD ATTCGCGGATCCACCATGGAAAAAAGCTTTGTGATTACCGA
1-183 (bp)	REV ATTCGCGGATCCTTAGCGAATCGCATCGCGAATTTT
Minisog 3	FWD ATTCGCGGATCCACCATGGAAAAAAGCTTTGTGATTACCGA
1-216 (bp)	REV ATTCGCGGATCCTTAGTTAATCAGCTGCACGGTAATTTCG
Minisog 4	FWD ATTCGCGGATCCACCATGGAAAAAAGCTTTGTGATTACCGA
1-276 (bp)	REV ATTCGCGGATCCTTACTGATCGCGCATCGGCT
Minisog 5	FWD ATTCGCGGATCCACCATGGAAAAAAGCTTTGTGATTACCGA
1-192 (bp)	REV ATTCGCGGATCCTTAGCGCTGATCGCGAATCGC
Minisog 6	FWD ATTCGCGGATCCACCATGGAAACCGATCAGGCGACCG
138-321 (bp)	REV ATTCGCGGATCCTTAGCCATCCAGCTGCACG
Minisog	FWD ATTCGCGGATCCGGACCAGCGGGAAATTACAGTCC
183-321 (bp)	REV ATTCGCGGATCCTTAGCCATCCAGCTGCACG
Minisog	FWD ATTCGCGGATCCTACACCAAGTCCGGCAAGAAGTT
216-321 (bp)	REV ATTCGCGGATCCTTAGCCATCCAGCTGCACG
Minisog	FWD ATTCGCGGATCCACCATGAAAGGCGAACTGCAGTATTTTATTGGC
276-321 (bp)	REV ATTCGCGGATCCTTAGCCATCCAGCTGCACG

The second step was made by sub cloning MiniSOG fragments into the pcDNA3.1 STAT3 destination vector, substituting the venus BiFC fragments. The MiniSOG fragments were obtained by digestion of the previously produced pcDNA3.1-MiniSOG fragment plasmids with *Nhe*I and *Xho*I for 2 hours at 37 ºC. The STAT3 destination vector was digested

in the same conditions and incubated with alkaline phosphatase for 1 hour at 37 ºC to prevent unspecific religation of the vector. Insert and vector were then purified (Section 2.1 above) and ligated (Section 2.2 above).

7. Generation of GFAP BiFC constructs

7.1. Venus-GFAP/GFAP-Venus regular BiFC constructs

Initially, four different GFAP BIFC constructs were generated by inserting *Venus* fragments in the N- or C-terminus of GFAP in pcDNA3.1 vector. These constructs encoded for GFAP fused to three different non-fluorescent halves of the *Venus* fluorescent protein: VN, amino acids 1-210; a short version of VC, amino acids 211-238; and a long version of VC, amino acids 159-238. For the sake of simplicity, we will refer to *Venus* C (211-238) as S-VC (short), and *Venus* C (159-238) as L-VC (long) throughout the present thesis.

Fusion proteins were cloned in a pcDNA 3.1 backbone. S-VC halves were inserted in the N- or C-termini of *GFAP*, L-VC in the C-terminal part of GFAP and Venus N in the N-terminus of GFAP. A fourth BiFC fusion gene was synthesized in a pcDNA 3.1 backbone, where S-VC was located in the C-terminus of GFAP.

7.2. Insert/Vector preparation

The VN-GFAP construct was made using two cloning steps. First, VN was inserted in the pcDNA 3.1 vector. The VN insert was obtained by digestion of a previously synthesized gene (*Venus*) with *Nhe*I and *Xba*I for 2 hours at 37 ºC. The pcDNA 3.1 vector was digested in the same conditions and incubated with alkaline phosphatase for 1 hour at 37 ºC.

Insert and vector were then purified (Section 2.1 above) and ligated (Section 2.2 above).

The GFAP insert was amplified by PCR using a pcDNA 3.1-human GFAP kindly provided by Dr. Michael Brenner (University of Alabama at Birmingham, USA) as a template. PCR was carried out using 20 ng of template DNA, 0.2 µM of primers (FWD 5' GCCGCTCGAGGAGAGGAGACGCATCACCTC 3' and REV 5' CTGAGGCGGATCCATCACATCACATCCTTGTGCTCC 3') and 250 µM of dNTPs in a total volume of 50 µl containing 2.5 units of Phusion DNA polymerase and the corresponding amplification buffer. The following thermocycling conditions were used: initial denaturation at 98ºC of 30s followed by 35 cycles of denaturation at 98ºC for 10s; annealing at 60ºC for 30 sec; and extension at 72ºC for 1 min. The GFAP PCR product and the pcDNA-VN construct were digested with XhoI and BamHI for 2 hours at 37ºC and the vector was incubated with alkaline phosphatase for 1 hour at 37ºC. Insert and vector were then purified (Section 2.1 above) and ligated (Section 3.2 above) to obtain the final VN-*GFAP* clones.

The pcDNA-S-VC-GFAP construct was made by just one cloning step. The S-VC-*GFAP* insert was obtained by digestion of a previously synthesized plasmid containing the insert with *BamH*I for 2 hours at 37 ºC. The pcDNA 3.1 destination vector was digested in the same conditions and incubated with alkaline phosphatase for 1 hour at 37 ºC. Insert and vector were then purified (Section 2.1 above) and ligated (Section 2.2 above).

The pcDNA-GFAP-L-VC construct was also made by just one cloning step. *GFAP* was inserted in the pcDNA 3.1 vector carrying L-VC. The *GFAP* insert was obtained by digestion of a previously synthesized plasmid containing *GFA*P with *Nhe*I and *Xho*I for 2 hours at 37 ºC. The pcDNA-L-VC destination vector was digested in the same conditions and

incubated with alkaline phosphatase for 1 hour at 37 ºC. Insert and vector were then purified (Section 2.1 above) and ligated (Section 2.2 above).

8. **Mammalian cell cultures**

All constructs were eventually tested in cultured mammalian cells. HEK, U251 and HeLa cells were maintained in DMEM supplemented with 10% FBS and 1% of penicillin/streptomycin commercial antibiotic mixture, at 37ºC and 5% CO_2. Cells were always plated at a density of 10.000 cells/cm^2 in order to obtain comparable results with different techniques and plates and between experiments. Cells were transfected with different combinations of constructs, and analyzed 24 hours later by flow cytometry, fluorescence microscopy, immunoblotting, cell proliferation/viability assays and ATP assays. Transfections were done using jetPRIME™ (Polyplus transfection, New York, USA) in a proportion of 3:1 (µl of jetPRIME: µg of DNA). Briefly, the jetPRIME™ transfection reagent and the DNA were mixed with 200 µl of jetPRIME buffer, and incubated for 10 minutes at room temperature before adding the transfection mixture to the plates. For 35 mm or 60 mm dishes, 65 µl or 130 µl of transfection mixture were added, respectively. Twenty-four hours after transfection, cells were processed specifically for each analytical method.

9. **Flow cytometry**

Cells were washed once with PBS and incubated with Trypsin 0.05% w/v for 5 min at 37ºC to detach cells from the substrate. Trypsin was neutralized with complete DMEM and cells were collected into sterile 15 ml tubes and centrifuged at 300xg for 5 min. The supernatant was removed and cells were resuspended in 500 µl of PBS. Ten thousand cells

per experimental group were analyzed by means of a FACSCalibur flow cytometer equipped with a low-power aircooled 15mW blue laser (488nm) argon laser and a red (635nm) diode laser (band-pass filter 530/30) at Instituto Gulbenkian de Ciência or by means of AccuriC6 equipped with a blue laser (488nm) and a red laser (640nm) at Instituto de Medicina Molecular. Data were analyzed and represented by means of FlowJo software (Tree Star Inc., Ashland, United States).

10. **Diaminobenzidine (DAB) reaction**

Cells were fixed with 1% glutaraldehyde and 1% paraformaldehyde in 0.1M cacodylate buffer for 30 min. Samples were rinsed 2 x 30 sec and 3 x 5 min with 0.15M cacodylate buffer (chilled). After the wash, blocking buffer was added (50mM glycine; 10mM KCN; 5mM aminotriazole) for 30 min. Samples were rinsed 2 x 30 sec with 0.15M cacodylate buffer (chilled). After the wash, DAB was added and then the samples were illuminated using a standard FITC filter set with intense light from a 150W Xenon lamp on 20x objective (on 780-R, in the locate tab, 100% Hg lamp + 488 filter cube set) for 2-10min. Rinse 2 x 30 sec and 3 x 5 min with 0.15M cacodylate buffer. Cells were incubated with 3% potassium ferrocyanide, 2% OsO4 in 0.15M cacodylate buffer for 1hr on ice. Samples were rinsed 2 x 30 sec and 3 x 5 min with water. Aminotriazole solution was filtered with a 0.22 µm filter and cells were incubated in the filtered aminotriazole solution for 20 min at RT. Cells were rinsed 2 x 30 sec and 3 x 5 min with water. Incubated in 2% OsO4 in water for 20 min at RT and rinsed 2 x 30 sec and 3 x 5 min with water. Samples were incubated in 1% UA overnight at 4 degrees. Cells were rinsed 2 x 30 sec and 3 x 5 min with water and then Incubated in lead solution for 30 min at 60 degrees. Rinsed 2 x 30 sec and 3 x 5 min with water and dehydrated using acetone or EtOH (started with 35% in that case) on ice for 5 minutes each. It was

prepared fresh Durcupan and EtOH mixtures and incubated for 2 hours at RT.

11. **Microscopy**

Images from living or fixed cells were acquired at Instituto Gulbenkian de Ciência on a custom-built Nikon Eclipse TE2000-S inverted fluorescence microscope equipped with a Hamamatsu Flash 2.8 sCMOS camera. For fixation, cells were washed with PBS and fixed and permeabilized in 100% ice-cold methanol at -20ºC for 10 min. They were washed again and stored in PBS at 4ºC. Pictures were taken using the 100X objective and analyzed by means of the ImageJ free online software (http://rsbweb.nih.gov/ij/). For STAT3 experiments, cells were classified qualitatively in three categories according to the relative intensity and localization of the fluorescence signal (Fig. 17A, 17B, 17C): 1) predominantly in the cytoplasm, 2) predominantly in the nucleus, or 3) homogeneously distributed through nucleus and cytoplasm. These categories are mutually exclusive meaning their sum is 100% of cells. Furthermore, the percentage of cells with mitochondrial signal, where the fluorescent signal co-localized with Mitotracker Red (Life Technologies; Eugene, OR, USA), or aggregates where the fluorescent signal did not co-localize with the dye (Fig. 17D), was also determined.

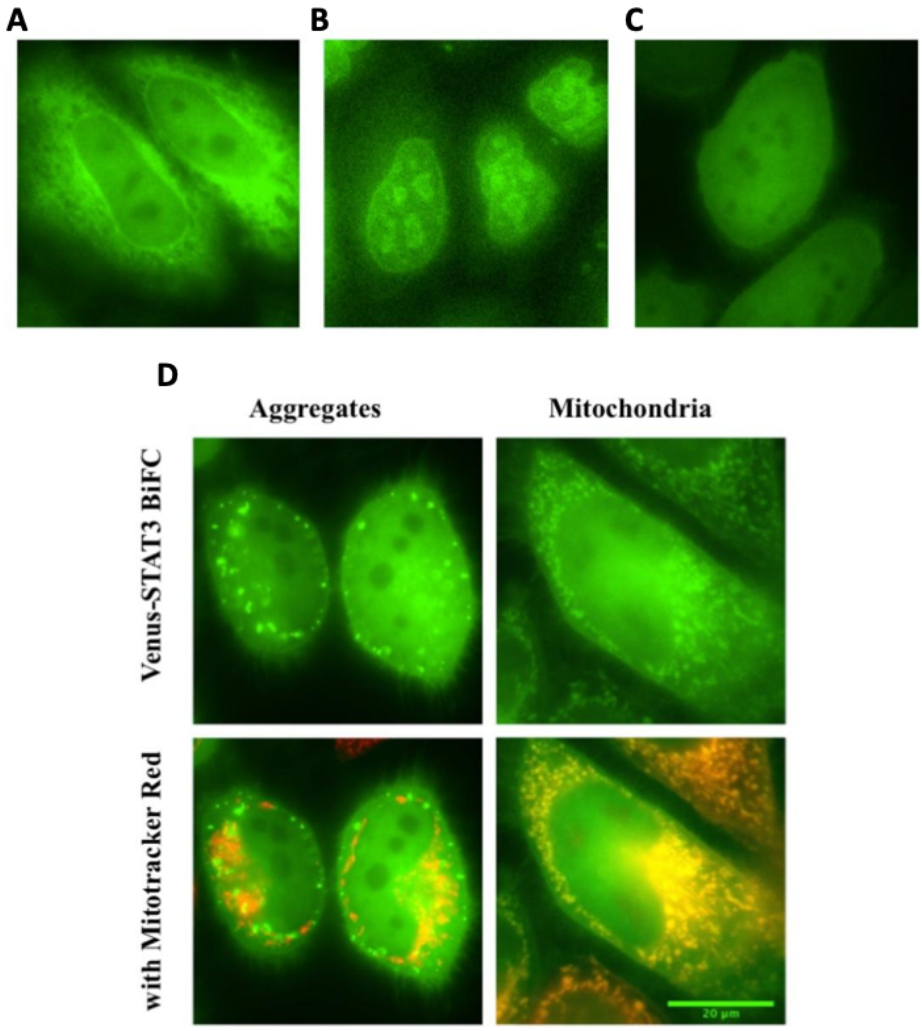

Figure 17 - Representative fluorescence microscopy pictures of the qualitative classification of STAT3 distribution in HeLa cells - A, Predominantly in the cytoplasm. B, Predominantly in the nucleus. C, Homogenously in the cytoplasm and nucleus. D, Mitochondrial localization and aggregates with and without Mitotracker Red. Scale bar: 20 µm

12. **Immunoblotting**

12.1. Total protein extraction

Cells were washed once with PBS, and then lysed with a lysis buffer (NaCl 150 mM, NP-40 1% v/v, Tris-HCl 50 mM pH 8.0) containing protease inhibitors. Cells were scrapped directly from the plates, transferred to microcentrifuge tubes, and incubated in ice for 10 min. Cells were sonicated for 5 seconds by means of a Sonifier W-450 D sonicator (Emerson, Danbury, United States) to disrupt the membranes and release intracellular proteins, allowing their isolation and detection by western blotting. To avoid protein degradation by cell proteases, cells were always kept in ice during extraction procedures. Protein concentration was quantified on a microplate reader (Multiskan Go, Thermo Scientific, Waltham, United States) by means of the Bradford method. Briefly, 2 µl of protein sample were added to 200 µl of the Bradford reagent and incubated for 10 minutes, and their absorbance was measured at 595 nm. Protein concentrations were calculated by means of a standard curve produced from known concentrations of bovine serum albumin (0.125 to 2 µg/µl).

12.2. Nuclear and cytoplasmic protein extraction

Nuclear and cytosolic proteins were extracted with the NE-PER Nuclear and Cytoplasmic Extraction Reagents kit from Thermo Scientific (MA, USA), following manufacturer´s instructions. Briefly, cells were washed once with PBS and incubated with Trypsin 1X for 5 min at 37ºC to detach cells from the substrate. Trypsin was neutralized with complete DMEM and cells were collected into a microcentrifuge tube and were centrifuged at 300xg for 5 min, the supernatant was discarded and the

pellet was resuspended in cold cytoplasmic extraction reagent I with protease inhibitors. The suspension was homogenized by vortex (15 seconds) and incubated in ice for 10 min. Cold cytoplasmic extraction reagent II was then added to the mixture, homogenized by vortex and incubated for 1 minute in ice. The mixture was once again vortexed and centrifuged at 16000xg for 5 min. The supernatant, corresponding to the cytoplasmic protein extract, was collected into a new sterile microcentrifuge tube and stored at –20°C. The pellet was resuspended in the nuclear extraction reagent with protease inhibitors and homogenized by vortex 4 times every 10 min. The sample was then centrifuged at 16000xg for 10 min and the supernatant, corresponding to the nuclear protein fraction, was collected into a new sterile microcentrifuge tube and stored at – 80°C. Protein concentration was quantified on a microplate reader (Multiskan Go, Thermo Scientific, Waltham, United States) by means of the Bradford method as described above (section 12.1).

12.3. Immunoblotting

Twenty µg of protein were mixed with 4x denaturing loading buffer (1 M Tris pH 7; 8% SDS; 40% glycerol; 6.3% β-mercaptoethanol; bromophenol blue), boiled at 95ºC for 5 min, and incubated at 4ºC for 5 min. Protein samples were run in SDS-PAGE 10% (w/v) Acrylamide gels made with Protogel reagents (United Diagnostics, Atlanta, United States). Samples were run at 125V for 60 min and transferred to a nitrocellulose membrane at 100V for 60 minutes. Membranes were stained with Ponceau S 0.1% (w/v) to verify protein transfer efficiency as well as equal sample loading. Membranes were washed with miliQ water and Tris-HCl buffer saline (TBS, 150 mM NaCl, 50 mM Tris pH 7.4) and blocked with 5% (w/v) non-fat dry milk in TBS for 1 hour at room temperature in agitation. Membranes were washed 3 times with TBS-Tween (0.05% v/v)

and incubated with the corresponding antibodies overnight at 4ºC in agitation: a Rabbit polyclonal anti-*GFAP* (1:1000, Millipore, Billerica, United States of America), a mouse monoclonal anti-GAPDH (1:1000, Ambion, West Palm Beach, United States), a mouse monoclonal anti-STAT3, (1:1000, Santa Cruz Biotechnology; Dallas, TX, USA); a rabbit polyclonal anti-P-STAT3(Y705), (1:1000, Cell Signaling Technology; Danvers, MA, USA) or anti-*Lamin* B, 1:1000, mouse monoclonal (Santa Cruz Biotechnology; Dallas, TX, USA), a mouse monoclonal anti-*GRIM19* (Santa Cruz Biotechnology; Dallas, TX, USA). Primary antibodies were diluted in 5% (w/v) bovine serum albumin (BSA) in TBS and sodium azide 0.02% (w/v) to prevent contaminations. Membranes were then washed 3 times for 10 min each with TBS-T and incubated with the corresponding anti-Rabbit or anti-Mouse horseradish peroxidase-conjugated secondary antibodies (GE-Healthcare, Little Chalfont, United Kingdom) for 2 hours in agitation at room temperature. Secondary antibodies were diluted at a 1:1000 concentration in 5% (w/v) non-fat dry milk. Membranes were washed 3 times for 10 min each with TBS-T, incubated with chemiluminescent HRP reagents (Millipore, Billerica, United States), and imaged by means of a Chemidoc device (XRS+, Biorad, California, United States).

13. **Cell proliferation/viability Assay**

For proliferation/viability assays, cells were plated on a 96-well plate at a density of $4x10^4$ per well in a final volume of 100 µl of medium. Twenty-four hours after the seeding, cells were transfected with a proportion of 1 µg of DNA to 3 µl of Transfection Reagent. Twenty-four hours after transfection, 10 µl of 3-(4,5-dimethyl-2-thiazolyl) 2,5-diphenyl-2H-tetrazolium bromide (MTT) solution in PBS (2 mg/ml) were added to each well. After 2 hours of incubation at 37ºC and 5% CO_2, the medium

was removed and 100 µl of Dimethyl Sulfoxide (100%) were added. Cells were incubated for 15 minutes at room temperature and the samples were measured at 570 nm in an automatic microplate reader (Sunrise 8708, Tecan Trading AG, Switzerland).

14. **ATP determination**

For determination of total ATP levels, cells were plated on a 6-well plate at a density of $1{,}2x10^6$ per well in a final volume of 3 ml of medium. Twenty-four hours after seeding, cells were transfected with a proportion of 1 µg of DNA to 3 µl of Transfection Reagent. Twenty-four hours after transfection cells were washed twice with PBS, lysed for 5 min with Extraction Buffer (6 M Guanidine-HCl 100mM Tris/HCl pH 7.8; 4 mM EDTA) and snap-frozen in liquid nitrogen. After 3 minutes of incubation at 95ºC, cells were centrifuged at maximum speed for 10 min and the supernatant was recovered to a new tube. The concentration of each sample was quantified using the Bradford method (see section 12.1) and the same quantity of each condition was mixed with a luminescent solution from the ATP Determination Kit (A22066, Thermo Fischer Scientific, Waltham, MA USA). ATP-containing solutions were added to a 96-well black transparent bottom plate and incubated in the dark for 10 min at room temperature. Luminescence was measured using a multitask microplate reader (Victor 3V, Perkin Elmer, Boston, MA USA).

15. ***STAT3*** **CRISPR/Cas9 Knockout**

Knockout of the endogenous *STAT3* gene from HeLa cell line was achieved by following the specifications of *STAT3* CRISPR Knockout plasmid manufacturer (Santa Cruz Biotechnology, Dallas, Texas, USA). The protocol was divided in 3 phases. First, 1 µg of *STAT3* CRISPR/Cas9

knockout pool DNA was mixed with 150 µl of Plasmid Transfection Medium provided in the kit to prepare solution A, and incubated for 5 min at RT. Five µl of UltraCruz Transfection Reagent were mixed with 150 µl of Plasmid Transfection Medium provided in the kit to prepare solution B, and incubated for 5 min at RT. Solution A was mixed with solution B and incubated for 20 min at RT. Prior to transfection, medium from cells was replaced with fresh free antibiotic medium. Cells at 80% confluence were transfected with the transfection mixture and incubated for 48 hours.

The second phase was the selection of the positive clones by fluorescence-assisted cell sorting (FACS). Cells transfected with CRISPR/Cas9 constructs expressed temporarily the green fluorescent protein (*GFP*), and this fluorescence allowed their clonal isolation by sorting. Cell sorting was carried out by means of a BD FACSAria III sorter at the Instituto de Medicina Molecular (Lisbon, Portugal). Single cells were distributed in 96-well plates containing 200µl of complete medium with antibiotics.

The third phase was the growth of single cell colonies and confirmation of gene removal. Cells were maintained in complete medium until they reached confluence, and then passed into larger plates. When there were enough cells to freeze, an aliquot of cells was lysed and the proteins extracted to confirm knockout by immunoblotting. A *STAT3*-knockout clone was selected for further growth and experiments.

16. **Statistical analysis**

Sigmaplot software (Systat Software, Inc, San Jose, CA, USA) was used to perform the statistical analysis and graphical representation of data. Results are shown as the average ± SEM of at least 3 independent experiments, unless otherwise indicated in figure legends. Statistical analysis was carried out by means of a one-way ANOVA followed by a

Bonferroni test adjusted for multiple comparisons. Results were in all cases considered significant when $p < .05$, but lower significance thresholds ($p<.01$) were specified in some cases.

17. **List of Plasmids**

A total of 42 plasmids have been generated through this thesis. The plasmids are described in the table below.

Table III - List of plasmids generated

Plasmid Name	Vector	Antibiotic
VN STAT3 Y45F	pcDNA3.1	Amp
VN STAT3 K49R	pcDNA3.1	Amp
VC STAT3 K49R	pcDNA3.1	Amp
VN STAT3 Y68F	pcDNA3.1	Amp
VC STAT3 Y68F	pcDNA3.1	Amp
VN STAT3 Y79F	pcDNA3.1	Amp
VN STAT3 K140R	pcDNA3.1	Amp
VC STAT3 K140R	pcDNA3.1	Amp
VN STAT3 Y176F	pcDNA3.1	Amp
VC STAT3 Y176F	pcDNA3.1	Amp
VN STAT3 S181A	pcDNA3.1	Amp
VC STAT3 S181A	pcDNA3.1	Amp
VN STAT3 C418S	pcDNA3.1	Amp
VC STAT3 C426S	pcDNA3.1	Amp
VN STAT3 Y539F	pcDNA3.1	Amp
VN STAT3 Y640F	pcDNA3.1	Amp
VC STAT3 Y640F	pcDNA3.1	Amp
VN STAT3 K685R	pcDNA3.1	Amp
VC STAT3 K685R	pcDNA3.1	Amp
VN STAT3 S691A	pcDNA3.1	Amp
VN STAT3 Y705F	pcDNA3.1	Amp

VC STAT3 Y705F	pcDNA3.1	Amp
VN STAT3 T708D	pcDNA3.1	Amp
VN STAT3 S727A	pcDNA3.1	Amp
VC STAT3 S727A	pcDNA3.1	Amp
VN STAT3 Y705F+S727A	pcDNA3.1	Amp
VC STAT3 Y705F+S727A	pcDNA3.1	Amp
VN STAT3ΔSH2	pcDNA3.1	Amp
STAT3MiniSog 1 (1-138)	pcDNA3.1	Amp
STAT3Minisog 6 (138-321)	pcDNA3.1	Amp
STAT3MiniSog 2 (1-183)	pcDNA3.1	Amp
STAT3Minisog 7 (183-321)	pcDNA3.1	Amp
STAT3Minisog 3 (1-216)	pcDNA3.1	Amp
STAT3Minisog 8 (216-321)	pcDNA3.1	Amp
STAT3Minisog 4 (1-276)	pcDNA3.1	Amp
STAT3Minisog 9 (276-321)	pcDNA3.1	Amp
STAT3Minisog 5 (1-192)	pcDNA3.1	Amp
GFAP VC(159-238)	pcDNA3.1	Amp
GFAP VN (1-158)	pcDNA3.1	Amp
VC (159-238) GFAP	pcDNA3.1	Amp
GFAP_eGFP(Transposon)	pcDNA3.1	Amp
GFAP_R239C_eGFP(Transposon)	pcDNA3.1	Amp

Chapter 3

Results (Part I)

Asymmetric PTMs change the subcellular distribution of *STAT3* homodimers

This chapter contains results published in:

Letra-Vilela, R., Cardoso, B., Silva-Almeida, C., Maia Rocha, A., Murtinheira, F., Branco-Santos, J., Herrera, F. (2020). Can asymmetric post-translational modifications regulate the behavior of STAT3 homodimers? FASEB BioAdvances, 2(2), 116–125.

Introduction

STAT3 is a transcription factor that plays key roles in development, immunity, response to injury and cancer (Srivastava & DiGiovanni, 2016; J. Yang & Stark, 2008). STAT3 is mainly found in the cytosol as a homodimer in unstimulated cells and is activated by phosphorylation at Y705 after stimulation with a variety of cytokines (Srivastava & DiGiovanni, 2016; J. Yang & Stark, 2008). After phosphorylation, STAT3 translocates to the nucleus where it is retained and activates the transcription of a specific set of genes, such as Mcl-1, Bcl-xL, Fascin, Vimentin, AKT and PIM-1 (Carpenter & Lo, 2014). However, unphosphorylated STAT3 is also able to translocate to the nucleus and bind to DNA, activating another set of genes, such as m-Ras, RANTES or cyclin B1 (Dasgupta et al., 2014; Schröder, Kroeger, Volk, Eidne, & Grütz, 2004; J. Yang et al., 2005).

To visualize STAT3 dimerization in living cells, three systems have been developed based on FRET (Domoszlai et al., 2014), BRET (Schröder et al., 2004) or the homoFluoppi tag (Okada et al., 2018). The first two allow us to visualize homo- and heterodimerization of STAT3 in real time and in a reversible manner (Domoszlai et al., 2014; Schröder et al., 2004), but they require very skilled users for sampling and analyses and are difficult to adapt for high-throughput experiments. Both approaches are based on the fusion of an energy donor and an energy acceptor, typically a fluorescent protein where the emission spectrum of the donor must overlap with the excitation spectrum of the acceptor (P. Wu & Brand, 1994). In contrast, the homoFluoppi system is simpler but only allows to visualize homodimerization. Two tags, PB1 and mAG1, are fused together to a protein of interest that facilitate the formation of fluorescent droplets once the proteins of interest interact. Other disadvantage when compared with FRET or BRET is that it is only useful for microscopy because the fluorescent levels inside the cell do not

change quantitatively upon STAT3 dimerization, fluorescence only changes its intracellular distribution, producing puncta upon cytokine stimulation (Okada et al., 2018).

Here, we decided to develop a new system to visualize STAT3 dimers in living cells based on BiFC assays, which is complementary to the existing ones. In BiFC assays, changes in fluorescence levels are proportional to the amount of STAT3 dimers, and therefore can be measured by flow cytometry or fluorimetry, not only by microscopy. They can also be used for the study of both homo- and heterodimerization and can be easily applied to high-throughput setups.

Results

Development and validation of a Venus-STAT3 BiFC system

We developed a suit of plasmids to study STAT3 dimerization in living cells, based on BiFC systems using Venus fragments as a reporter (Fig. 18A), as we did for other proteins in previous reports (Blum et al., 2014; Branco-Santos et al., 2017; Dias et al., 2013). When STAT3 dimerizes, the Venus fragments are brought together and reconstitute the fluorophore, fluorescence being proportional to the amount of dimers (Fig. 18B). This indicates that resting STAT3 can form dimers in the absence of stimulus.

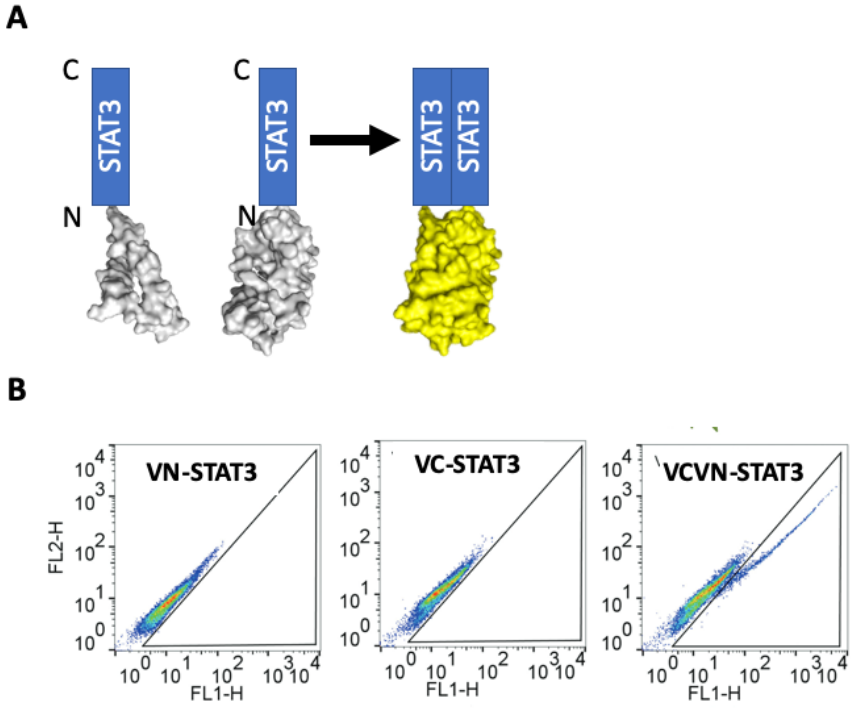

Figure 18 - Bimolecular Fluorescence Complementation (BiFC) system for *STAT3* – A, Venus BiFC fragments constituted by amino acids 1-158 (Venus N, VN) and 159-238 (Venus C, VC) were fused to the N-terminus of the STAT3 sequence in two independent constructs. B, Flow cytometry charts showing that VN-STAT3 and VC-STAT3 BiFC constructs do not produce fluorescence by themselves, but they fluoresce when they are transfected together.

Transfection of HEK293 or HeLa cells with the wild-type (WT) pair of Venus-STAT3 BiFC constructs led to successful expression of the chimeric proteins VN-STAT3 and VC-STAT3 (Fig. 19B). As expected, fluorescence was primarily cytoplasmic in both cell lines, with low but visible nuclear signal (Fig. 19A; Fig. 20C). Incubation with leukemia inhibitory factor (LIF, 100 ng/mL) induced STAT3 phosphorylation and translocation to the nucleus in HEK293 and HeLa cells (Fig. 19), but it did not enhance STAT3 dimerization (Fig. 19C; Fig. 20A). Single or double phosphoresistant mutants of key phosphorylatable residues Y705F/S727A did not decrease fluorescence either (Fig. 20A). These results support existing evidence indicating that STAT3 dimerization is actually independent of its phosphorylation (Okada et al., 2018; Schröder et al., 2004; Srivastava & DiGiovanni, 2016).

Incubation with STAT3 inhibitor Stattic (5 µmol/L) or removal of the C-terminus containing the SH2 domain partially prevented STAT3 dimerization (Fig. 20A), consistent with previous reports (Domoszlai et al., 2014; Schust, Sperl, Hollis, Mayer, & Berg, 2006). The combination of STAT3 with the corresponding BiFC constructs for Mdm2 or p53 proteins had extremely low levels of fluorescence (Fig. 20B). This is consistent with the fact that these proteins are not STAT3 interactors and supports the specificity of the Venus-STAT3 BiFC system.

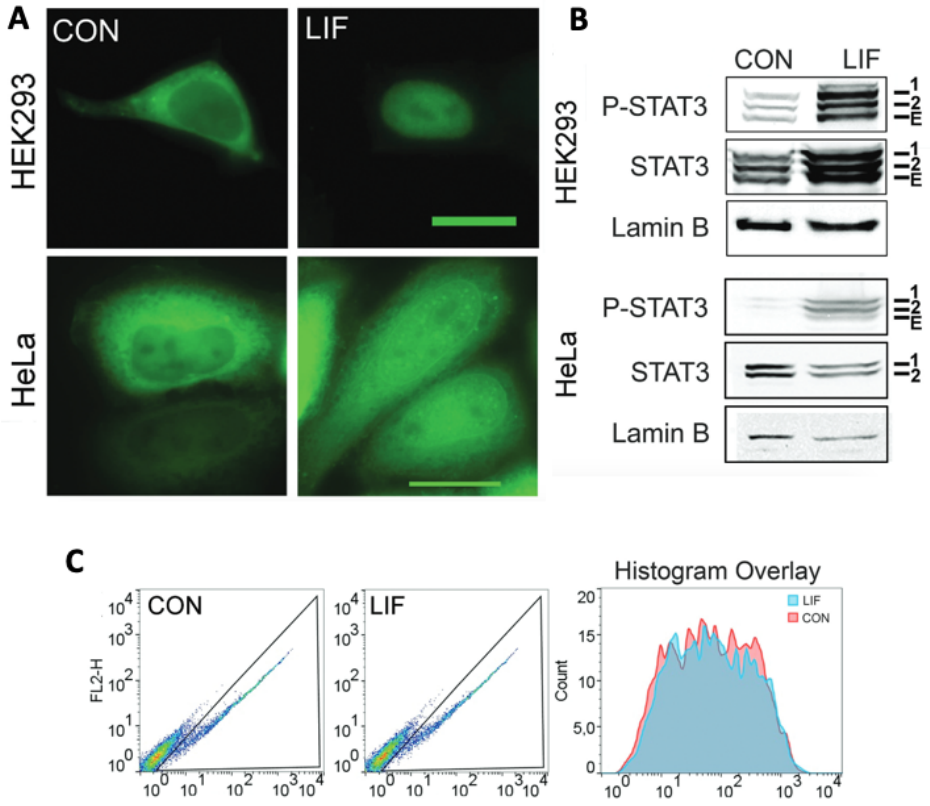

Figure 19. Resting *STAT3* dimers are mainly cytoplasmic, but accumulate in the nucleus upon cytokine stimulation – A, Representative fluorescence microscopy pictures of HEK293 or HeLa cells transfected with Venus-STAT3 constructs and incubated in the presence or absence of Leukemia Inhibitory Factor (LIF, 100 ng/ml) for 2 h or 15 min, respectively. STAT3 dimers translocate to the nucleus of stimulated cells, as expected (Scale bar, 20µm). B, Immunoblotting of *STAT3* in nuclear extracts from HEK293 or HeLa cells transfected with *Venus-STAT3* constructs and incubated in the presence or absence of LIF (100 ng/ml) for 2 h or 15 min, respectively. Three bands are observed, corresponding to VN-*STAT3* (1), VC-*STAT3* (2) and endogenous *STAT3* (E). C, LIF does not induce further *STAT3* dimerization, as determined by flow cytometry. The histogram (right) shows that there is almost perfect overlap between the fluorescent signal emitted by cells in the presence or absence of LIF.

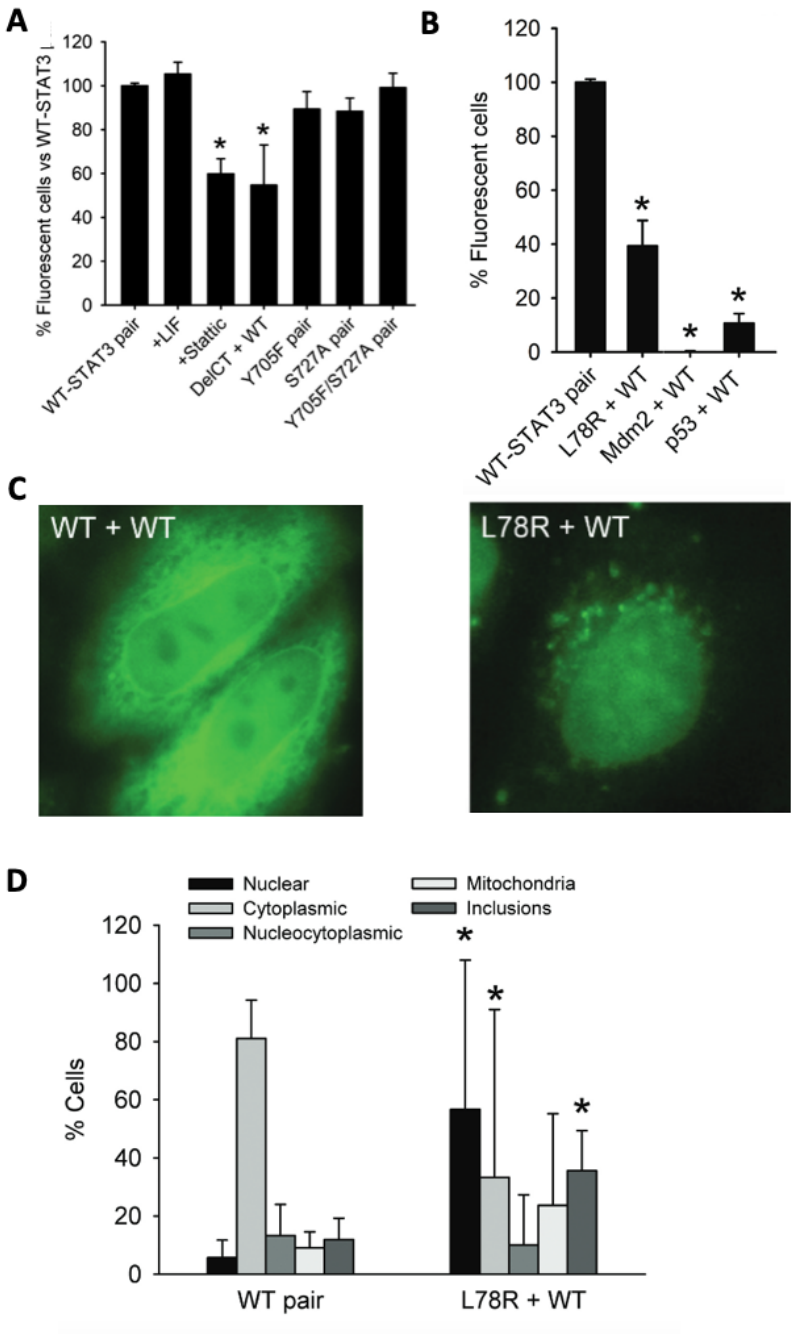

Figure 20 - The disease-associated L78R mutation inhibits *STAT3* dimerization, and promotes its aggregation and nuclear translocation – A, Wild-type (WT) *Venus-STAT3* constructs produced fluorescence in HeLa cells, and it was monitored by flow cytometry

24 h after transfection with BiFC constructs. Incubation with leukemia inhibitory factor (100 ng/mL) for 2 h in the absence of serum or the presence of the indicated drugs or mutant BiFC pairs (n = 3; P < .05). Results were normalized vs the WT *STAT3* pair (100%). B, HeLa cells were co-transfected with several BiFC combinations: the wild type (WT) *STAT3* pair (control), or WT *STAT3* with i) the L78R *STAT3* mutant (since L78R is a somatic, dominant *STAT3* mutation), or ii) *Mdm2* or *p53*, two proteins that in principle should not interact with STAT3 as negative controls. C, Representative cells for the WT *STAT3* pair and the combination containing the L78R mutant. While most cells transfected with the WT *STAT3* pair show a predominant cytoplasmic localization of the dimers, the introduction of the L78R mutation changes the distribution pattern towards the production of cytoplasmic inclusions and a predominantly nuclear location. D, Quantification of microscopy pictures. As explained in the main text, we classified cells according to the relative intensity and the location of the fluorescence signal in five categories: cytoplasmic, nuclear, both cytoplasmic and nuclear, mitochondrial and inclusions. Data are shown as the average ± SEM of n=12 (Wild-type, WT) or n=3 (L78R) independent experiments. *, significant vs the symmetric Wild-type *STAT3* pair, p<0.05

Naturally occurring STAT3 mutations cause hyper-immunoglobulin E syndrome or inflammatory hepatocellular adenoma (Pilati, Amessou, Bihl, Balabaud, Nhieu, et al., 2011; Woellner et al., 2010). The L78R mutation, in particular, inhibits STAT3 dimerization but has a strong tendency to go to the nucleus and activate transcription (Domoszlai et al., 2014; Pilati, Amessou, Bihl, Balabaud, Nhieu, et al., 2011). We created a L78R STAT3 mutant in our BiFC system and confirmed that it inhibited STAT3 dimerization (Fig. 20B), and induced nuclear translocation at the expense of cytoplasmic STAT3 (Fig. 20C, B). Furthermore, the analysis of microscopy images indicated that it also induces STAT3 aggregation into cytoplasmic inclusions (Fig. 20D). Taken altogether, our results indicate that the behavior of the Venus-STAT3 BiFC system is consistent with previous reports for tagged STAT3, and could be useful for the analysis of environmental or genetic modifiers of STAT3 dimerization, protein-protein interactions and intracellular traffic.

Specific symmetric PTM-resistant mutations cause changes in the intracellular localization of resting STAT3 dimers

STAT3 plays a role in a variety of biological functions where the fate of the protein is regulated by many PTMs, being phosphorylation, acetylation and methylation the most studied ones (Srivastava & DiGiovanni, 2016; J. Yang & Stark, 2008). The role that each PTM plays in STAT3 behavior and function still needs to be better understood.

Taking advantage of our BiFC Venus-STAT3 system previously validated, 16 mutated versions of STAT3 (Fig. 21A) were generated by means of site-directed mutagenesis. Ten plasmids carrying single inhibitory mutations: K to R in amino acid 49, 140 and 685, to avoid methylation (in the first two) and/or acetylation (in amino acid 49 and 685); and Y to F in amino acid 705 and S to A in amino acid 727, to avoid phosphorylation. The other 6 plasmids are double mutants, carrying the Y705F phosphoresistant mutation together with K49R, K685R or S727A mutations. This second set of constructs would allow to determine the role of these PTMs on unphosphorylated STAT3. Inhibitory mutations of PTMs on STAT3 do not affect STAT3 expression, presenting the same protein levels in all tagged forms of STAT3 (Fig. 21B).

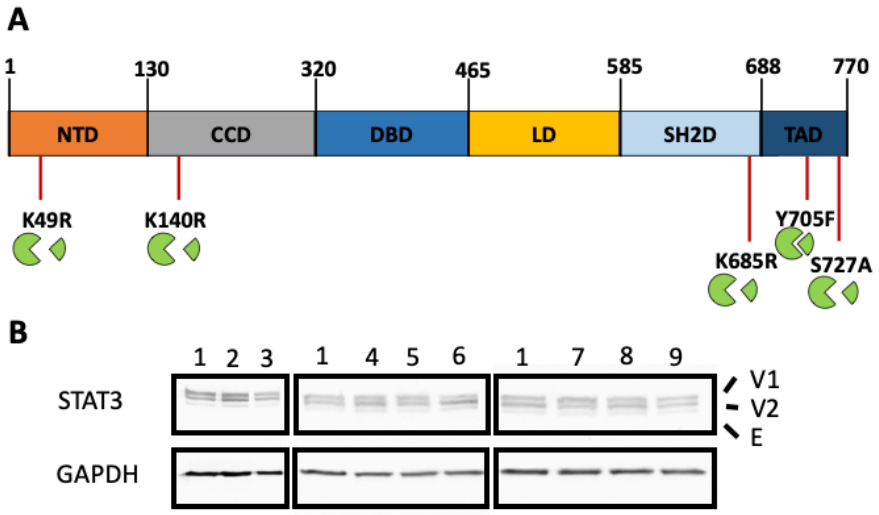

Figure 21 - Schematic representation of *STAT3* - The STAT3 protein can suffer different PTMs in 4 of the 6 domains. A, To understand the relation of this PTMs with the homodimerization of STAT3 and the pattern of distribution, a set of plasmids have been generated of STAT3 fused to two halves of the fluorescent protein Venus with inhibitory mutations of the STAT3 PTMs. The mutants were originated by means of Site Directed Mutagenesis using as template the STAT3 WT plasmids. For each mutation two plasmids are originated, one with the first halve of Venus (VN) and other with the second (VC). B, Immunoblotting of STAT3 from HeLa cells transfected with Venus-STAT3 constructs, WT-pair (1), K49R-pair (2), K140R-pair (3), K685R-pair (4), Y705F-pair (5), S727A-pair (6). Three bands are observed, corresponding to VN-STAT3 (V1), VN-STAT3 (V2) and endogenous STAT3 (E).

Next, we tried to elucidate the role that these particular residues susceptible to PTMs could play on the dimerization and intracellular localization of STAT3 homodimers without adding exogenous cytokines. The original idea was to establish a baseline for future experiments in the presence of cytokines, which enhance the frequency of these particular PTMs in STAT3. However, low levels of these PTMs in the absence of cytokines have been also described in the literature (Dasgupta et al., 2014; Kang et al., 2017; Ray, Boldogh, & Brasier, 2005b) and we also

wanted to know if these basal PTMs or the residues themselves had any influence in the dimerization and distribution of resting STAT3 homodimers. No combination of single or double mutants had a significant effect on unstimulated STAT3 dimerization, as determined by flow cytometry (Fig. 24). However, we observed a tendency to decrease dimerization in the combinations carrying the double mutants Y705F/S727A and Y705F/K685 together with single mutants K140R or S727A.

For the intracellular distribution studies, we classified cells qualitatively in three categories that are mutually exclusive (their sum is 100% of cells), according to the relative intensity and location of the fluorescence signal (Fig. 17): (a) predominantly in the cytoplasm (eg WT pair); (b) predominantly in the nucleus (eg upon LIF induction, Figs. 17B and Fig. 19A); or (c) homogeneously distributed through nucleus and cytoplasm (eg Y705F pair). We also determined the percentage of cells with mitochondrial signal or intracellular inclusions (Fig. 20 and Fig.23). We initially assumed that the two STAT3 molecules that form a dimer are identical in all aspects, including their PTMs (i.e. they were perfectly "symmetric"). Therefore, our analyses focused first on "symmetric" combinations. Although changes in patterns of STAT3 dimer distribution were observed in several symmetric BiFC pairs, only the Y705F pair induced a significant increase in the percentage of cells with homogeneous nucleocytoplasmic fluorescence (Fig. 22).

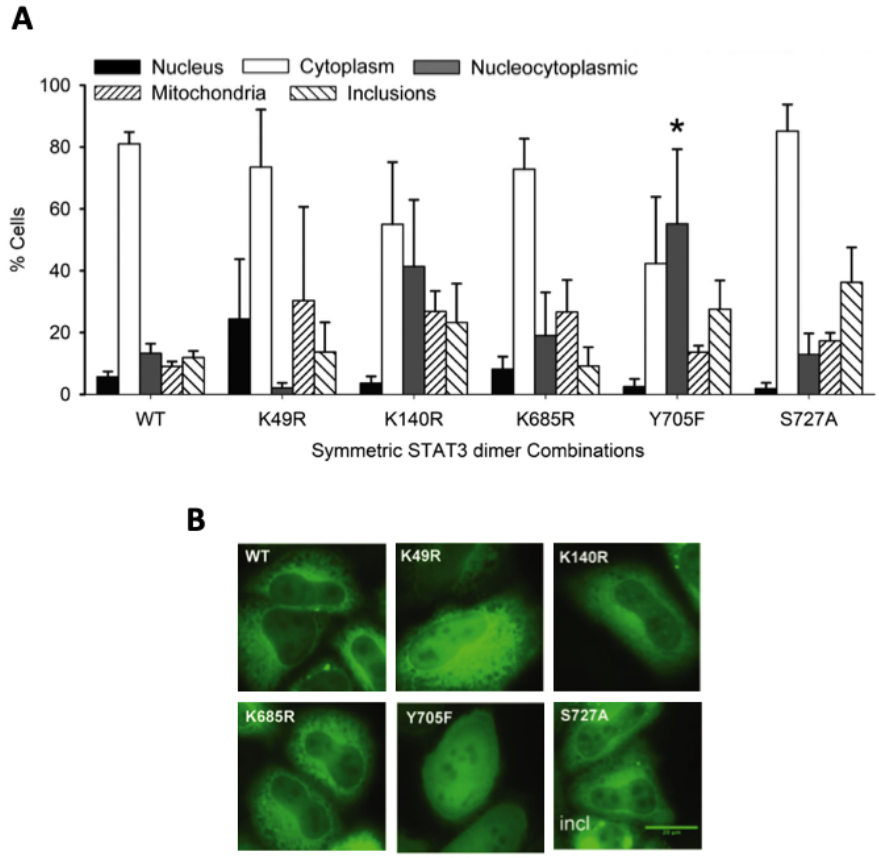

Figure 22 – The Y705F phosphoresistant mutation led to an increase in nucleocytoplasmic distribution – A, Percentage of cells displaying fluorescence predominantly in the Nucleus (black bar), predominantly in the Cytosol (white bar), homogeneously distributed in cytoplasm and nucleus (nucleocytoplasmic, grey bar), in the mitochondria or in non-mitochondrial inclusions. Data are shown as the average ± SEM of n = 12 WT or n = 3 (rest of combinations) independent experiments. *Sign. vs the symmetric WT STAT3 pair, P < .05. B, Microscopy pictures of representative cell phenotypes in the different symmetric combinations of BiFC Venus-STAT3 constructs (Incl, inclusions; scale bar, 20 μm).

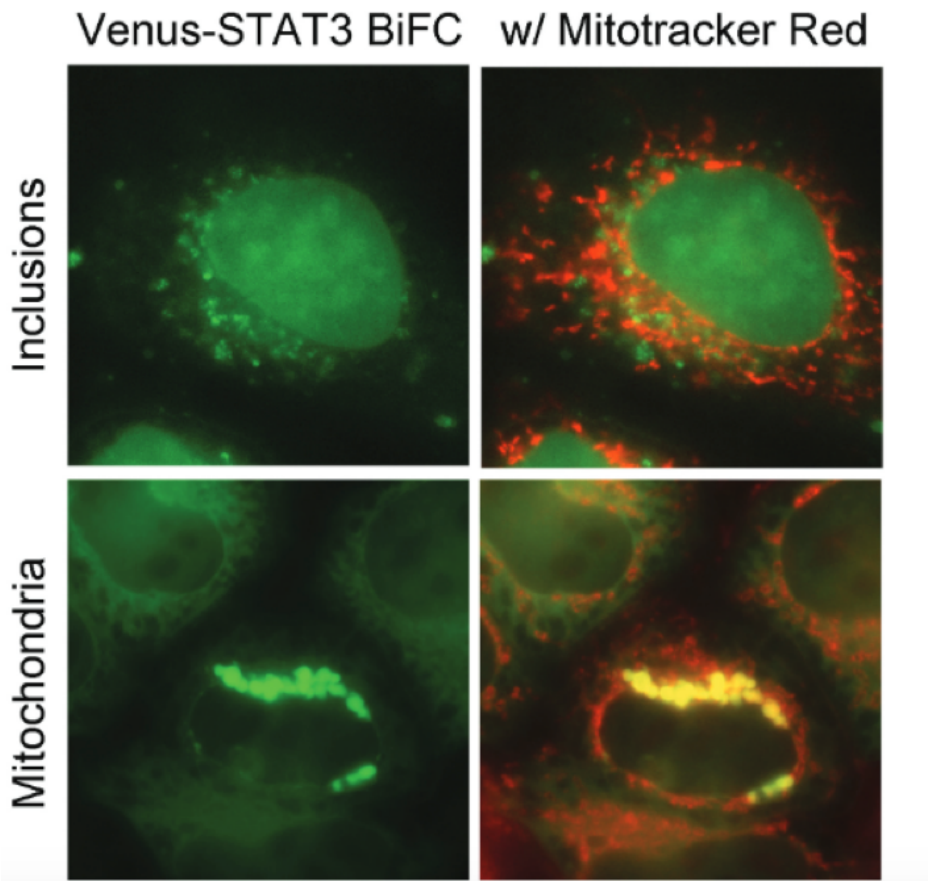

Figure 23 - Examples of cells showing mitochondrial localization of *STAT3* dimers versus *STAT3* inclusions - Mitochondrial localization of STAT3 dimers was monitored by co-localization of fluorescent foci with Mitotracker Red. When there were fluorescent foci that did not co-localize with Mitotracker Red we classified them as "Inclusions"

Relative contribution of specific residues to STAT3 dimerization, intracellular location, and cell proliferation

To the best of our knowledge, the existing scientific literature on STAT3 implicitly assumes that STAT3 homodimers are formed by two identical molecules in all aspects, including PTMs. For example, it is still relatively easy to find articles and reviews where STAT3 is described to homodimerize only upon phosphorylation of both molecules at Y705 (Sgrignani et al., 2018), and we worked under this same assumption until

recently (Mesquita et al., 2016). Here, we made use of the unique properties of our BiFC system to determine the relative contribution of each residue to the dimerization and intracellular distribution of unstimulated STAT3 dimers, in an experimental paradigm similar to the one we used previously for mutant huntingtin (Branco-Santos et al., 2017).

HeLa cells were transfected with all the possible combinations containing PTM-resistant mutations for key STAT3 acetylation/methylation (K49R, K140R, K685R) or phosphorylation (Y705F, S727A) events, as well as a few double-mutant versions (Y705F plus K49R, K685R or S727A) to determine the relative contribution of these residues to the behavior of Y705-phosphorylated or -unphosphorylated STAT3 homodimers. Combinations containing K140R or K658R mutations did not reveal significant differences in the percentage of fluorescent cells when compared with the WT STAT3 pair (Fig. 24). The same result was observed when we transfected combinations containing one construct carrying the Y705F mutant (Fig. 25). When we transfected combinations containing the K49R and S727A mutants together we observed a significant decrease in the levels of fluorescence when compared with the WT pair. This decrease was only observed for that pair, while in all the other combinations carrying these mutations it was not possible to observe significant differences. In cells transfected with all the possible combinations containing double mutants Y705F + S727A or Y705F + K685R was observed an increase in the fluorescent levels when between both proteins of the same dimer we have inhibition methylation (K49R) and phosphorylation (S727A and Y705F) while in all the other combinations it is not possible to observe significant differences versus WT pairs (Fig. 26). These results indicate that the majority of PTMs do not have an effect on STAT3 dimerization leading to the possibility that they can regulate the interaction of STAT3 dimers with

other proteins or complexes or can participate in the fate of *STAT3* distribution.

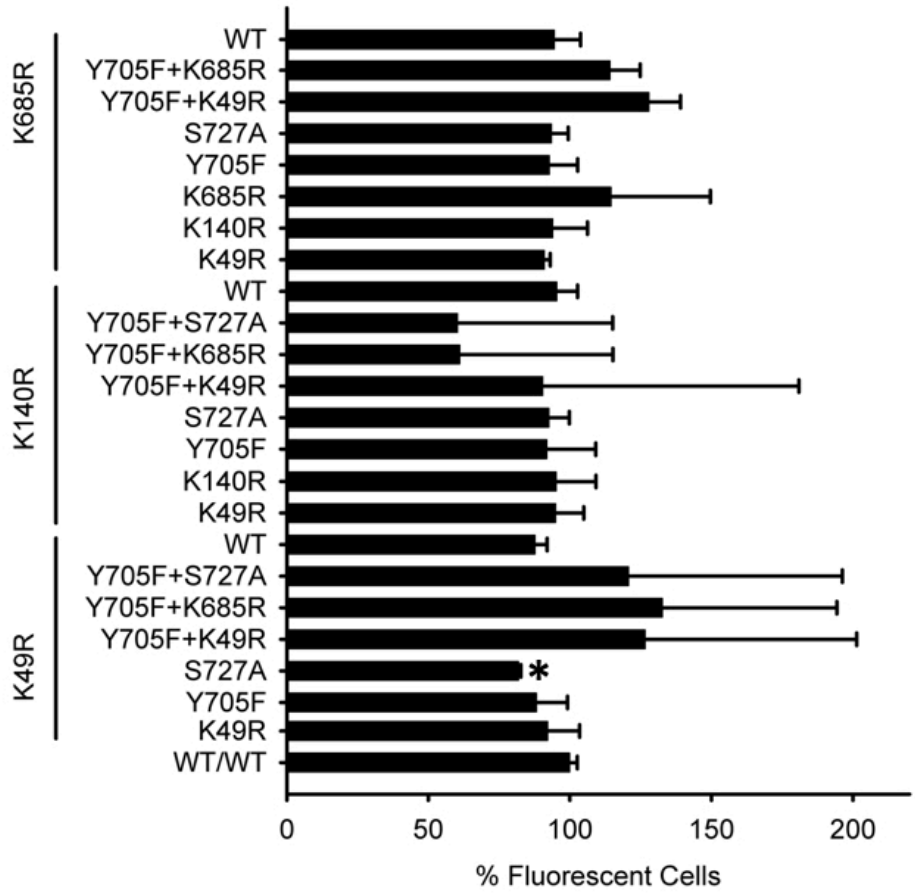

Figure 24 - Inactivating mutations in key lysine residues only regulate unstimulated *STAT3* dimerization in pairs containing a mutation in residues K49 and S727 - The graph represents the percentage of fluorescent cells observed in each *Venus-STAT3* BiFC combination by means of flow cytometry, normalized versus the symmetric wild type pair (WT/WT). Errors represent the Standard Deviation. Statistical analysis was carried out by means of a ANOVA. Data are shown as the average ± SD, n=3. Significant vs the symmetric WT STAT3 pair, *, $P < .05$

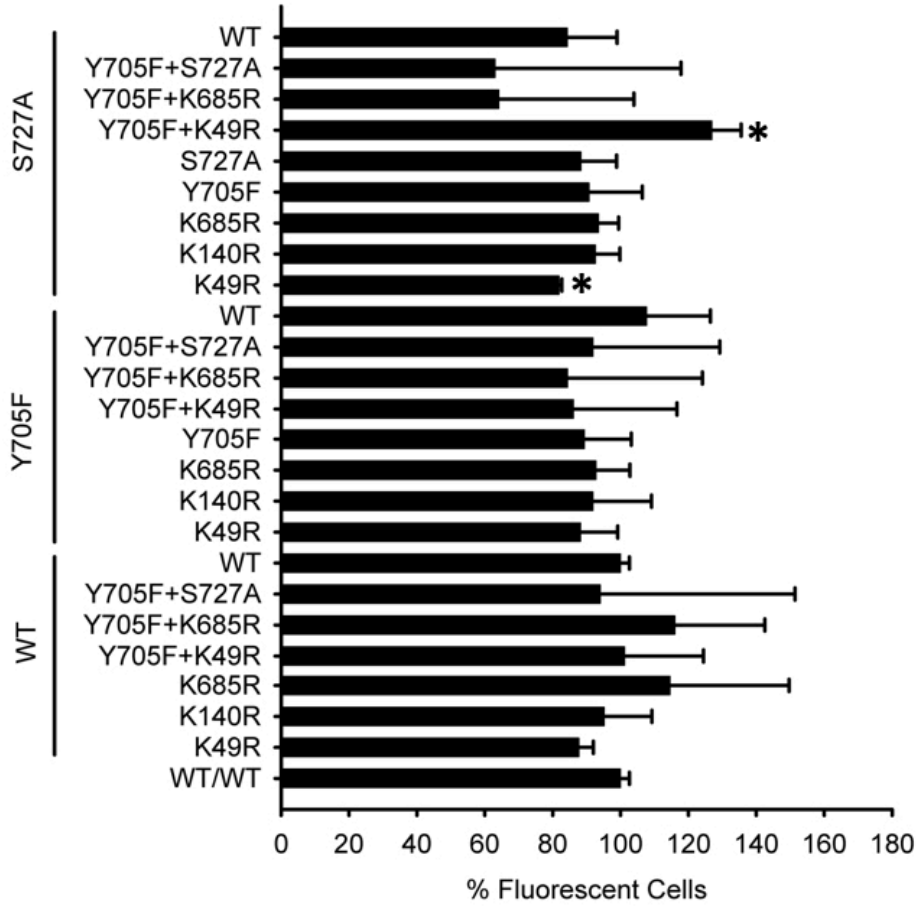

Figure 25 - Genetic blockage of key phosphorylatable residues only regulate unstimulated *STAT3* dimerization in pairs containing mutation in residue S727 and K49 - The graph represents the percentage of fluorescent cells observed in each *Venus-STAT3* BiFC combination by means of flow cytometry, normalized versus the symmetric wild type pair (WT/WT). Errors represent the Standard Deviation. Statistical analysis was carried out by means of ANOVA. Data are shown as the average ± SD, n=3. Significant vs the symmetric WT *STAT3* pair, *, $P < .05$

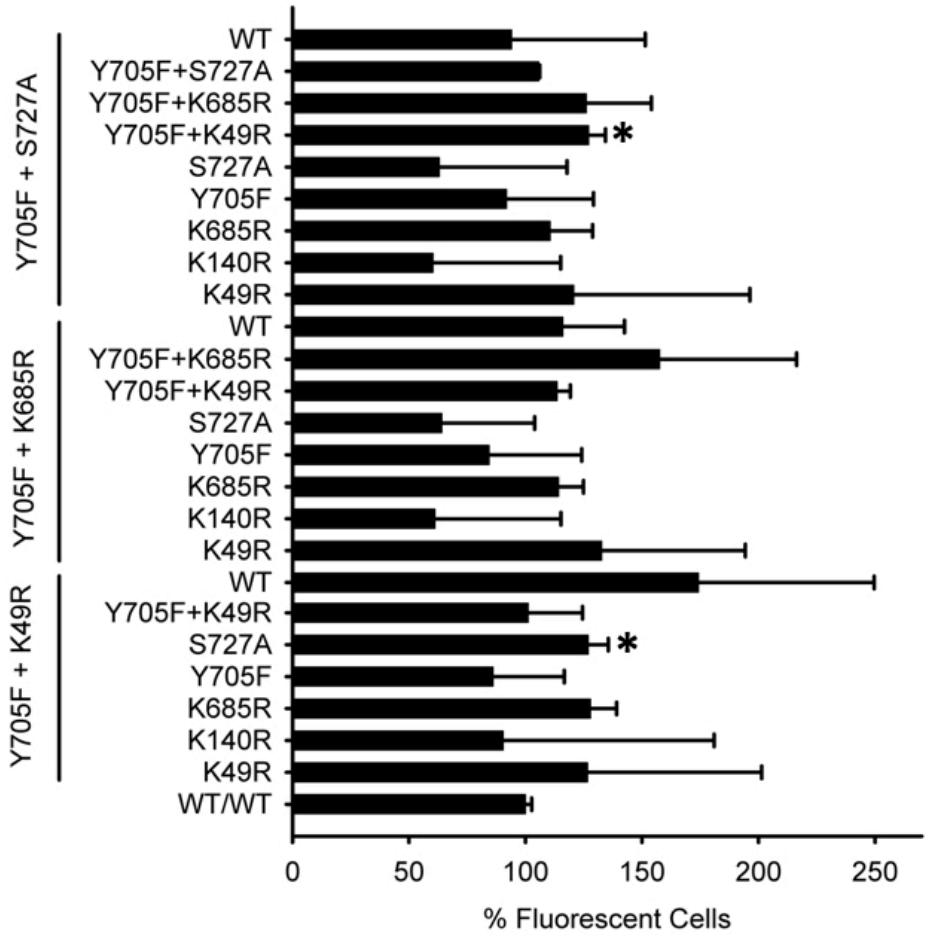

Figure 26 - Double PTM mutations containing S727A or K49R in a dimer containing also S727A or K49R increase homodimerization of unstimulated *STAT3* - The graph represents the percentage of fluorescent cells observed in each Venus-STAT3 BiFC combination by means of flow cytometry, normalized versus the symmetric wild type pair (WT/WT). Errors represent the Standard Deviation. Statistical analysis was carried out by means of ANOVA. Data are shown as the average ± SD, n=3. Significant vs the symmetric WT STAT3 pair, *P < .05

However, the intracellular distribution of STAT3 homodimers was significantly altered by specific combinations of STAT3 molecules (Fig. 27). Unlike the K49R symmetric pair (Fig. 22), K49R asymmetric

combinations dominantly induced an increase in cells with homogeneous nucleocytoplasmic fluorescence at the expense of cytoplasmic location (Fig. 27), similar to the Y705F symmetric pair (Fig. 22). K140R- or K685R-containing pairs showed some tendency to shift cytoplasmic location toward the nucleus, but only the K140R + S727A combination achieved significance. This phenotype was almost identical to the Y705F + S727A asymmetric pair (Fig. 27).

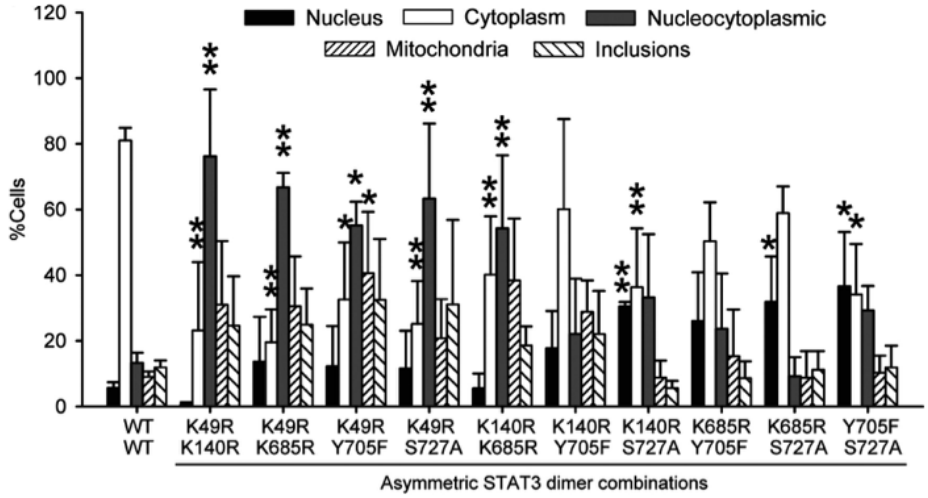

Figure 27 - Asymmetric signal transducer and activator of transcription 3 (*STAT3*) post-translational modifications regulate intracellular distribution of *STAT3* homodimers - Intracellular distribution of fluorescence in asymmetric combinations of Venus-STAT3 bimolecular fluorescence complementation (BiFC) constructs (and the WT symmetric pair as reference). Data are shown as the average of n = 12 (WT, wild-type) or n = 3 (rest of combinations) independent experiments ± SEM. Statistical analysis was carried out by means of a two-way ANOVA followed by a Bonferroni test adjusted for multiple comparisons. Significant vs the symmetric WT STAT3 pair, *, P < .05, **, P < .01.

We then pooled and re-analyzed all results according to the number and type of PTM mutations present in each BiFC pair.

Combinations carrying any one (asymmetric) or two K-R substitutions (symmetric or asymmetric) significantly increased mitochondrial translocation, while decreasing the percentage of cells with STAT3 dimers predominantly in the cytoplasm (Fig. 28A). As a reminder, K-R substitutions prevented all possible modifications at the corresponding lysine (K) residues, such as acetylation, methylation or ubiquitination. Asymmetric combinations of one K-R substitution and one phosphoresistant mutant also increased nuclear translocation, but only 2×K-R combinations increased homogeneous nucleocytoplasmic distribution. Combinations carrying any two phosphoresistant mutations (symmetric or asymmetric) had no significant effect on cellular distribution of resting STAT3 homodimers (Fig. 28A). These results indicated that specific asymmetric PTMs on STAT3 dimers can prevent their nuclear import/export. This was later confirmed by pooling the data according to whether the STAT3 pair was symmetric or asymmetric in their PTM mutations (Fig. 28B). We found that only asymmetric PTM mutant combinations increased nucleocytoplasmic or nuclear distribution at the expense of decreasing cytoplasmic localization of STAT3 homodimers. Asymmetric combinations were also sufficient to produce an increase in

mitochondrial localization of STAT3 dimers (Fig. 28).

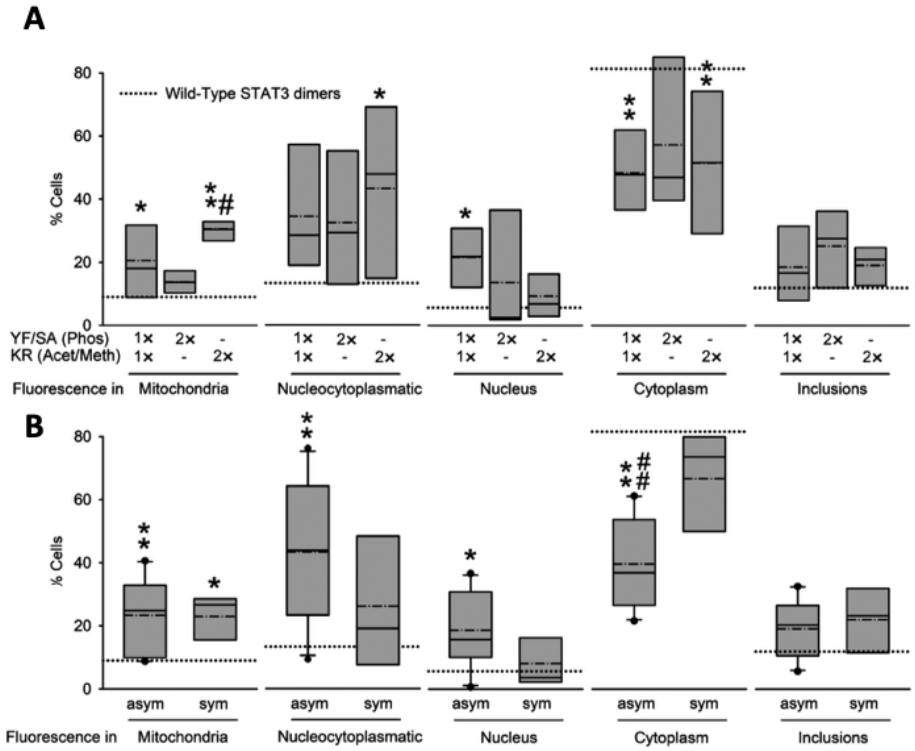

Figure 28- Asymmetric dimers lead to higher differences in *STAT3* dimer localization - Intracellular distribution of fluorescence in asymmetric combinations of Venus-STAT3 bimolecular fluorescence complementation (BiFC) constructs (and the WT symmetric pair as reference). Data are shown as the average of n = 12 (WT, wild-type) or n = 3 (rest of combinations) independent experiments ± SEM. Statistical analysis was carried out by means of a two-way ANOVA followed by a Bonferroni test adjusted for multiple comparisons. Significant vs the symmetric WT STAT3 pair, *P < .05, **P < .01. B, The same original data from Figure 22 and 27 but pooled according to the number and nature of substitutions (A) or the symmetry or asymmetry of substitutions (B) in the STAT3 homodimer, and represented as box plots. The limits of the boxes represent the smallest and largest values, the straight line represents the median, the dashed line represents the average, and the dotted line represents the average for WT STAT3 pair. Statistical analysis was carried out on the Average ± SEM of each pool of data (1×YF/SA:1×KR, n = 6; 2×YF/SA, n = 3; 2×KR, n = 6; sym, n = 5; asym, n = 10). Significant vs the symmetric WT STAT3 pair, *P < .05, **P < .01; significant vs 2×YF/SA substitution (A) or the symmetric mutant pairs (B), #P < .05, ##P < .01

STAT3 contributes to cancer cell survival, proliferation and malignant transformation even in conditions where it is not stimulated by cytokines (Burke et al., 2001; R. Garcia et al., 1997; M. Huang, Page, Reynolds, & Lin, 2000; Srivastava & DiGiovanni, 2016; Turkson & Jove, 2000), and mitochondrial STAT3 could promote oncogenic transformation in certain biological contexts (Gough et al., 2009; Q. Zhang et al., 2013). In order to know if there were biological consequences of the observed changes of behavior in unstimulated STAT3 dimers, HeLa cells were transfected with the different combinations of constructs and their proliferation was determined 24 hours later (Fig. 29). The asymmetric combinations K49R/K140R, K140R/K685R and K685R/S727A increased significantly the number of cells versus control cultures transfected with wild type STAT3. Among the symmetric combinations, only the K49R pair showed a smaller but significant increase in cell proliferation. These results indicate that asymmetric dimers of STAT3 could have differential biological effects.

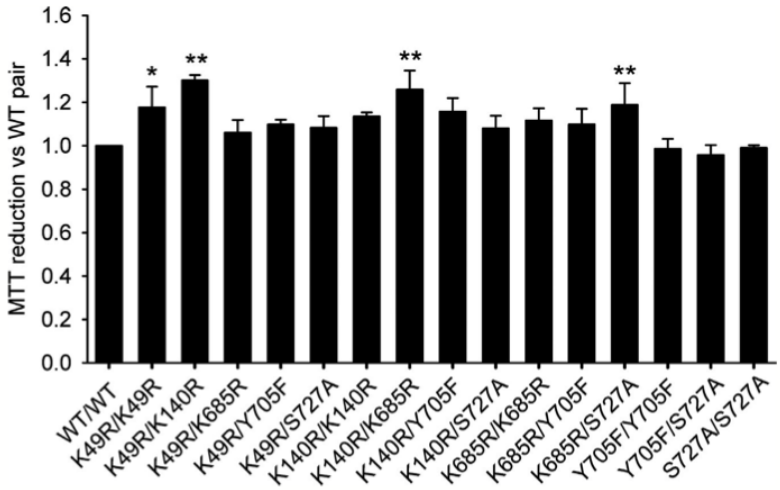

Figure 29 - Post-translational modifications regulate cell proliferation after unstimulated *STAT3* dimerization - HeLa cells transfected with different combinations of the STAT3 BiFC constructs reveal significant differences in the increase of MTT

reduction, in the pairs K49R/K49R, K49R/K140R, K140R/K685R and K685R/S727A when compared with the WT STAT3 pair. *p<.,05, **p<0.01

Generation of a HeLa cell line knocked out for endogenous STAT3

HeLa cell lines express endogenous STAT3 that could interfere with the behavior of exogenous STAT3 BiFC constructs, and this was a criticism raised by reviewers during the publication of our paper on STAT3 (Letra-Vilela et al., 2020). Thus, we produced a HeLa STAT3-/- cell line by means of a CRISPR/Cas9 approach (Fig. 30). However, in our conditions, the level of expression of endogenous STAT3 was very low in comparison to the expression of transfected STAT3 (Fig. 31), making it difficult for endogenous STAT3 to interfere significantly with exogenous STAT3.

Figure 30 - *STAT3* levels of HeLa knockout cells - Total proteins (40 µg) have been extracted from HeLa WT and STAT3 KO cell lines. Blot probed for *STAT3*. KO of *STAT3* from HeLa cells do not express endogenous *STAT3* as expected.

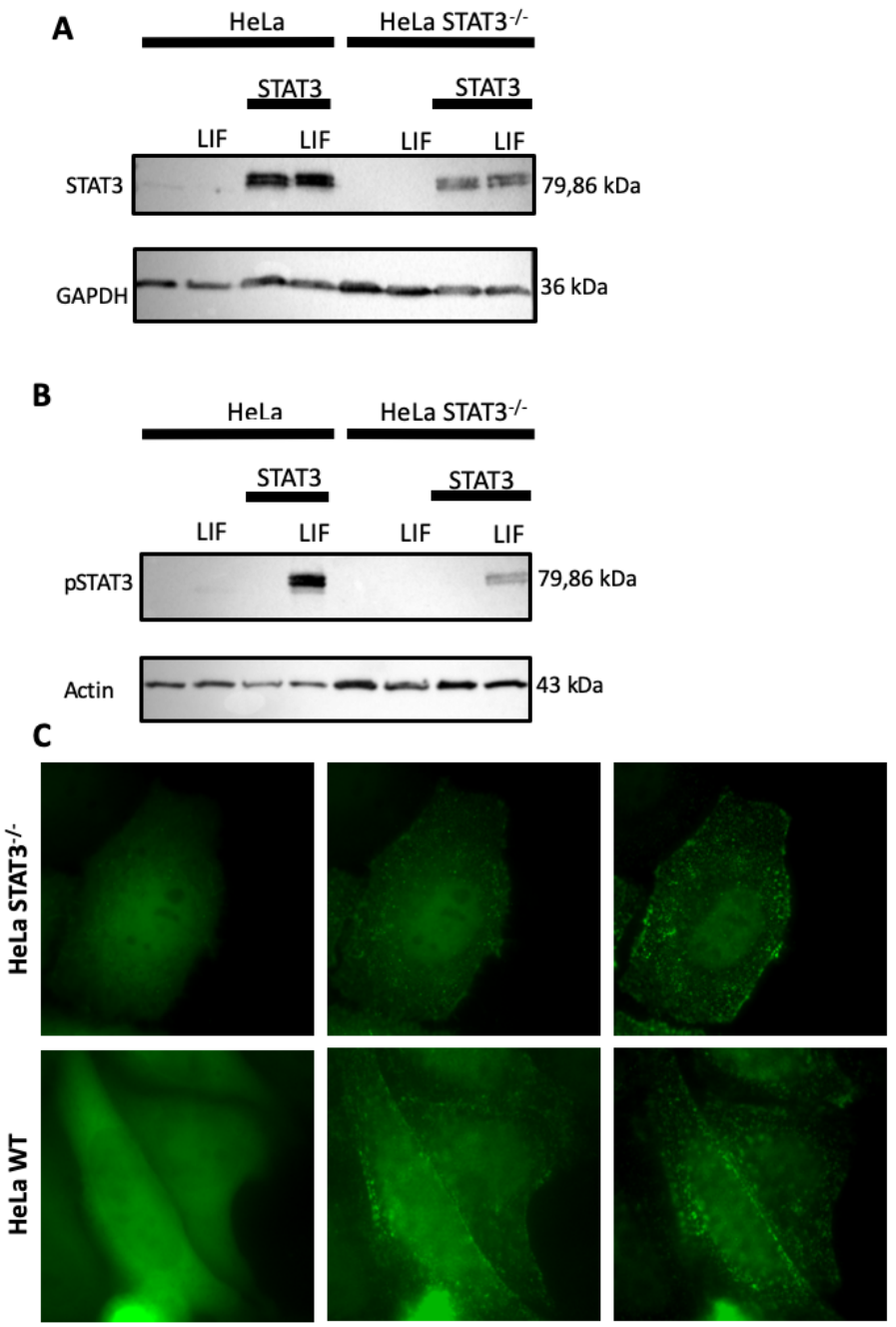

Figure 31 - Expression and phosphorylation of *STAT3* in HeLa WT and *STAT3* KO cells- Total proteins (40 µg) have been extracted from HeLa WT and STAT3 KO cell lines. In both cell lines STAT3 BiFC pair have been transfected and stimulated with LIF

(100ng/nl) after 2 hours of serum starvation. A) Blot probed for STAT3. KO of STAT3 from HeLa cells decrease the expression of transfected STAT3. B) Blot probed for pSTAT3. C, WT and $STAT3^{-/-}$ HeLa cells present nuclear translocation of transfected WT STAT3 after stimulation with 100 ng/mL of LIF. 2 hours after LIF stimulation it was performed a time lapse of both experimental groups.

LIF stimulation (100 ng/mL) for 2 hours in the absence of serum produced nuclear translocation of STAT3 dimers in both wild type and $STAT3^{-/-}$ HeLa cells transfected with STAT3 BiFC constructs (Fig. 31). More tests need to be done to fully characterize the cell line in order to determine the effects of the lack of endogenous STAT3 in the physiology of the cell. The HeLa STAT3-free system is currently in use in Dr. Herrera´s laboratory.

Development of new BiFC constructs for the study of underexplored STAT3 PTM sites

K49, K140, K685, Y705 and S727 are the most studied PTM sites, and we have shown above that they are also relevant to intracellular localization and pro-tumoral action of unstimulated STAT3. However, STAT3 has more than 80 possible PTMs, which have been barely explored. Plasmids containing WT STAT3 fused to the Venus halves were used as template to synthetize 12 additional mutated versions of STAT3 targeting phosphorylatable residues Y45, Y68, Y79, Y176, S181 and S691 (Fig. 32). Mutations were induced in both VN and VC BiFC constructs, which will allow symmetric and asymmetric combinations of the different PTM-mutants.

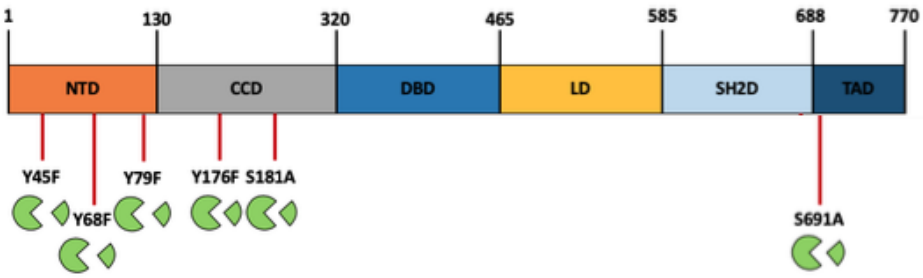

Figure 32 - PTM-mutants of underexplored phosphorylatable sites at *STAT3* - To understand the relation of underexplored phosphorylation events with the homodimerization and the pattern of intracellular distribution of STAT3, different Venus-STAT3 BiFC plasmids were generated. VN and VC plasmids are represented by the complementary fragments of green circles. The mutants were originated by means of Site Directed Mutagenesis using as template the Venus-STAT3 WT BiFC plasmids. For each mutation, two plasmids were originated, one with the first halve of Venus (VN) and other with the second (VC). The residues mutated are present in the N-Terminal Domain (NTD), Coiled Coil Domain (CCD) and Transcription Activation Domain (TAD), which play key roles in STAT3 dimerization and protein-protein interactions, among other regulatory functions.

With these new constructs, it will be possible to study the effect of the different PTMs in the dimerization and distribution of the respective dimers. There are 27 new possible combinations of VN and VC STAT3 versions, but more than 100 possible combinations if we combine them with the previous PTM mutants. We have not proceeded with the analysis of these mutants due to the time constrains for this thesis, but they will serve for future studies in the main line of work of Herrera´s lab.

Polo-like kinase (PLK)-1 inhibitors reduce spontaneous STAT3 dimerization

Our STAT3 BiFC system could allow pharmacological or genetic high-throughput screenings to test STAT3 homodimerization. To establish a proof-of-concept, we used the BiFC system to carry out a pharmacological screening with a library of 194 kinase inhibitors, of which

I have tested 82. We established stringent criteria to accept a hit as positive. First, it had to produce a fold-change in the fluorescence levels lower than 0.5 or higher than 2. Second, the inhibitor should not be significantly toxic to cells nor modify STAT3 protein levels. Third, several different inhibitors for the same kinase –when available- should show similar results.

As we can observe in figure 33, some kinase inhibitors decreased the percentage of fluorescence (black bars), namely Hesperadin (73), PHA-680632 (75) and SNS-314 Mesylate (76) for Aurora (Fig. 33 B), BI 2536 (57), GSK 461364 (58), HMN-214 (59) and ON-01910 (60) for PLK1, Flavopiridol (Alvocidib) (62) for CDK, AZD7762 (68) for CHK and AS703026 (79) for MEK (Fig. 33 C). However, in most cases they were isolated cases. Only four kinase inhibitors belonging to the PLK-1 seemed to have a consistent pattern, decreasing the percentage of fluorescence more than 50% (57, 58, 59 and 60, Fig. 33 C, black bars). PLK-1 inhibitors were not significantly toxic for cells at the concentration tested (Fig. 33 C, white bars). Aside from the PLK-1 family, the Aurora (3 out of 12), the cyclin-dependent kinase (CDK) (1 out of 7) and the MEK (1 out of 4) families and also the checkpoint kinase (CHK) inhibitor have all shown a significant decrease in the levels of STAT3 dimerization.

Only one of the tested inhibitors increased the percentage of fluorescence more than 2-fold: Sunitinib Malate (28) for VEGFR (Fig. 32 A, black bars). However, this inhibitor was auto fluorescent (Fig. 34). Of the c-met family of inhibitors, 4 out of 6 showed a tendency towards the increase of percentage of fluorescence, but the most noteworthy were PF-2341066 (49) and SU11274(PKI-SU11274) (51). These two, however, did not overcome the threshold set for the needed increase in fluorescence and so were excluded from these preliminary experiments.

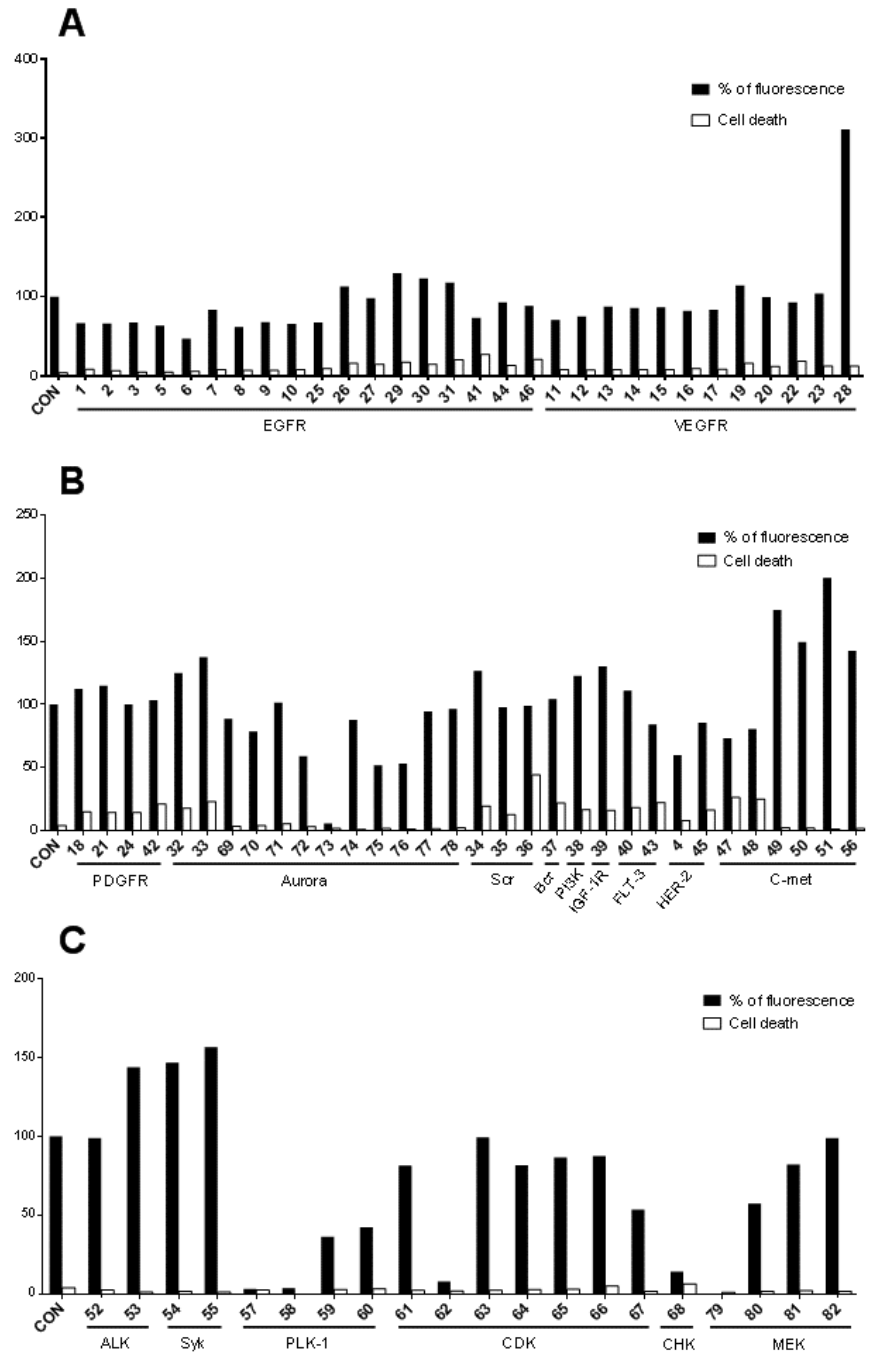

Figure 33 - Screening with a library of kinase inhibitors - HEK cells were transfected with both *Venus-STAT3* BiFC plasmids (N-STAT3 and C-STAT3) and treated with a library of kinase inhibitors (1μM). Flow cytometry results show the amount of *STAT3* dimers in

the presence of the inhibitors (black bars) and also the toxicity of the inhibitors to cells (white bars). *Venus-STAT3* BiFC construct was used as control (CON).

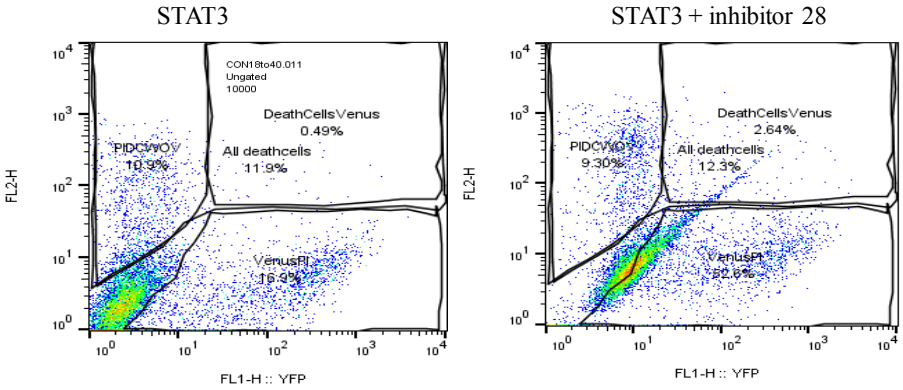

Figure 34 –Kinase inhibitor 28 is autofluorescent - HEK cells were transfected with both Venus-STAT3 BiFC plasmids (VN-STAT3 and VC-STAT3) and treated kinase inhibitor 28 (1μM). Flow cytometry results show a shift to the right when the cells were exposed to the inhibitor. STAT3 without the inhibitor was used as control.

Discussion

We have successfully developed and validated a new BiFC assay for the visualization and study of STAT3 interactions in living cells. The STAT3 BiFC system shows the expected responses to pharmacological activation and inhibition, to mutations linked to genetic disorders and the interaction with other proteins (Fig. 20B). As other systems reported for the study of STAT3 dimerization, BiFC also has some limitations. The reconstitution of the fluorophore is irreversible, stabilizing interactions that otherwise would be transient. However, it is also true that this same property allows for the detection of low frequency and very fast interactions that could be missed by other methods. The Venus BiFC systems are prone to high background, but our experiments with pharmacological inhibitors and a high number of mutant combinations indicate that the system is still sensitive to changes in STAT3 dimerization. Furthermore, only the dimers with complementary reporter fragments are observed, and it is possible that non-fluorescent dimers are formed between STAT3 molecules that carry the same Venus fragments, as well as with endogenous STAT3. This limitation is unavoidable, but at least we can observe a representative population of STAT3 dimers, and by the properties of the system, we know exactly which is the nature of the two monomers involved. However, we have developed a HeLa STAT3 KO cell line in order to prevent the interactions with endogenous STAT3. This line is currently being used in Herrera´s lab for analysis of the effects of PTMs on cytokine-stimulated STAT3 dynamics. Nevertheless, our Venus-STAT3 BiFC system can be applied to any type of protein-protein interaction in living cells, is easy to use and scale up for high-throughput and is complementary to existing methods for the analysis of STAT3 dimerization in living cells.

We have observed that asymmetric PTMs could constitute a new level of regulation of unstimulated STAT3 behavior and function. This

result raises a new hypothesis of dimer formation different from what have been described until now in the literature. Studies performed until now do not differentiate between monomers and dimers (Dasgupta et al., 2015, 2014; Kang et al., 2017; Ray et al., 2005b; Wegrzyn, Potla, Chwae, Sepuri, Zhang, et al., 2009; J. Yang et al., 2005, 2010; Q. Zhang et al., 2013) and use or assume a single population of STAT3 molecules, either mutated or normal (Domoszlai et al., 2014; Okada et al., 2018; Schröder et al., 2004). However, the probability for two identical STAT3 molecules to form a dimer should be low in the complex and crowded intracellular environment, although it could certainly be enhanced by either total absence or presence of stimuli. As an example, most of STAT3 molecules do not suffer phosphorylation in the absence of cytokine stimulation, although there are small amounts of phosphorylated STAT3 in resting state. Unphosphorylated and phosphorylated STAT3 should coexist at similar levels in many situations, and the literature presents evidence that this could be equally true for other STAT3 PTMs induced by cytokines (Dasgupta et al., 2015; Kang et al., 2017; Ray et al., 2005b; J. Yang et al., 2010).

We have performed all our experiments in cells that express endogenous STAT3, which could somewhat interfere with the system. However, we can argue that we have observed changes in asymmetric combinations but not in symmetric combinations, with endogenous STAT3 present in both cases. Assuming that endogenous STAT3 interfere homogeneously in all possible combinations, it is unlikely that our results are explained by interference of endogenous STAT3. Therefore, the presence of endogenous STAT3 does not necessarily invalidate our hypothesis, although new experiments in STAT3 knockout context should be performed.

Our results have showed that some asymmetric PTMs lead STAT3 towards mitochondria. There, it is possible that it can act at the level of

transcriptional modulation of mitochondrial genes related to the electron transport chain (Macias, Rao, Carbajal, Kiguchi, & DiGiovanni, 2014) or as a direct regulator of the mitochondrial electron transport activity (Wegrzyn, Potla, Chwae, Sepuri, Zhang, et al., 2009). Until now, it is not defined the exact mechanism that lead to STAT3 translocation, or the exact PTMs that regulate each possible function of STAT3 inside mitochondria. Our results could indicate that PTM configuration play a role in STAT3 localization inside of mitochondria, function and even in translocation.

It is also important to note that all the experiments were done in the absence of cytokine stimuli making all the PTMs studied relevant for the function of unphosphorylated STAT3. USTAT3 can homodimerize, translocate to the nucleus, interact with transcriptional regulators, bind to DNA and regulate the transcription of a set of genes, such as E2F1, M-Ras or Met (Braunstein et al., 2003; Nkansah et al., 2013a; J. Yang et al., 2005, 2007). In fact, when compared with canonical STAT3 phosphorylation and signaling, USTAT3 persists several days after IL-6 induction and supports gene expression in a prolonged manner (Cheon, Yang, & Stark, 2011). Our system can be a useful tool for the validation and study of all these processes.

Chapter 3

Results (Part II)

STAT3 PTMs regulate its interaction with *GRIM-19* and consequent function

Introduction

The intracellular distribution of unphosphorylated STAT3 is not restricted to the cytoplasm and the nucleus. It can also be found in the mitochondria and endoplasmic reticulum (Avalle et al., 2019; Su et al., 2020). Mitochondrial STAT3 is responsible for the transcriptional regulation of specific mitochondrial genes (R. Yang & Rincon, 2016), but also to the transcription-independent regulation of mitochondrial respiration (Tammineni et al., 2013). STAT3 binds directly and increases the activity of components of the electron transport chain, such as succinate oxidoreductase (complex II), ATP synthase (complex V) and lactate dehydrogenase (Wegrzyn, Potla, Chwae, Sepuri, Zhang, et al., 2009). Mitochondrial STAT3 promotes tumor growth and metastasis in breast cancer (Q. Zhang et al., 2013). However, how STAT3 enters mitochondria remains a matter of discussion. No mitochondrial localization signal has been identified in the STAT3 amino acid sequence, although the C-terminus is clearly necessary for mitochondrial localization (Tammineni et al., 2013). There is evidence indicating that the GRIM19 protein could be a transporter for STAT3 to the mitochondria.

The human GRIM19 gene encodes for a small mitochondrial protein that can be also found in the nucleus and cytoplasm (J E Angell et al., 2000; Fearnley et al., 2001). This gene was initially described as a mediator of IFN/Retinoic acid-induced cell death (Jon E. Angell et al., 2000). Later, GRIM19 was also reported as a component of complex I in the electron transport chain, and also localized in the nucleus, where it has been described as a negative transcriptional regulator of STAT3 (Jon E. Angell et al., 2000; Fearnley et al., 2001; Guochang Huang et al., 2004; Kalakonda, Nallar, Gong, et al., 2007; Lufei et al., 2003; Okamoto et al., 2010; J. Zhang et al., 2003). GRIM19 interacts with STAT3 directly, and their interaction promotes mitochondrial accumulation and inhibits STAT3 translocation to the nucleus (Okamoto et al., 2010; J. Zhang et al., 2003).

Phosphorylation at residue S727 is necessary for STAT3-GRIM19 interaction, although phosphorylation at Y705 has been also observed in mitochondrial STAT3 (Gough et al., 2009; Wegrzyn, Potla, Chwae, Sepuri, Koeck, et al., 2009). In cancer cells where STAT3 is highly expressed, the presence of GRIM19 can stop the cell cycle in G1 phase and lead to cell death. STAT3 and GRIM19 interaction can therefore have two distinct roles, negatively regulating STAT3 pathway and participating in the respiratory chain.

Results

Generation of a BiFC system for STAT3 - GRIM19 interaction

In the previous chapter, we described the presence of STAT3 in mitochondria in a small percentage of cells (Fig. 20), and an increased mitochondrial STAT3 localization induced by some asymmetric combinations of STAT3 homodimers (Fig. 27). The same constructs used to study STAT3 homodimerization are useful to analyze STAT3 interactions with other proteins (heterodimerization). To analyze the interaction between STAT3 and GRIM19, we synthesized a new BiFC construct carrying human GRIM19 tagged in the N-terminus with the VC Venus fragment.

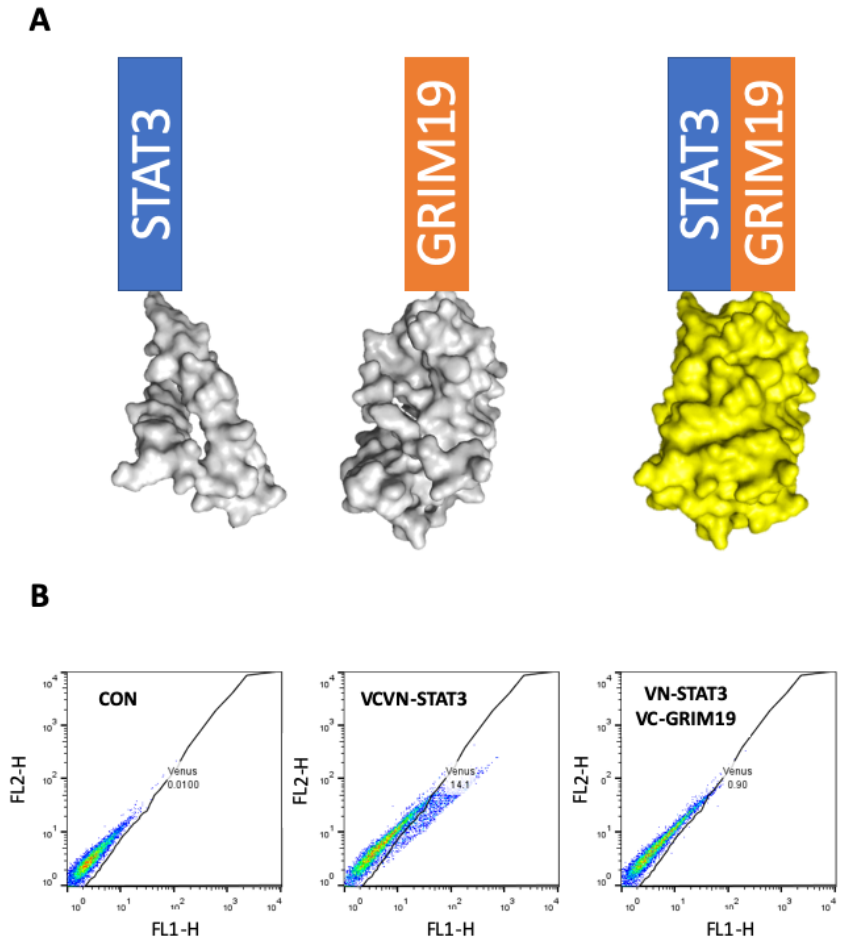

Figure 35 - Unstimulated cells do not present interaction between *GRIM19* and *STAT3* - A, BiFC system developed for the study of STAT3 and GRIM19 interaction. B, Hela cells were transfected with the STAT3-GRIM19 BiFC pair or STAT3-STAT3 pair and analyzed by means of Flow Cytometry 24h after transfection. Ten thousand events were counted and plotted. The STAT3 - GRIM19 BiFC pair did not show any fluorescence, similar to non-transfected cells (negative control). Cells transfected with the WT STAT3-STAT3 BiFC pair were used as a positive control.

When unstimulated cells were transfected with the STAT3/GRIM19 BiFC constructs, there was very little fluorescence, indicating that unstimulated STAT3 did not interact with GRIM19 (Fig. 35B). By microscopy, it was possible to observe that the very few

fluorescent cells detected by flow cytometry had their signal localized in the mitochondria (Fig. 36).

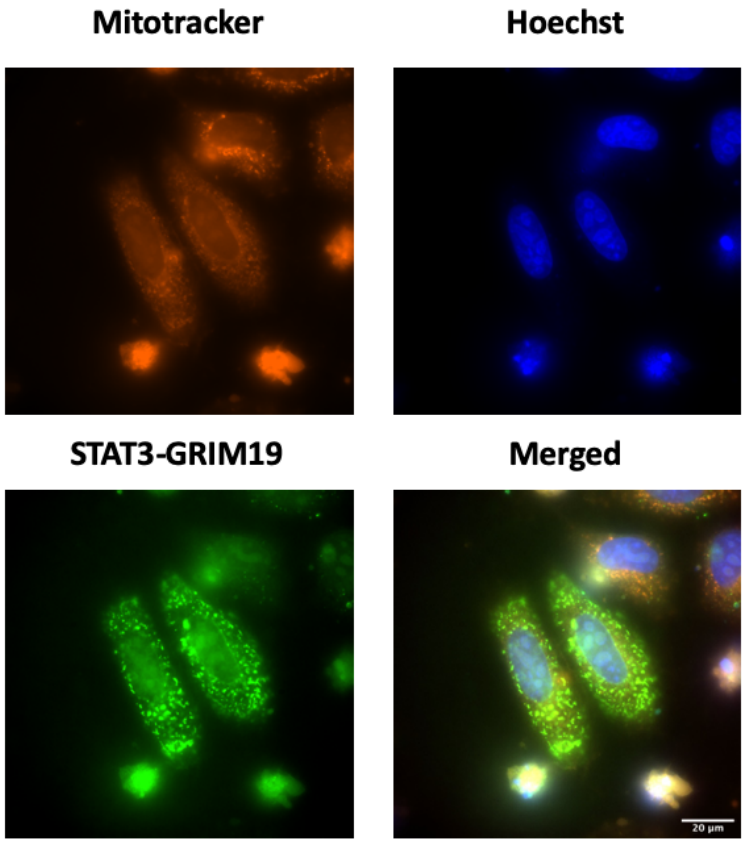

Figure 36 - *STAT3-GRIM19* dimers localize to the mitochondria - HeLa cells were transfected with the V2-GRIM19 and VN-STAT3 WT BiFC constructs. In red, mitochondria stained with Mitotracker dye; in blue, nuclei stained with Hoechst 33342 dye; and in green, STAT3-GRIM19 dimers (Venus fluorescence). STAT3-GRIM19 heterodimers mainly localize to the mitochondria. Scale bar - 20µm

Dimerization between GRIM19 and STAT3 is induced by cytokines and affected by specific PTMs

Taking advantage of the STAT3 PTM mutants previously generated, we analyzed the effect of specific PTMs on GRIM19-STAT3 interaction in the presence or absence of LIF, a cytokine known to induce STAT3 activation. In the absence of cytokines, the wild type and PTM-mutant versions of STAT3 barely interacted with GRIM19 (Fig. 37). However, after LIF stimulation for 2 hours in the absence of serum, a significant increase in the interaction was observed for all BiFC pairs. K49R, K140R and S727A STAT3 mutants showed a significant increase in the percentage of fluorescent cells versus STAT3 WT, suggesting that these specific residues played a key role in STAT3-GRIM19 interaction. The K685R and Y705F mutants did not change significantly the level of interaction with GRIM19 in comparison to WT STAT3.

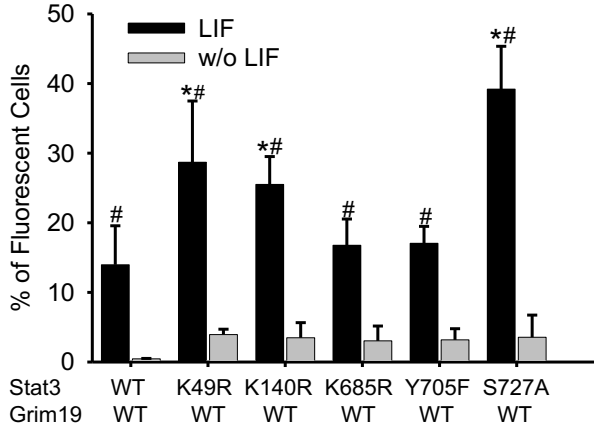

Figure 37 – Genetic blockage of PTMs at the residues K49, K140 and S727 led to potentiation of the interaction with *GRIM19* after LIF stimulation - Hela cells transfected with BiFC pairs of Mut STAT3 and GRIM19 were analyzed by means of Flow Cytometry before and after LIF stimulation. All the pairs increase the levels of fluorescent cells after LIF stimulation indicating and increase when compared with the respective pairs in unstimulated cells. The K49R, K140R and S727A PTM-inactivating mutations in STAT3 induced a significant increase in the percentage of fluorescent cells versus the combination containing wild type STAT3 upon LIF stimulation. Flow cytometry was performed 24h after transfection with BiFC constructs. Cells were incubated with leukemia inhibitory factor (100ng/mL) for 2h in the absence of serum. Results were normalized vs the WT STAT3

pair (100%). Data are shown as the average of n = 3 independent experiments ± SD. Statistical analysis was carried out by means of a two-way ANOVA followed by a Bonferroni test adjusted for multiple comparisons. P < .05.

STAT3-GRIM19 dimers control intracellular ATP levels

The interaction between STAT3 and GRIM19 can have an effect in the expression of genes regulated by STAT3 (Lufei et al., 2003; J. Zhang et al., 2003) or in the activity of the electron transport chain at the mitochondria (Demaria et al., 2010). Since the electron transport chain is the main source of ATP, measuring the intracellular levels of ATP can give an indirect hint of the functional consequences of the interaction of STAT3-GRIM19 dimers with the mitochondrial electron transport chain (Fig. 38). HeLa cells were transfected with GRIM19 and STAT3 BiFC pairs and stimulated with LIF (100 ng/mL) for 2 hours before determination of ATP levels. PTM-inhibitory mutations at K49, K140 and Y705 residues decreased the ATP content to half when compared with cells transfected with WT STAT3. The remaining inhibitory mutations, K685R and S727A did not lead to significant differences when compared WT pair.

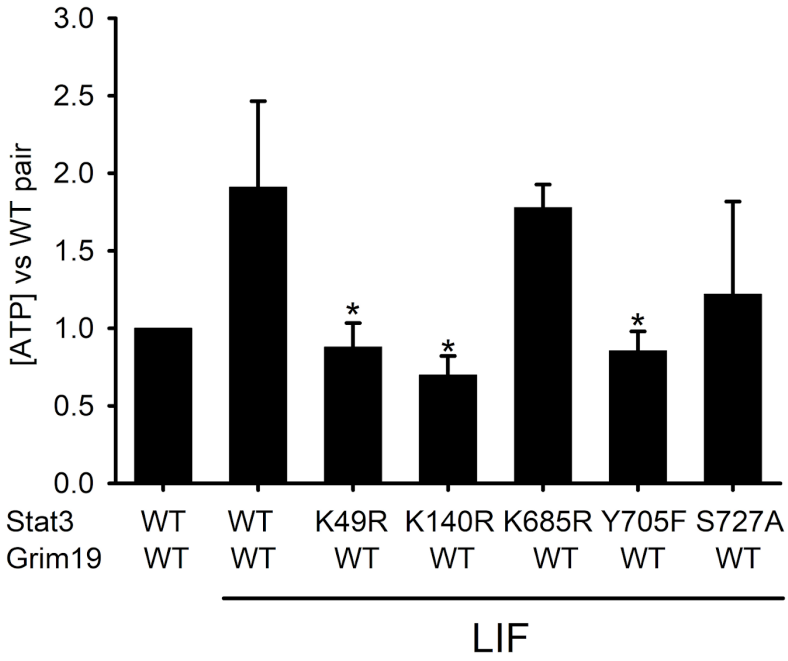

Figure 38 - Inhibitory mutations of PTMs of the residues K49 and K140 led to a decrease of ATP levels after LIF stimulation - ATP content of Hela cells transfected with BiFC pairs of mutant STAT3 and GRIM19 were analyzed after 2 hours of LIF (100ng/mL) stimulation. Cells transfected with STAT3/GRIM19 pair (WT without LIF) and cells without transfection and LIF stimulation (NC) were used as controls. All the groups under LIF stimulation correspond to the BiFC pairs of GRIM19 and STAT3 (WT or mutated). K49R STAT3/GRIM19 and K140R STAT3/GRIM19 pairs decrease the levels of ATP content after LIF stimulation in comparison with WT/GRIM19 pair and unstimulated cells. Results were normalized vs the WT STAT3 pair. Data are shown as the average of n = 3 independent experiments ± SD. Statistical analysis was carried out by means of a one-way ANOVA followed by a Bonferroni test adjusted for multiple comparisons. *, $P < .05$.

Development of a new system for STAT3 visualization by correlated fluorescence and electron microscopy (CLEM)

STAT3 interaction with GRIM19 could lead to different STAT3 localizations beyond mitochondria (e.g. the endoplasmic reticulum) or within mitochondria (e.g. external membrane versus internal membrane).

Ultrastructural localization of STAT3 could be useful to understand if any PTM would lead to different patterns of distribution inside smaller cell compartments. Thus, STAT3 was fused to the MiniSOG protein (Fig. 39), a relatively recent protein tag that allows detection by both fluorescence and electron microscopy (Qi, Garren, Shu, Tsien, & Jin, 2012; Shu et al., 2011).

Figure 39 - Schematic representation of MiniSOG-STAT3 construct – The miniSOG fluorescent tag was inserted in the C terminus of STAT3.

MiniSOG produces green fluorescence upon excitation at 450 nm. During this reaction, MiniSOG photogenerates $^1O_2$, which in the presence of Diaminobenzidine (DAB) forms an electron-dense polymer visible by transmission electron microscopy. These properties would allow correlated light and electron microscopy (CLEM) experiments (Qi, Garren, Shu, Tsien, & Jin, 2012; Shu et al., 2011). In figure 40, it is possible to see green fluorescent cells once they are excited and the formation of a dark polymer after the addition of DAB, which should be visible by electron microscopy.

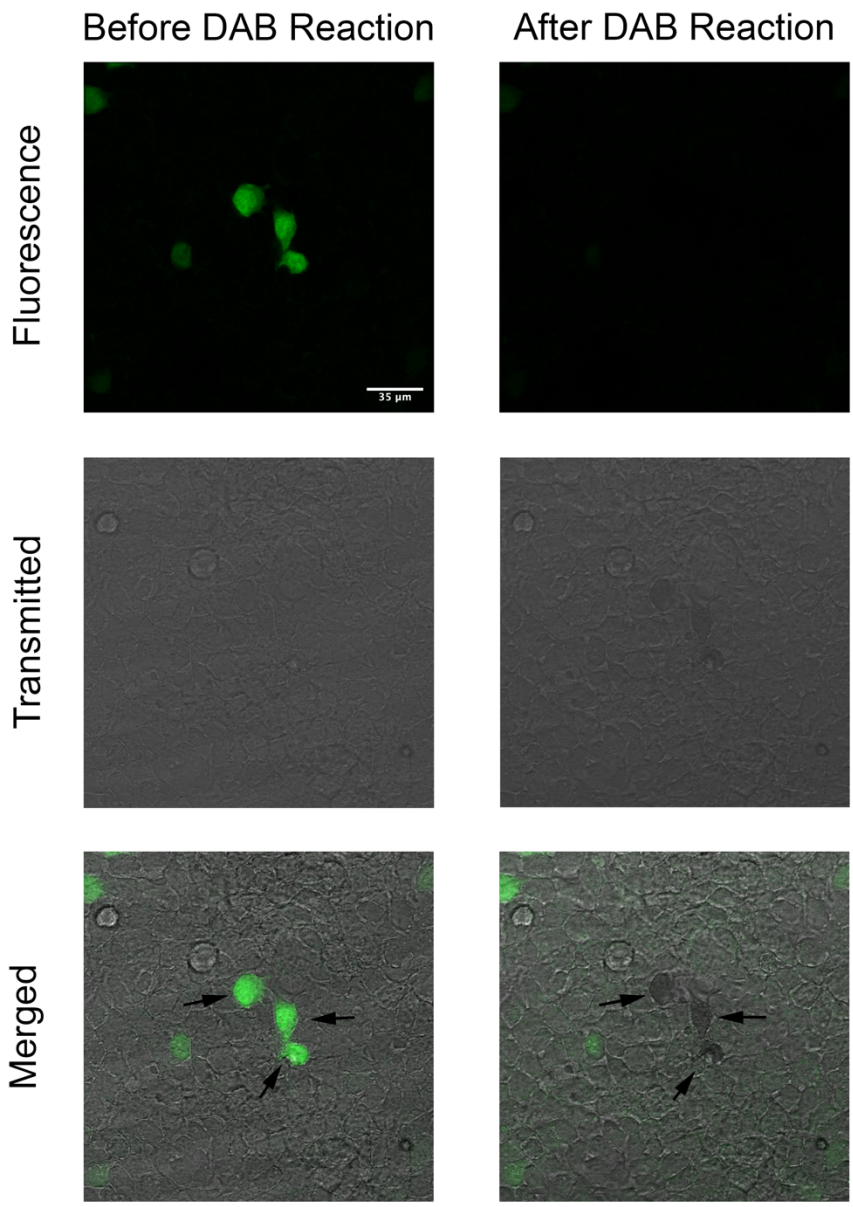

Figure 40 - *MiniSOG* properties - HEK cells have been transfected with a plasmid containing MiniSOG. Under the excitation of a blue laser, MiniSOG emits a green light and produce singlet oxygen that, in contact with DAB, it originates a dark polymer. Merging the photos obtained with transmitted light and with the blue laser excitation it is possible to localize the dark polymer originated in the same cells with the green light. Scale bar - 35µm

Complementary MiniSOG fragments are able to recover fluorescence

We next tried to generate split versions of the MiniSOG protein, in order to produce a BiFC system that would allow to detect protein-protein interactions at an ultrastructural level. Split locations were chosen in regions of the protein that were not alpha helix or beta sheet according to the existing structural data, and mammalian expression constructs carrying a series of complementary MiniSOG fragments were produced (Fig. 41). The fragments produced were 5 carrying the N-terminal part (from amino acid 1 to 138, 1 to 183, 1 to 192, 1 to 216 and 1 to 276) and 4 carrying the C-terminal part (from amino acid 138 to 321, 183 to 321, 216 to 321 and 276 to 321). Cells were transiently transfected with potentially complementary pairs of constructs and 24 hours later analyzed by flow cytometry to observe if complementary fragments regained fluorescence.

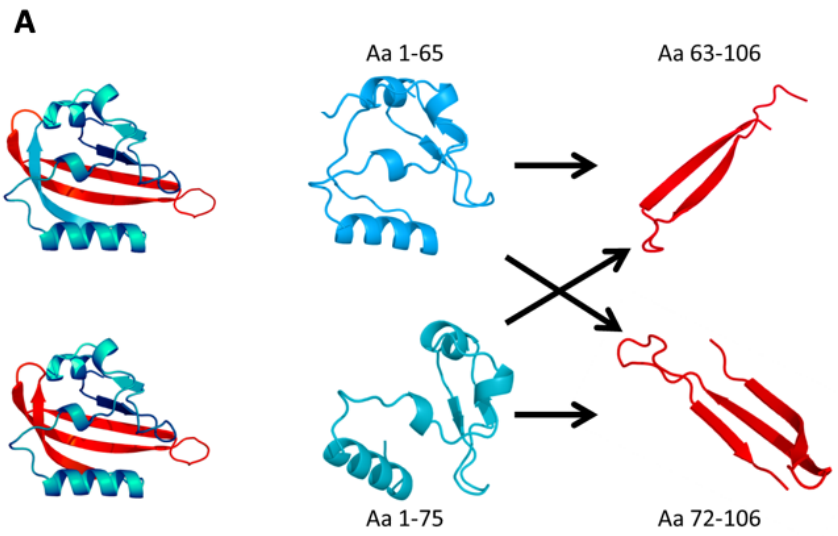

B

Nucleotides	138-321	183-321	216-321	276-321
1-138	+++			
1-183	+++	++		
1-192	+	+		
1-216	+	-	-	
1-276	-	-	-	-

Figure 41 - A split-*MiniSOG* system to visualize protein-protein interactions by CLEM - A, In the example, fragments comprised amino acids 1-65, 63-106, 1-75 and 72-106. In blue, the N-terminal fragment; in red, the C-terminal fragment. Fragments are not necessarily sequential and, in theory, could be intercombined. B, We designed 9 different fragments and combined them in all possible combinations. The output of this experiment was the recovery of MiniSOG green fluorescence (+, ++, or +++, according to the intensity of the recovered signal) being the +++ signal closer to the fluorescence emitted by the full-length protein.

Our results indicated that split versions of MiniSOG can recover fluorescence without the attachment to a protein of interest. The pairs that produced higher fluorescence intensity were N(1-138)+C(138-321), N(1-183)+C(138-321), followed by N(1-183)+C(183-321) and with less fluorescence signal N(1-192)+C(138-321), N(1-192+)C(183-321) and N(1-216)+C(138-231). The remaining ones, N(1-216)+C(183-321), N(1-216)+C(216-321), N(1-276)+C(138-321), N(1-276)+C(183-321), N(1-276)+C(216-321) and N(1-276)+C(276-321), did not produce fluorescence.

The fact that some of the combinations produce little or no fluorescence when coexpressed does not mean that they could not produce a functional fluorophore if they are brought together, e.g. by fusing them to potential protein-protein interactions. In order to determine whether these fragments could be useful to detect protein-protein interactions in CLEM experiments, we produced a series of constructs where we fused MiniSOG fragments to STAT3. These constructs comprised the fusion of all the N terminal halves of MiniSOG (1 to 138, 1 to 183, 1 to 192, 1 to 216 and 1 to 276 aminoacids) and the C terminal halves (138 to 321, 183 to 321, 216 to 321 and 276 to 321 aminoacids) to the N terminal part of STAT3. However, we failed to detect any fluorescence in these conditions. We are considering the possibility to introduce a linker sequence between MiniSOG tags and STAT3, in order to increase the flexibility of the chimeric proteins, and improve the chances of reconstituting the functional MiniSOG protein. Such system could be a major breakthrough in the field, as it would allow us to observe homo- and heterodimerization of STAT3 at an ultrastructural level, providing unprecedented spatial resolution.

Discussion

In this chapter, we have shown that the interaction of STAT3 with GRIM19 is induced by LIF stimulation on cells and that specific STAT3 residues can influence these interactions. K49R, K140R and S727A STAT3 mutants showed a significant increase in the percentage of fluorescent cells versus STAT3 WT. Phosphorylation at S727 is important for the interaction of STAT3 with the Complex I and it could be important for the interaction with GRIM19 (Jon E. Angell et al., 2000; Fearnley et al., 2001; Guochang Huang et al., 2004; Kalakonda, Nallar, Gong, et al., 2007; Lufei et al., 2003; Okamoto et al., 2010; J. Zhang et al., 2003). Inhibition of phosphorylation in the residue S727 and Y705 did not affect the ATP levels to the same extent as the other mutations, raising the hypothesis that other PTMs can be more important for the ETC function. STAT3 dimers can bind to mitochondrial DNA (R. Yang & Rincon, 2016), although it is also described that GRIM19 plays a critical role in the translocation of STAT3 to the mitochondria (Jon E. Angell, Lindner, Shapiro, Hofmann, & Kalvakolanu, 2000; Guochang Huang et al., 2004; Su et al., 2020; Tammineni et al., 2013; J. Zhang et al., 2003). PTMs in the residues K49 and K140 have not been previously described as a key step for the interaction between STAT3 and GRIM19 and its translocation to the mitochondria. Some authors describe that there is no translocation of STAT3 to mitochondria in mouse models. After mitochondria isolation, western blots do not reveal any STAT3 signal (Su et al., 2020). Our experiments have proven STAT3 interactions with GRIM19 and mitochondrial translocation after LIF stimulation and inhibition of specific PTMs while in the authors of the papper described before isolate mitochondria in normal conditions. Since these experiments were carried out in HeLa cells expressing endogenous STAT3, they should be repeated in the STAT3-KO cells to rule out the possible influence of endogenous STAT3 in these interactions.

The interaction between STAT3 and GRIM19 can have an effect in the activity of the electron transport chain at the mitochondria (Demaria et al., 2010) and since the electron transport chain is the main source of ATP, measuring the intracellular levels of ATP can be an indirect measure of the effect of their interaction. PTM-inhibitory mutations at K49, K140 and Y705 residues decreased ATP content. These data indicate that STAT3 interacts with GRIM19 and STAT3 PTMs interfere in the distribution and function of both proteins.

We also developed a STAT3 construct with a new tag for the visualization of STAT3 by both fluorescent and electron microscopy. The MiniSOG protein produces green fluorescence, but also photogenerates $^1O_2$, which in the presence of Diaminobenzidine (DAB) forms an electron-dense polymer visible by transmission electron microscopy. This characteristic allows correlated light and electron microscopy (CLEM) experiments. We have observed the green fluorescence signal of MiniSOG and DAB precipitates when fused to STAT3 and transfected in HEK cells.

This relatively recent protein tag that allows detection by both fluorescence and electron microscopy (Qi, Garren, Shu, Tsien, & Jin, 2012; Shu et al., 2011) it was recently described as capable of being split in two non-fluorescent fragments and recover all the functions when the protein is reconstituted after interaction of both fragments (Boassa et al., 2019). Here we also present new split versions, capable of recover fluorescence when transfected in the same cells.

Our data indicate that STAT3 can carry the MiniSOG tag, and that more split versions of MiniSOG can be discovered. In the future, the use of this tag could be important for a high spatial resolution of STAT3 distribution as a monomer or a dimer, as well as its interactions.

Chapter 3

Results (Part III)

New tools for the visualization of *STAT3*-regulated genes

This chapter contains results published in:

Letra-Vilela, R., Quiteres, R., Murtinheira, F., Crevenna, A., Hensel, Z., & Herrera, F. (2020). New tools for the visualization of glial fibrillary acidic protein in living cells. Experimental Results, 1, E4. doi:10.1017/exp.2020.1.

Introduction

STAT3 regulates the transcription of different sets of genes depending on the cell line and cytokine stimulus. One of the genes up-regulated after cytokine stimulation is the intermediate filament glial fibrillary acidic protein (GFAP) (Xu et al., 2011).

GFAP is an intermediate filament widely known as a molecular marker for astroglia (Michael Brenner, 2014; Middeldorp & Hol, 2011). GFAP expression is strikingly enhanced in conditions of stress, inflammation or injury (David & Ness, 1993; D. Li et al., 2020; Middeldorp & Hol, 2011). However, GFAP structure and function remain poorly understood. This is due, at least in part, to the intolerance of GFAP to tags at the N- or C-terminus. Most GFAP studies were restricted to fixed cells and immunocytochemistry (Hsiao et al., 2005; M.-D. Perng et al., 2008), and early attempts to tag human GFAP (hGFAP) had mixed success, as cells often showed GFAP aggregation or poor filament formation (Bachetti et al., 2008; M.-D. Perng et al., 2008; Tulyeu et al., 2019). Mouse GFAP (mGFAP) was successfully tagged with EGFP by introducing a linker between the filament and the fluorescent protein (Mignot et al., 2007). Although mGFAP shares 95% homology to hGFAP (David & Ness, 1993; Middeldorp & Hol, 2011), there are relevant differences that could determine different mechanisms of regulation and function.

The generation of a tagged version for GFAP is not only important for studies in physiological context but also in disease. Protein aggregation is a hallmark in many neurodegenerative disorders (Weydt & La Spada, 2006). Mutations in the GFAP gene are associated to Alexander disease (Tsuji, 2007), being the most common the substitution of an arginine (R) in the position 239 by a cysteine (C) (Prust et al., 2011). GFAP mutations lead to its aggregation in Rosenthal Fibers, which are composed by GFAP and other intermediate filaments, small heat shock proteins alphaB-crystallin and Hsp27, plectin and Cyclin D2, and usually

localize surrounding the nucleus (A. A. Sosunov, McKhann, & Goldman, 2017; Tang, Perng, Wilk, Quinlan, & Goldman, 2010).

Results

STAT3 phosphorylation regulates GFAP expression

Hela STAT3-/- cells were transfected with a plasmid containing the luciferase cDNA under the control of the rat GFAP promoter and three different STAT3 BiFC pairs: WT pair, Y705F pair and the asymmetric WT + Y705F pair. In the absence of stimulation by LIF the levels of luciferase activity do not present significant differences (Fig. 42). After stimulation with LIF (100 ng/ml) for 2 hours only the WT STAT3 BiFC pair led to an increase in the levels of Luciferase Activity. This was the first indication that our Venus-STAT3 BiFC system is actually transcriptionally active, an interesting property that we could not give for granted, and will be certainly used in Herrera´s lab for future studies on the control of STAT3 transcriptional activity by PTMs. The fact that the WT+Y705F asymmetric combination showed no transcriptional activity upon cytokine stimulation strongly indicates that both STAT3 monomers need to be phosphorylated for STAT3 dimers to induce GFAP expression.

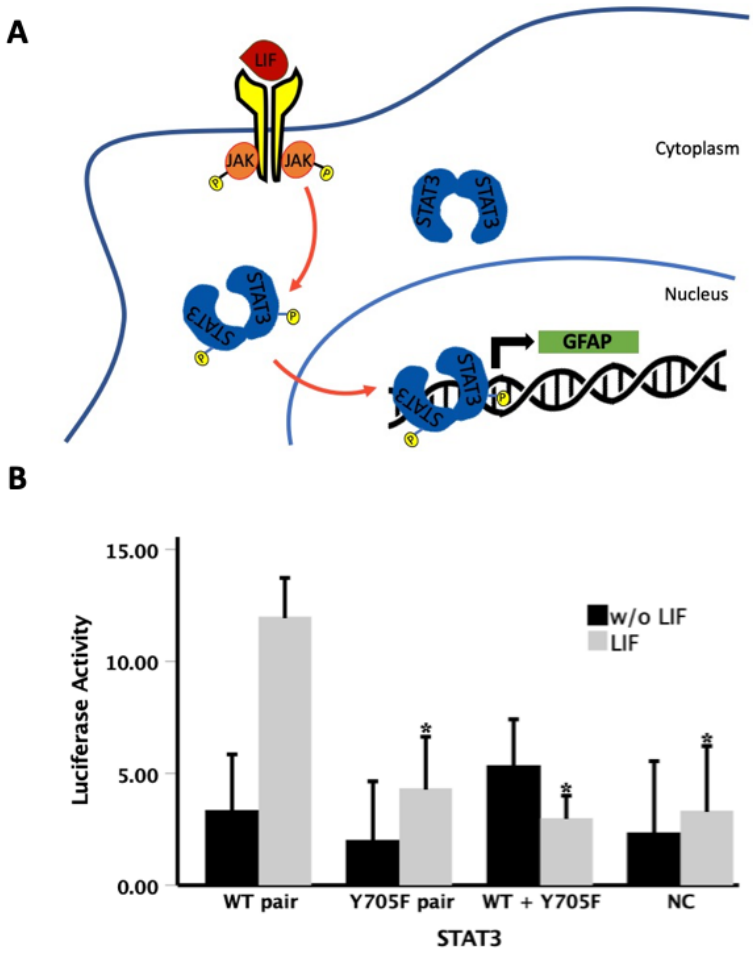

Figure 42 – *STAT3* BiFC system is able to bind to *GFAP* promotor and regulate trascription - A, representative scheme of JAK-STAT pathway activation for GFAP expression, B, Quantification of luciferase activity in Hela STAT3-/- cells transfected with WT-WT STAT3 pair, Y705F-Y705F STAT3 pair and WT-Y705F STAT3 pair, in LIF stimulated cells (grey bar) and unstimulated cells (black bar). Data are shown as the average of n = 3 independent experiments ± SD. Statistical analysis was carried out by means of a one-way ANOVA followed by a Bonferroni test adjusted for multiple comparisons. *, significant vs WT, $p < 0.001$

First attempts to generate a BiFC system for the visualization of GFAP dimerization and oligomerization

Our first approach was to generate a BiFC system to visualize GFAP dimerization and oligomerization into fibers in living cells. Back then, we were warned by GFAP expert Dr. Michael Brenner (Personal Communication) that tagging the protein may prove difficult, but we were not aware of the results by Mignot, where they used a linker to fuse GFAP with a fluorescent tag (Mignot et al., 2007). On the other hand, we were trying to test new split Venus systems that were reported to have lower background (Ohashi et al., 2012). Thus, we generated four constructs containing fusions of GFAP with different Venus halves, but no linker between them: One of VN in GFAP N terminal, and 3 of VC in N and C terminal, being the two in the C terminal of different sizes. This allowed us to test three different BiFC combinations (Fig. 43).

When analyzed by Flow Cytometry, the only pair that produced fluorescence after transfections was the one containing the Longer V2 halve in the C-Terminal (Fig. 43B and D). However, when we compared our results with the Huntingtin-Venus BiFC system previously developed (Herrera & Fleming, 2011), the level of fluorescence produced was very low.

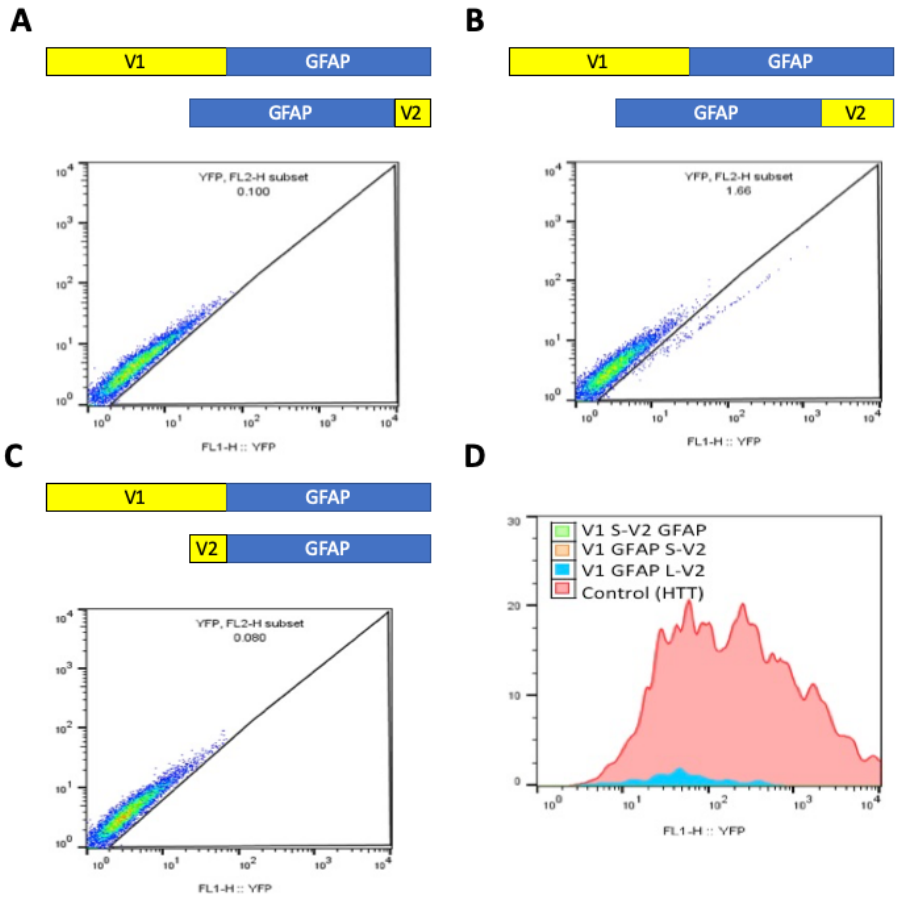

Figure 43 - BiFC pairs show very low fluorescence levels - A) Cells were transfected using three different combinations of BiFC constructs. B) Only the Venus 1–GFAP/GFAP – L-Venus 2 combination showed some fluorescence, as determined by Flow Cytometry. C) Fluorescence is always much lower than the signal from the Huntigtin BiFC pair previously developed by Dr. Herrera.

Western Blot analysis discarded the hypothesis of lack of expression in cells that did not have fluorescent signal. HEK cells transfected with the BiFC pair clearly expressed the respective bands of the constructs (Fig. 44A). Due to the lack of endogenous GFAP, two bands are visible for each pair. Differences in the size correspond to the different sizes of BiFC Venus fragments. Knowing that GFAP has a molecular weight of 50 KDa, the expected bands are higher being the

Venus N- GFAP tag the one with higher molecular weight. Between the Venus C constructs, two of them share the same molecular weight because the only difference is the position of the tag relatively to GFAP and the last one higher when compared with the other due to the larger length of the VC half (Fig. 44A).

Microscopy results were consistent with flow cytometry (Fig. 44B). The only pair producing fluorescence was the same that present fluorescent signal in flow cytometry, the pair VN-GFAP transfected with GFAP-Longer VC. The number of cells presenting fluorescence was low and the pattern of GFAP distribution did not correspond to the regular intermediate filament network. Our results were therefore inconclusive, but we now believe that introducing a linker between GFAP and the Venus fragments could solve this issue. Nevertheless, we decided to try first a different, unprecedented approach to tag GFAP.

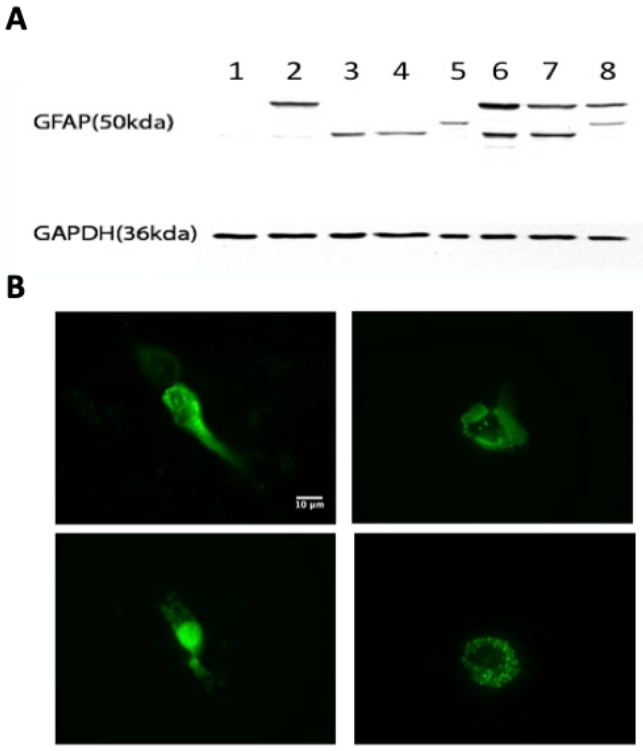

Figure 44 - *GFAP* expression is not compromised by the addition of a Tag - A) Immunoblots show that GFAP-Venus fusion proteins are expressed in transfected HEK cells. Lanes: 1) Control, 2) Venus N GFAP, 3) S-VC-GFAP, 4) GFAP–S-VC, 5) GFAP–L-VC, 6) Venus N–GFAP/S-VC-GFAP, 7) Venus N–GFAP/GFAP–S-VC, 8) Venus N–GFAP/GFAP–L-VC. B) HEK cells transfected with the Venus N–GFAP/GFAP – L-Venus C combination show aberrant patterns of intracellular distribution. Scale bar 10 µm,

Generation of a transposon tag for GFAP

Using a transposase reaction in vitro, it is possible to randomly insert a transposon in a plasmid in order to create fusion proteins where the fluorescent tag is not inserted in the N- or the C-terminus of the target gene, but within that gene (Sheridan et al., 2002). The authors generated two fluorescent fusion proteins for glutamate receptor subunit, GluR1, and for the *G* protein subunit, α_s, without compromising the normal behavior of

both proteins. Applying the same methodology, we generated a fluorescent fusion protein of GFAP with EGFP. The transposase reaction led to three sites of in frame insertion, where two of them produced fluorescence when analyzed by means of Flow Cytometry (Fig. 45).

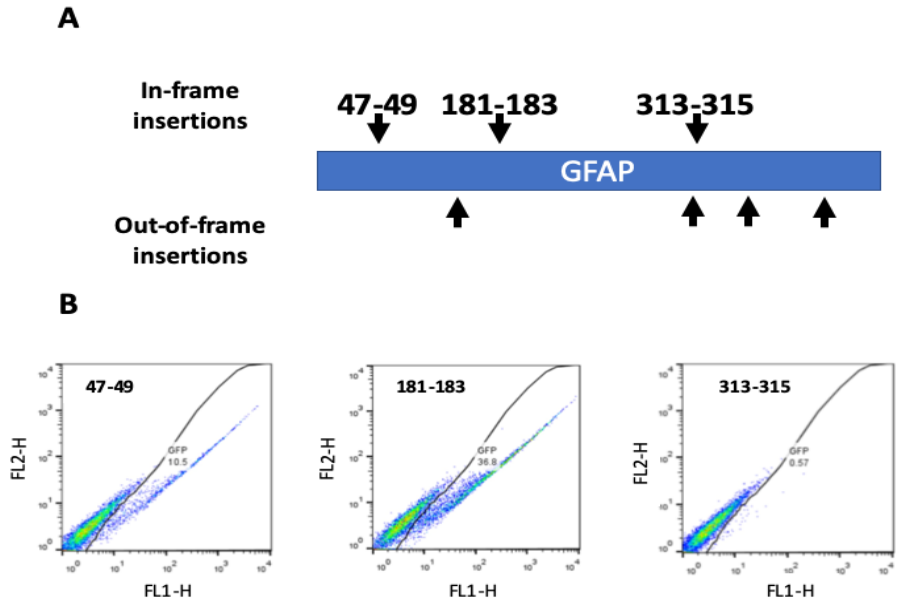

Figure 45 - Sites of EGFP insertion in GFAP – A, of the EGFP-containing transposon integrated in 7 different sites of the human GFAP cDNA were detected, 3 in frame and 4 out of frame. Some sites were found in several colonies, indicating that they could be preferential insertion sites for the transposon. B, When HeLa cells were transfected with the in-frame constructs, only one did not present fluorescent signal. This can be due to the incapacity of acquire the normal conformation of the fluorescent protein. Insertions between the amino acids 47-49 and 181-183 lead to fluorescent signals. Ten thousand events were counted and plotted.

These results proved the normal frame, assembly and function of the fluorophore, but only one of the insertions presented the normal pattern of distribution of GFAP when analyzed by fluorescent microscopy. The insertion of EGFP between the amino acids 47 and 49 led to a successful GFAP fluorescent fusion protein with EGFP (Fig. 46).

When compared with a EGFP-tagged mouse GFAP version previously described, our construct exhibited a normal GFAP filamentous network. Both of the constructs were able to express GFAP versions capable of incorporate into the IF network and form a normal filamentous pattern when transfected in U251 human glioblastoma cells.

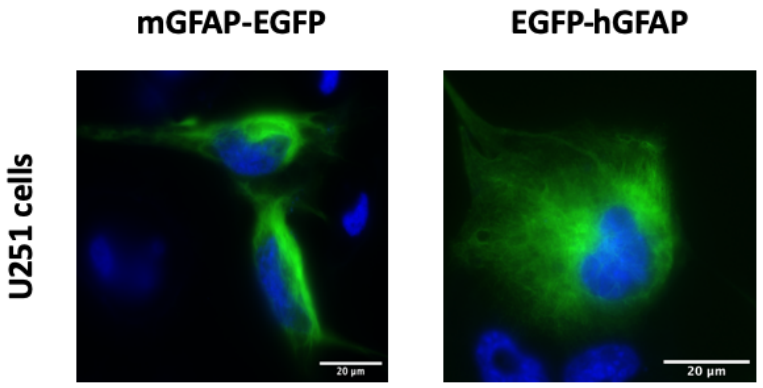

Figure 46 - EGFP-hGFAP incorporates to IF network - When transfected into U251 human glioblastoma cells EGFP-hGFAP and mGFAP-EGFP exhibited a normal GFAP filamentous network. Scale bar, 20 µm.

Generation of new tagged versions of human and mouse GFAP

Since GFAP supports an insertion of a coding region within its sequence, we generated two more constructs substituting the EGFP tag for an N-terminal Venus fragment (amino acids 1 to 157) or a C-terminal Venus fragment (from amino acid 158 to 238), in order to create a BiFC system. Unfortunately, U251 cells transfected with this new attempt of GFAP BiFC system presented very low levels of fluorescence by flow cytometry, as it occurred with our previous attempts. When analyzed by microscopy, the results were consistent, presenting a low number of fluorescent cells with low overall fluorescence. Once again, like in the previous attempt, cells presenting fluorescent signal failed to form the

filamentous network typical of *GFAP* (Fig. 47) and observed in our transposon EGFP-hGFAP construct.

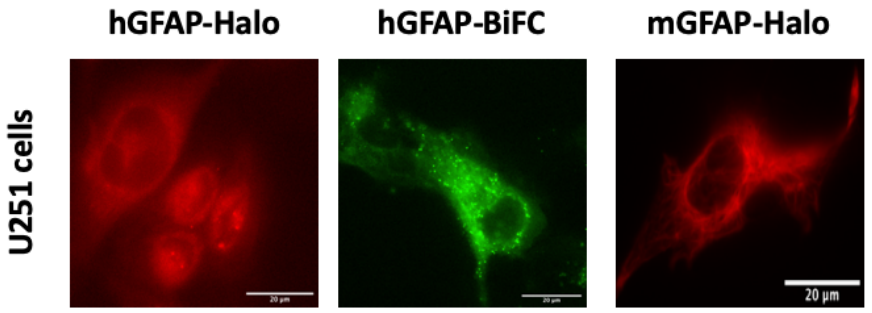

Figure 47 – Tagged versions of *GFAP* - mGFAP-Halo constructs (incubated with the JF549 Halo ligand, 100 nM) also produced normal filaments in U251 cells. Our attempts to substitute EGFP for bimolecular fluorescence complementation (BiFC) tags Venus N (amino acids 1–157) and Venus C (amino acids 158–238) or *Halo* Tag were unsuccessful. These are representative images of U251 cells transfected with these constructs, where residual fluorescence can be observed but has no recognizable pattern (i.e. filaments, bundles or aggregates). Scale bar, 20 µm.

In our lab, we had previously generated successfully a *Halo*-tagged version for mGFAP in order to carry out single-molecule analyses. Thus, we also tried to insert the Halo tag in the hGFAP-EGFP construct. Like the hGFAP-BiFC system, this new construct also presented problems to produce the pattern of distribution characteristic from intermediate filaments (Fig. 48). Our results indicate that our transposon approach is tag-sensitive, probably due to changes in the 3-dimensional folding of the chimeric proteins.

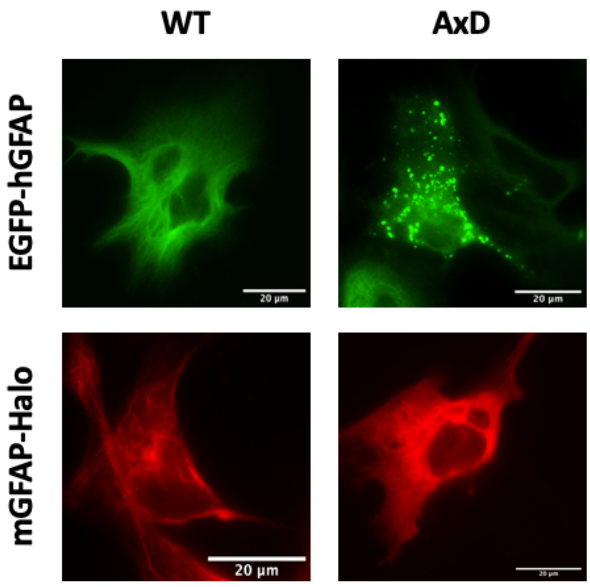

Figure 48 – Pattern of distribution of WT and Mutant GFAP - U251 cells were transiently transfected with either wild type (WT) or Alexander disease (AxD)-related versions of EGFP-hGFAP or mGFAP-*Halo* (R239C or R236H, respectively), and pictures were taken 24 h later. In the case of the mGFAP-Halo constructs, cells were incubated with the JF647 *Halo* ligand (100 nM) prior to imaging. WT hGFAP or mGFAP assembled into filaments (left panels), but AxD mutations changed this pattern (right panels). *hGFAP* R239C produced protein aggregates in the cytoplasm, while mGFAP R236H formed a homogeneous pattern throughout the cytoplasm without apparent filament structures. Scale bar, 20 µm.

The Alexander disease-associated R239C mutation led to GFAP aggregation in U251 cells

Our previous results demonstrated that our version of EGFP-tagged hGFAP tagged can incorporate into the IF network and exhibit the normal GFAP filamentous network. Next, we generated a R239C mutant form of GFAP that causes Alexander Disease by means of Site Directed Mutagenesis, using our construct as a template. When compared with U251 cells expressing WT GFAP, the ones expressing the mutated form presented higher levels of protein aggregation (Fig. 49). However, this

depended on intracellular protein concentration, since transfection with higher amounts of plasmid (2 micrograms) also led to aggregation of WT GFAP (Fig. 49).

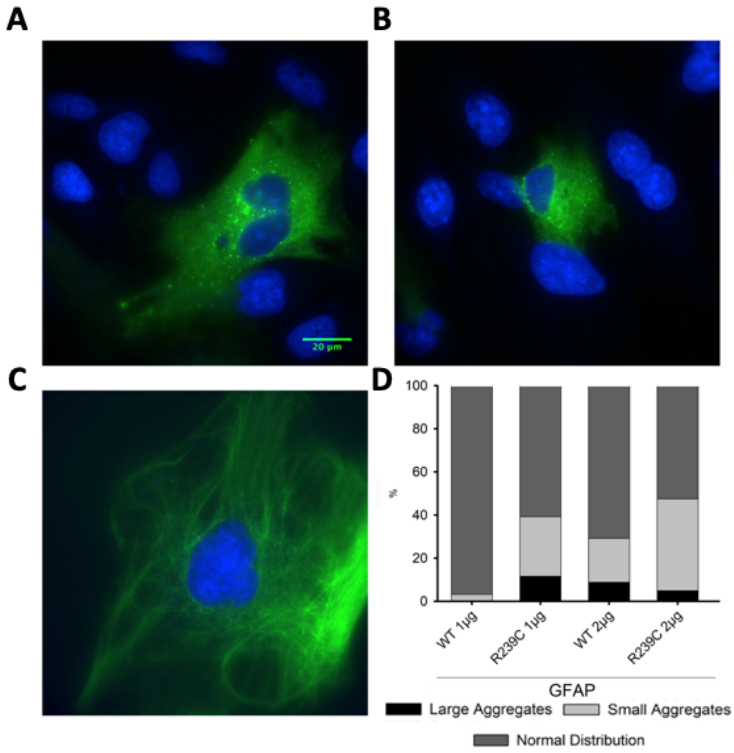

Figure 49 - GFAP tag does not compromise distribution in living cells - U251 cell line were transfected with a plasmid containing the EGFP-GFAP construct and with a plasmid containing the same construct but with the Alexander Disease mutation R239C in GFAP. Two different conditions were tested, 1µg and 2µg of DNA in each transfection. The cells presented three distinct patterns of distribution, large aggregates (A), small aggregates (B) and the normal pattern (C). Increasing the amount of DNA and the mutation in the GFAP protein tend to increase the levels of aggregation (D). Scale bar - 20µm

Our microscopy analysis revealed that about 90% of cells transfected with WT GFAP led to filamentous network, while cells transfected with the mutant form of GFAP showed only 40%. This difference was also observed in the pattern of aggregation, aggregates being visible in 3% of the cells transfected with WT GFAP versus 48% of

cells transfected with the Alexander disease mutant (Fig. 50 A). A similar pattern of aggregation is observed in cells transfected with the mouse GFAP WT and the mouse equivalent of the Alexander disease mutant (R236H).

By western-blot it was possible to observe that both constructs, WT and mutant, expressed similar levels of GFAP (Fig. 50 D). The aggregation visible by microscopy could be classified in distinct classes, with the pattern and size of the aggregates displaying differences between cells. While some cells exhibit less numerous but larger aggregates, others exhibit small aggregates in a large number (Fig. 50).

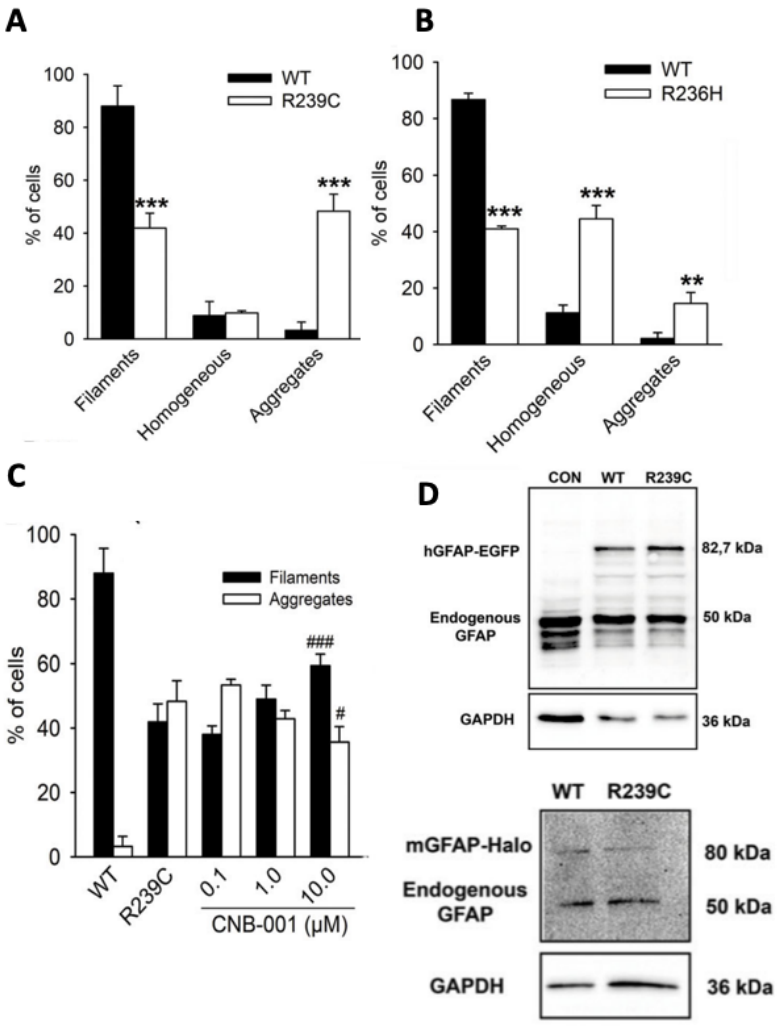

Figure 50 – CNB-001 decreases GFAP aggregation - A-B, Quantification of the various patterns observed in U251 cells transfected with (A) WT EGFP-hGFAP (black bars) and mutant EGFP-hGFAP (white bars) or (B) the equivalent mGFAP-Halo constructs. **, significant *vs* WT, $p < 0.01$; ***, $p < 0.001$. C, Quantification of U251 cells transfected with the EGFP-hGFAP R239C mutant that displayed a normal filamentous network (black bars) or aggregates (white bars) after treatment with increasing concentrations (0.1–10 μM) of the neuroprotective compound CNB-001. All groups were statistically significant versus WT EGFP-hGFAP, $p < 0.001$. #, significant vs EGFP-hGFAP R239C, $p < 0.05$; ###, $p < 0.001$. D, Western blots showing similar levels of expression in U251 cells transfected with hGFAP-EGFP and mGFAP-Halo constructs.

Our results indicate that these new systems can be useful for the screening of drugs and compounds targeting GFAP aggregation. Until now, there is still no treatment for AxD, and several studies have been done to target GFAP expression and accumulation (A. Messing, 2019). Knowing the beneficial effects of curcumin in a cellular model of Alexander Disease (Bachetti et al., 2012), we decided to test the effects of two synthetic curcumin derivatives, J147 and CNB-001, as neuroprotective compounds targeting GFAP accumulation. For that, cells transfected with *h*GFAP and R239C GFAP, were exposed to 100 nM, 1 μM or 10 μM of each drug. Only CNB-001 at 10 μM lead to a significant increase in filament formation and a corresponding decrease in GFAP aggregation (Fig. 50C).

Discussion

Astrocytes have a very important role in the response to CNS injury, being GFAP one of the principal components of astroglial filaments (Carmen et al., 2007; Eng et al., 1971). GFAP has an important role in astroglial proliferation, is overexpressed during traumatic, hypoxic or disease-related CNS injury, and its expression is correlated with lower malignancy of gliomas (a D. R. Garcia et al., 2004; Seri et al., 2001). However, there are just a few methods to analyze human GFAP behavior in living cells.

With the aim of studying GFAP oligomerization in all these processes we initially tried to produce a BiFC system by inserting *Venus* halves in the N- and C- terminus of GFAP. However, it was not possible to obtain the typical pattern of distribution from intermediate filaments and the fluorescent signal was really low. This attempt was done with different partitions of *Venus* halves due to the disadvantages of BiFC like higher background, lower signal-to-noise ratios and saturated signals (Herrera et al., 2012b; Shyu et al., 2006). Some authors had described a new split of *Venus* (in residue 210) that overcome these disadvantages leading to better signal-to-noise ratios (Ohashi et al., 2012). However, it did not work in GFAP in our hands. This is probably the result of the already mentioned difficulties to tag GFAP, and our lab is currently trying to implement this split Venus in their new constructs.

Our results are consistent with the literature, where some authors defend that human GFAP is not able to oligomerize in a correct way do to the incorporation of a tag (Ming-der Perng et al., 2008). When we use mouse GFAP, the results are not the same. It was described that EGFP-tagged mouse GFAP was used for the study of GFAP function and dynamics (Mignot et al., 2007). The authors were the first ones to describe a successfully tagged version for GFAP where they inserted a flexible linker between the tag and the *GFAP* sequence (Mignot et al., 2007). The

authors were able to study the correct folding of GFAP and the integration of GFAP within the endogenous intermediate filament network.

The absence of a tag for the human GFAP led us to a new attempt. We successfully developed the first tagged version of human *GFAP* inserting the coding sequence for *EGFP* inside the GFAP sequence. The site of insertion, between the amino acids 181 and 183, was randomly discovered using the same approach described for the insertion of *EGFP* inside the coding sequence of other proteins (Sheridan et al., 2002). When analyzed, we observed that the region where the insertion of the tag was successful contains very few mutations related with Alexander Disease (A. Messing et al., 2012b). Like the tag for mouse GFAP, our new construct allows human GFAP to integrate a healthy IF network.

We had previously developed a HaloTag mouse *GFAP* construct with successful results, so we also tried to achieve the same result for human GFAP using the site of insertion discovered with the transposon reaction, although once again we did not succeed. Both constructs were not able to produce proteins able to integrate the filament network forming small aggregates in the cytoplasm of the cell.

Previous studies have shown that Alexander Disease mutations affect GFAP oligomerization leading to aggregation (Hsiao et al., 2005; Mignot et al., 2007). The most common mutation related with AxD is R239C in human *GFAP* and the corresponding R236H in mouse GFAP. Bearing this in mind, we developed constructs carrying these mutations to analyze if our system could also be useful to study the behavior of GFAP in pathological conditions. Our results were consistent with the literature due to the presence of GFAP aggregation and disruption of IF network in the majority of the cells. When we observe cells expressing mutant human GFAP it is possible to see inclusions, while in *Halo*-tagged mouse GFAP we observed a homogeneous pattern without filament structures. Previous studies described mutant mouse GFAP accumulation as

aggregates (Mignot et al., 2007) presenting differences with our model, although we need to have in mind that the tags used were different, raising the hypothesis that *Halo* Tag might be inhibiting the formation of aggregates.

Having a model that allow us to study GFAP in physiological and pathological conditions, we next tried to test possible compounds that could recover GFAP abnormal behavior. It has been described recently that the use of spice curcumin can have beneficial effects reducing GFAP accumulation (Bachetti et al., 2012). At Dr. Schubert's Laboratory (The Salk Institute, La Jolla, CA, USA), two synthetic derivatives of curcumin were synthetized, J147 (Q. Chen et al., 2011) and CNB-001 (Y. Liu, Dargusch, Maher, & Schubert, 2008) in an attempt to improve the effectiveness of curcumin. J147 is the most studied and with more results that indicate an effectiveness in various rodent models of neurodegenerative disease and memory enhancement (Currais et al., 2015; Prior et al., 2016). Our results show an opposite effect being CNB-001 more efficient than J147, reducing *GFAP* accumulation. However, more studies need to be done with increased concentrations of both compounds.

Chapter 4
General Discussion and Conclusions

In this thesis, we have covered different aspects of the *JAK*/*STAT3*/*GFAP* axis that is so relevant for astrogliogenesis during development and in pathological conditions. We have developed a series of molecular tools that will allow new perspectives on this signaling pathway. They are deposited in a public repository (Addgene) to make them fully available to researchers worldwide, in our commitment to Open data and Open resources policies. Our approaches and tools could be relevant to biological phenomena beyond the central nervous system. For example, the *JAK*/*STAT3*/*GFAP* axis is also involved in glioblastoma or Crohn´s disease. Additionally, some of our findings could be translated to other signaling systems, such as the hypothesis that asymmetric PTMs could be a new regulatory level for any protein which activity depends on homodimerization.

Our work gives a new perspective of dimer formation different from what have been described in the literature (Dasgupta et al., 2015, 2014; Kang et al., 2017; Ray et al., 2005b; Wegrzyn, Potla, Chwae, Sepuri, Zhang, et al., 2009; J. Yang et al., 2005, 2010; Q. Zhang et al., 2013). We have observed that symmetric combinations of STAT3 do not alter dimer formation or distribution in unstimulated cells, although when we transfect cells with asymmetric *STAT3* pairs it is possible to observe significant changes in the patterns of intracellular distribution of *STAT3* dimers. Asymmetric pairs containing K49R substitution in one protein of the dimer lead to a homogeneous distribution of *STAT3* through all the cell (nucleocytoplasmic distribution). While the pair K140R + S727A lead to an increase in nuclear localization. This tendency can be observed in pairs containing one K140R- or K685R- substitution but with no significant differences.

USTAT3 can homodimerize, translocate to the nucleus, interact with transcriptional regulators, bind to DNA and regulate the transcription of a specific set of genes, such as *E2F1*, *M-Ras* or *Met* (Braunstein et al.,

2003; Nkansah et al., 2013a; J. Yang et al., 2005, 2007). The development of our system can be a key factor in the study of all these distinct processes inside the cell, although more studies need to be done and with the support of other techniques.

With that in mind, we started to use our BiFC *STAT3* system in the study of *STAT3* transcriptional regulation. *GFAP* is one of the genes regulated by *STAT3* (Xu et al., 2011) so we used it as a surrogate of *STAT3* transcriptional activity, through luciferase assays where we test the binding of *STAT3* dimers to the GFAP promoter. We have presented preliminary results where the WT *STAT3* BiFC pair but not pairs containing the Y705F phosphoresistant mutant led to an increase in the levels of Luciferase Activity after stimulation with LIF. This was the first indication that our Venus-*STAT3* BiFC system is actually transcriptionally active, and although more studies need to be done to confirm our results it can open an opportunity to use BiFC systems, and in our case the *STAT3* system, for future studies on the control of transcriptional activity.

Our system also presented intriguing results with *STAT3* interactors. In our analysis of *STAT3* distribution we also found that combinations carrying any one (asymmetric) or two K-R substitutions (symmetric or asymmetric) significantly increased mitochondrial translocation. *GRIM19* interacts with *STAT3* directly, and their interaction promotes mitochondrial accumulation and inhibits STAT3 translocation to the nucleus (Okamoto et al., 2010; J. Zhang et al., 2003). *GRIM19* was originally described as the principal mediator of IFN/Retinoic acid-induced cell death (Jon E. Angell et al., 2000), also as a component of complex I in the electron transport chain, and besides mitochondria was also localized in the nucleus where it has been described as a negative transcriptional regulator of STAT3 (Jon E. Angell et al., 2000; Fearnley et al., 2001; Guochang Huang et al., 2004; Kalakonda, Nallar, Gong, et al., 2007; Lufei et al., 2003; Okamoto et al., 2010; J. Zhang et al., 2003). Some authors

also described the absence of mitochondrial localization of STAT3 in mouse models under normal physiological conditions (Su et al., 2020). The development of a system that allows the study of all these possible roles of *GRIM19* and how *STAT3* PTMs can regulate the interaction and fate of *GRIM19* can be useful for many biological fields. For example, *STAT3* is constitutively activated in 70% of solid tumors and mitochondrial STAT3 could play a key role on cancer progression; and the presence of *GRIM19* can stop the cell cycle in G1 phase and lead to cell death (Guanizo, Fernando, Garama, & Daniel, 2018; Turkson & Jove, 2000). Knowing which STAT3 PTMs lead to specific functions of his interaction with GRIM19 can be useful for cancer therapy or further studies in mitochondrial functions. We observed that if we use cytokines for cell stimulation, and transfect the cells with *STAT3* proteins carrying inhibitory mutations in K49, K140 and S727 there is an increase in the interaction with *GRIM19*. To better understand this interaction and the localization of these dimers in mitochondria new systems need to be developed.

Having that in mind, we can try to apply the concept of protein complementation in fluorescent tags that can be used in electron microscopy, such as *MiniSOG*, for a better resolution and a more accurate observation of intracellular distribution. During the development of our *MiniSOG* complementation system, it was published an article using the same approach with the same tag. *MiniSOG* is a fluorescent flavoprotein derived from the light, oxygen, voltage (LOV)-2 domain of Arabidopsis phototropin. When the split fragments interact with each other, the fragments reconstitute a functional reporter that permits tagged protein complexes to be visualized by fluorescence light microscopy (LM), and then by standard as well as ‘‘multicolor’’ electron microscopy (EM) (Boassa et al., 2019). The authors highlight the advantages of split-miniSOG complementation in visualizing intracellular protein-protein interactions with high spatial resolution.

We also started the development of a similar system where *STAT3* was fused to complementary *MiniSOG* fragments to provide a higher spatial resolution. We presented split versions of *MiniSOG* protein that are able to recover fluorescent protein and the next step should be the addition of the split versions to our protein of interest, *STAT3*, for cell transfections, analyses of function recoveries of the *MiniSOG* protein and the effect of the tag in *STAT3* function and distribution. When we use the full protein, we have shown that the fluorescent capacities of *MiniSOG* are retained and the *STAT3* is distributed in the cytoplasm.

The development of new versatile molecular tools is also needed for genes regulated by *STAT3*. This allows us to study the functions of *STAT3* at different levels, from regulation of *STAT3* PTMs to the effect of this regulation in the genes regulated by *STAT3*. GFAP is one of the proteins regulated by *STAT3*, and it lacks a good tag for the study of its dynamics in living cells. We developed several GFAP constructs where it was fused with tags that allowed single-molecule and superresolution microscopy (e.g. Halo Tag) and visualization in living cells in both normal and pathological conditions, such as Alexander´s disease (e.g. *EGFP* within the *GFAP* gene) The key roles of GFAP in CNS injury or disease, as well as brain cancer and Alexander disease, make our GFAP tools an important addition to the field.

In summary, our results open a wide field of research. Our hypothesis that asymmetric dimerization can be a new regulatory mechanism for *STAT3* signaling needs more studies to be confirmed but the idea that dimers of the same protein can be formed with each molecule containing different PTMs regulating in this way the behavior and function of the dimers is a new possibility. We can start to do some questions, like, if *STAT3* regulate a wide variety of genes can this asymmetric dimerization regulate specific sets of genes? Can this dimerization play a role in the

gradation of *STAT3* transcriptional or mitochondrial activities? How can cells control dimerization of proteins in such a perfect way that guarantees the exact dimerization of two molecules with the same PTMs in a pool of a wide variety of proteins? If PTMs have such importance in homodimerization how they influence heterodimerization?

Our results also present advances in the interaction of *STAT3* with *GRIM19*. This relation has been studied in the last years although we still need to reveal the influence of specific PTMs for *STAT3* behavior and function in all cell compartments. Our work describes new systems to study *STAT3* interaction with other proteins and, in the case of *MiniSOG*, with the BiFC system will allow the study of all these interactions with more accurate location. How PTMs regulate the interaction of *STAT3* with other proteins? Can we target specific PTMs to the distribution of *STAT3* or to *STAT3* interactions? Are PTMs specific for only one function?

Our last findings also allow us to study the *JAK-STAT3* pathway from the cytokine stimulation to the regulation of gene expression and function. We have showed that intermediate filaments are able to incorporate tags inside the protein structure like it was previously reported for other proteins.

We have been able to develop systems to study unstimulated and stimulated *STAT3* behavior and distribution. Systems that can be useful for the study of heterodimerization and precise location and systems for genes regulated by *STAT3*.

Based on these results, our main conclusions are:

1. Asymmetric *STAT3* homodimerization regulates the intracellular distribution of *STAT3* dimers, and has biological consequences at the level of cell proliferation;

2. Asymmetric homodimerization could represent a new level of regulation of cell signaling for proteins that exert their actions as homodimers;
3. *STAT3* heterodimerization with other proteins is also key to regulate intracellular *STAT3* distribution and function;
4. The interaction between *GRIM19* and *STAT3* is dependent on cytokine stimuli and specific *STAT3* PTMs, and has functional consequences in intracellular energy storage;
5. A split *MiniSOG* system is possible and would allow the visualization of protein-protein interactions by correlated light and electron microscopy (CLEM) at an ultrastructural level, enabling the monitorization of *STAT3* through subcellular compartments such as the mitochondria, the ER or the mitochondrial-associated membranes (MAMs);
6. Intermediate filaments can support a tag inside the coding sequence, but not all tags seem to be accepted (a linker may be also needed between these inserts and the target genes);
7. GFAP oligomerization is dependent on cellular environment and the tags to which it is fused; and
8. Curcumin derivatives are capable of recovering mutant GFAP aggregation or aberrant distribution.

References

Acarin, L., González, B., & Castellano, B. (2000). STAT3 and NFκB Activation Precedes Glial Reactivity in the Excitotoxically Injured Young Cortex but not in the Corresponding Distal Thalamic Nuclei. *Journal of Neuropathology & Experimental Neurology*, *59*(2), 151–163. https://doi.org/10.1093/jnen/59.2.151

Aebersold, R., Agar, J. N., Amster, I. J., Baker, M. S., Bertozzi, C. R., Boja, E. S., … Zhang, B. (2019). How many human proteoforms are there? *Nature Chemical Biology*, *14*(3), 206–214. https://doi.org/10.1038/nchembio.2576.How

Aigner, P., Just, V., & Stoiber, D. (2019). STAT3 isoforms: Alternative fates in cancer? *Cytokine*, *118*(January 2018), 27–34. https://doi.org/10.1016/j.cyto.2018.07.014

Alexander, W. S. (1947). PROGRESSIVE FIBRIXOID DEGENERATION OF FIBRILLARY ASTROCVTES ASSOCIATED WITH MENTAL RETARDATION IN A HYDROCEPHALIC INFANT 1 IN the following case of progressive hvdrocephalus in an infant , the brain displays on histological examination a type of degenerat, 373–381.

ALEXANDER, W. S. (1949). Progressive fibrinoid degeneration of fibrillary astrocytes associated with mental retardation in a hydrocephalic infant. *Brain : A Journal of Neurology*, *72*(3), 373–381, 3 pl. https://doi.org/10.1093/brain/72.3.373

Alfaro, J. F., Gong, C. X., Monroe, M. E., Aldrich, J. T., Clauss, T. R. W., Purvine, S. O., … Smith, R. D. (2012). Tandem mass spectrometry identifies many mouse brain O-GlcNAcylated proteins including EGF domain-specific O-GlcNAc transferase targets. *Proceedings of the National Academy of Sciences of the United States of America*, *109*(19). https://doi.org/10.1073/pnas.1200425109

Alford, S. C., Ding, Y., Simmen, T., & Campbell, R. E. (2012). Dimerization-dependent green and yellow fluorescent proteins. *ACS Synthetic Biology*, *1*(12), 569–575. https://doi.org/10.1021/sb300050j

Alonzi, T., Maritano, D., Gorgoni, B., Rizzuto, G., Libert, C., & Poli, V. (2001). Essential Role of STAT3 in the Control of the Acute-Phase Response as Revealed by Inducible Gene Activation in the Liver. *Molecular and Cellular Biology*, *21*(5), 1621–1632. https://doi.org/10.1128/mcb.21.5.1621-1632.2001

Angell, J E, Lindner, D. J., Shapiro, P. S., Hofmann, E. R., & Kalvakolanu, D. V. (2000). Identification of GRIM-19, a novel cell death-regulatory gene induced by the interferon-beta and retinoic acid combination, using a genetic approach. *The Journal of Biological Chemistry*, *275*(43), 33416–33426. https://doi.org/10.1074/jbc.M003929200

Angell, Jon E., Lindner, D. J., Shapiro, P. S., Hofmann, E. R., & Kalvakolanu, D. V. (2000). Identification of GRIM-19, a novel cell death-regulatory gene induced by the interferon-β and retinoic acid combination, using a genetic approach. *Journal of Biological Chemistry*, *275*(43), 33416–33426. https://doi.org/10.1074/jbc.M003929200

Arai, R., Nakagawa, H., Tsumoto, K., Mahoney, W., Kumagai, I., Ueda, H., & Nagamune, T. (2001). Demonstration of a Homogeneous Noncompetitive Immunoassay Based on Bioluminescence Resonance Energy Transfer. *Analytical Biochemistry*, *289*(1), 77–81. https://doi.org/https://doi.org/10.1006/abio.2000.4924

Avalle, L., Camporeale, A., Morciano, G., Caroccia, N., Ghetti, E., Orecchia, V., … Poli, V. (2019). STAT3 localizes to the ER, acting as a gatekeeper for ER-mitochondrion Ca 2+ fluxes and apoptotic responses. *Cell Death and Differentiation*, *26*(5), 932–942. https://doi.org/10.1038/s41418-018-0171-y

Avalle, L., & Poli, V. (2018). Nucleus, Mitochondrion, or Reticulum? STAT3 à La Carte. *International Journal of Molecular Sciences*, *19*(9), 2820. https://doi.org/10.3390/ijms19092820

Aznar, S., Valerón, P. F., Del Rincon, S. V., Pérez, L. F., Perona, R., & Lacal, J. C. (2001). Simultaneous tyrosine and serine phosphorylation of STAT3 transcription factor is involved in RhoA GTPase oncogenic transformation. *Molecular Biology of the Cell*, *12*(10), 3282–3294. https://doi.org/10.1091/mbc.12.10.3282

Becker, S., Groner, B., & Müller, C. W. (1998). Three-dimensional structure of the Stat3beta homodimer bound to DNA. *Nature*, *394*(6689), 145–151. https://doi.org/10.1038/28101

Bhattacharya, S., & Schindler, C. (2003). Regulation of Stat3 nuclear export. *Journal of Clinical Investigation*, *111*(4), 553–559. https://doi.org/10.1172/jci200315372

Bianchini, D., De Martini, I., Cadoni, A., Zicca, A., Tabaton, M., Schenone, A., … Mancardi, G. L. (1992). GFAP expression of human Schwann cells in tissue culture. *Brain Research*, *570*(1–2), 209–217. Retrieved from http://www.ncbi.nlm.nih.gov/pubmed/1617413

Boassa, D., Lemieux, S. P., Lev-Ram, V., Hu, J., Xiong, Q., Phan, S., … Ngo, J. T. (2019). Split-miniSOG for Spatially Detecting Intracellular Protein-Protein Interactions by Correlated Light and Electron Microscopy. *Cell Chemical Biology*, *26*(10), 1407-1416.e5. https://doi.org/10.1016/j.chembiol.2019.07.007

Boengler, K., Hilfiker-Kleiner, D., Heusch, G., & Schulz, R. (2010). Inhibition of permeability transition pore opening by mitochondrial STAT3 and its role in myocardial ischemia/reperfusion. *Basic Research in Cardiology*, *105*(6), 771–785. https://doi.org/10.1007/s00395-010-0124-1

Boeuf, H., Hauss, C., De Graeve, F., Baran, N., & Kedinger, C. (1997). Leukemia inhibitory factor-dependent transcriptional activation in embryonic stem cells. *Journal of Cell Biology*, *138*(6), 1207–1217. https://doi.org/10.1083/jcb.138.6.1207

Bongcam-Rudloff, E., Nistér, M., Betsholtz, C., Wang, J.-L., Stenman, G., & Huebner, K. (1991). Human Glial Fibrillary Acidic Protein: Complementary DNA Cloning,

Chromosome Localization, and Messenger RNA Expression in Human Glioma Cell Lines of Various Phenotypes. *Cancer Research*, *51*(5), 1553–1560.

Boute, N., Jockers, R., & Issad, T. (2002). The use of resonance energy transfer in high-throughput screening: BRET versus FRET. *Trends in Pharmacological Sciences*, *23*(8), 351–354. https://doi.org/10.1016/s0165-6147(02)02062-x

Braun, P., Tasan, M., Dreze, M., Barrios-Rodiles, M., Lemmens, I., Yu, H., … Vidal, M. (2009). An experimentally derived confidence score for binary protein-protein interactions. *Nature Methods*, *6*(1), 91–97. https://doi.org/10.1038/nmeth.1281

Braunstein, J., Brutsaert, S., Olson, R., & Schindler, C. (2003). STATs Dimerize in the Absence of Phosphorylation. *Journal of Biological Chemistry*, *278*(36), 34133–34140. https://doi.org/10.1074/jbc.M304531200

Brenner, M, Johnson, a B., Boespflug-Tanguy, O., Rodriguez, D., Goldman, J. E., & Messing, a. (2001). Mutations in GFAP, encoding glial fibrillary acidic protein, are associated with Alexander disease. *Nature Genetics*, *27*(1), 117–120. https://doi.org/10.1038/83679

Brenner, Michael. (2014). Role of GFAP in CNS injuries. *Neuroscience Letters*, *565*, 7–13. https://doi.org/10.1016/j.neulet.2014.01.055

Brenner, Michael, Kisseberth, W. C., Su, Y., Besnard, F., & Messing, A. (1994). GFAP promoter directs astrocyte-specific expression in transgenic mice. *The Journal of Neuroscience : The Official Journal of the Society for Neuroscience*, *14*(3 Pt 1), 1030–1037.

Buettner, R., Corzano, R., Rashid, R., Lin, J., Senthil, M., Hedvat, M., … Williams, J. C. (2011). Alkylation of cysteine 468 in Stat3 defines a novel site for therapeutic development. *ACS Chemical Biology*, *6*(5), 432–443. https://doi.org/10.1021/cb100253e

Burda, J. E., & Sofroniew, M. V. (2014). Reactive gliosis and the multicellular response to CNS damage and disease. *Neuron*, *81*(2), 229–248. https://doi.org/10.1016/j.neuron.2013.12.034

Cabantous, S., Nguyen, H. B., Pedelacq, J. D., Koraïchi, F., Chaudhary, A., Ganguly, K., … Waldo, G. S. (2013). A new protein-protein interaction sensor based on tripartite split-GFP association. *Scientific Reports*, *3*, 1–9. https://doi.org/10.1038/srep02854

Chakraborty, A., & Tweardy, D. J. (1998). Granulocyte colony-stimulating factor activates a 72-kDa isoform of STAT3 in human neutrophils. *Journal of Leukocyte Biology*, *64*(5), 675–680. https://doi.org/10.1002/jlb.64.5.675

Chen, X., Zaro, J. L., & Shen, W.-C. (2013). Fusion protein linkers: property, design and functionality. *Advanced Drug Delivery Reviews*, *65*(10), 1357–1369. https://doi.org/10.1016/j.addr.2012.09.039

Chernyatina, A. A., Guzenko, D., & Strelkov, S. V. (2015). Intermediate filament structure: the bottom-up approach. *Current Opinion in Cell Biology*, *32*, 65–72. https://doi.org/10.1016/j.ceb.2014.12.007

Chrétien, A.-È., Gagnon-Arsenault, I., Dubé, A. K., Barbeau, X., Després, P. C., Lamothe, C., … Landry, C. R. (2018). Extended Linkers Improve the Detection of Protein-protein Interactions (PPIs) by Dihydrofolate Reductase Protein-fragment Complementation Assay (DHFR PCA) in Living Cells. *Molecular & Cellular Proteomics : MCP*, *17*(2), 373–383. https://doi.org/10.1074/mcp.TIR117.000385

Chung, J., Uchida, E., Grammer, T. C., & Blenis, J. (1997). STAT3 serine phosphorylation by ERK-dependent and -independent pathways negatively modulates its tyrosine phosphorylation. *Molecular and Cellular Biology*, *17*(11), 6508–6516. https://doi.org/10.1128/mcb.17.11.6508

Cimica, V., Chen, H. C., Iyer, J. K., & Reich, N. C. (2011). Dynamics of the STAT3 transcription factor: Nuclear import dependent on ran and importin-β1. *PLoS ONE*, *6*(5). https://doi.org/10.1371/journal.pone.0020188

Coriano, C., Powell, E., & Xu, W. (2016). Monitoring Ligand-Activated Protein-Protein Interactions Using Bioluminescent Resonance Energy Transfer (BRET) Assay. *Methods in Molecular Biology (Clifton, N.J.)*, *1473*, 3–15. https://doi.org/10.1007/978-1-4939-6346-1_1

Dasgupta, M., Dermawan, J. K. T., Willard, B., & Stark, G. R. (2015). STAT3-driven transcription depends upon the dimethylation of K49 by EZH2. *Proceedings of the National Academy of Sciences*, *112*(13), 3985–3990. https://doi.org/10.1073/pnas.1503152112

De Pablo, Y., Nilsson, M., Pekna, M., & Pekny, M. (2013). Intermediate filaments are important for astrocyte response to oxidative stress induced by oxygen-glucose deprivation and reperfusion. *Histochemistry and Cell Biology*, *140*(1), 81–91. https://doi.org/10.1007/s00418-013-1110-0

Decker, T., & Kovarik, P. (2000). Serine phosphorylation of STATs. *Oncogene*, *19*(21), 2628–2637. https://doi.org/10.1038/sj.onc.1203481

Deiss, L. P., & Kimchi, A. (1991). A genetic tool used to identify thioredoxin as a mediator of a growth inhibitory signal. *Science (New York, N.Y.)*, *252*(5002), 117–120. https://doi.org/10.1126/science.1901424

Deol, K. K., Lorenz, S., & Strieter, E. R. (2019). Enzymatic Logic of Ubiquitin Chain Assembly. *Frontiers in Physiology*, *10*, 835. https://doi.org/10.3389/fphys.2019.00835

Der Perng, M., Su, M., Wen, S. F., Li, R., Gibbon, T., Prescott, A. R., … Quinlan, R. A. (2006). The Alexander disease-causing glial fibrillary acidic protein mutant, R416W, accumulates into Rosenthal fibers by a pathway that involves filament aggregation and the association of alpha B-crystallin and HSP27. *American Journal of Human Genetics*, *79*(2), 197–213. https://doi.org/10.1086/504411

Derouet, D., Rousseau, F., Alfonsi, F., Froger, J., Hermann, J., Barbier, F., … Chevalier, S. (2004). Neuropoietin, a new IL-6-related cytokine signaling through the ciliary neurotrophic factor receptor. *Proceedings of the National Academy of Sciences of the United States of America*, *101*(14), 4827–4832. https://doi.org/10.1073/pnas.0306178101 Dimri, S., Sukanya, & De, A. (2017). Approaching non-canonical STAT3 signaling to redefine cancer therapeutic strategy. *Integrative Molecular Medicine*, *4*(1), 1–10. https://doi.org/10.15761/imm.1000268

Diallo M, Herrera F. The role of understudied post-translational modifications for the behavior and function of Signal Transducer and Activator of Transcription 3. FEBS J. 2022 Oct;289(20):6235-6255. doi: 10.1111/febs.16116. Epub 2021 Jul 17. PMID: 34235865.

Droescher, M., & Vinkemeier, U. (2012). Self-association of STAT Proteins from Monomers to Paracrystals. In T. Decker & M. Müller (Eds.), *Jak-Stat Signaling : From Basics to Disease* (pp. 47–63). Vienna: Springer Vienna. https://doi.org/10.1007/978-3-7091-0891-8_4

Eng, L. F., Vanderhaeghen, J. J., Bignami, a, & Gerstl, B. (1971). An acidic protein isolated from fibrous astrocytes. *Brain Research*, *28*(2), 351–354. https://doi.org/10.1016/0006-8993(71)90668-8

Etienne-Manneville, S. (2018). Cytoplasmic Intermediate Filaments in Cell Biology. *Annual Review of Cell and Developmental Biology*, *34*, 1–28. https://doi.org/10.1146/annurev-cellbio-100617-062534

Fearnley, I. M., Carroll, J., Shannon, R. J., Runswick, M. J., Walker, J. E., & Hirst, J. (2001). GRIM-19, a cell death regulatory gene product, is a subunit of bovine mitochondrial NADH:ubiquinone oxidoreductase (complex I). *The Journal of Biological Chemistry*, *276*(42), 38345–38348. https://doi.org/10.1074/jbc.C100444200

Furtek, S. L., Backos, D. S., Matheson, C. J., & Reigan, P. (2016). Strategies and Approaches of Targeting STAT3 for Cancer Treatment. *ACS Chemical Biology*, *11*(2), 308–318. https://doi.org/10.1021/acschembio.5b00945

Galarneau, A., Primeau, M., Trudeau, L.-E., & Michnick, S. W. (2002). Beta-lactamase protein fragment complementation assays as in vivo and in vitro sensors of protein protein interactions. *Nature Biotechnology*, *20*(6), 619–622. https://doi.org/10.1038/nbt0602-619

Gao, P., Niu, N., Wei, T., Tozawa, H., Chen, X., Zhang, C., … Liu, J. (2017). The roles of signal transducer and activator of transcription factor 3 in tumor angiogenesis. *Oncotarget*, *8*(40), 69139–69161. https://doi.org/10.18632/oncotarget.19932

Gao, X., Wang, H., Yang, J. J., Liu, X., & Liu, Z.-R. (2012). Pyruvate kinase M2 regulates gene transcription by acting as a protein kinase. *Molecular Cell*, *45*(5), 598–609. https://doi.org/10.1016/j.molcel.2012.01.001

Garcia, a D. R., Doan, N. B., Imura, T., Bush, T. G., & Sofroniew, M. V. (2004). GFAP-expressing progenitors are the principal source of constitutive neurogenesis in adult mouse forebrain. *Nature Neuroscience*, *7*(11), 1233–1241. https://doi.org/10.1038/nn1340 Gegg, C. V, Bowers, K. E., & Matthews, C. R. (1997). Probing minimal independent folding units in dihydrofolate reductase by molecular dissection. *Protein Science : A Publication of the Protein Society*, *6*(9), 1885–1892. https://doi.org/10.1002/pro.5560060909

Geisler, N., & Weber, K. (1983). Amino acid sequence data on glial fibrillary acidic protein (GFA); implications for the subdivision of intermediate filaments into epithelial and non-epithelial members. *The EMBO Journal*, *2*(11), 2059–2063. Retrieved from http://www.pubmedcentral.nih.gov/articlerender.fcgi?artid=555409&tool=pmcentrez&rendertype=abstract

Ghosh, I., Hamilton, A. D., Regan, L., V, Y. U., & V, N. H. (2000). Antiparallel Leucine Zipper-Directed Protein Reassembly : Application to the Green Fluorescent Protein The dissection and subsequent reassembly of a protein from peptidic fragments provides an avenue for controlling its tertiary structure and hence its fu, (11), 5658–5659.

Gomi, H., Yokoyama, T., Fujimoto, K., Ikeda, T., Katoh, A., Itoh, T., & Itohara, S. (1995). Mice devoid of the glial fibrillary acidic protein develop normally and are susceptible to scrapie prions. *Neuron*, *14*(1), 29–41. https://doi.org/10.1016/0896-6273(95)90238-4

Gonçalves, S. A., Matos, J. E., & Outeiro, T. F. (2010). Zooming into protein oligomerization in neurodegeneration using BiFC. *Trends in Biochemical Sciences*, *35*(11), 643–651. https://doi.org/10.1016/j.tibs.2010.05.007

Gookin, T. E., & Assmann, S. M. (2014). Significant reduction of BiFC non-specific assembly facilitates in planta assessment of heterotrimeric G-protein interactors. *The Plant Journal : For Cell and Molecular Biology*, *80*(3), 553–567. https://doi.org/10.1111/tpj.12639

Gough, D. J., Corlett, A., Schlessinger, K., Wegrzyn, J., Larner, A. C., & Levy, D. E. (2009). Mitochondrial Stat3 Supports Ras-Dependent Oncogenic Transformation. *Science*, *324*(5935), 1713–1716. https://doi.org/10.1126/science.1171721.Mitochondrial

Grinberg, A. V, Hu, C.-D., & Kerppola, T. K. (2004). Visualization of Myc/Max/Mad family dimers and the competition for dimerization in living cells. *Molecular and Cellular Biology*, *24*(10), 4294–4308. https://doi.org/10.1128/mcb.24.10.4294-4308.2004

Gupta, M., Han, J., Stenson, M., Wellik, L., & Witzig, T. (2012). Regulation of STAT3 by histone deacetylase-3 in diffuse large B- cell lymphoma: implications for therapy. *Bone*, *23*(1), 1–7. https://doi.org/10.1038/leu.2011.340.Regulation

Guryanova, O. A., Wu, Q., Cheng, L., Lathia, J. D., Huang, Z., Macswords, J., … Rich, J. N. (2011). Non-Receptor Tyrosine Kinase BMX Maintains Self-Renewal and Tumorigenic Potential of Glioblastoma Stem Cells by Activating STAT3. *Cancer Cell*, *19*(4), 498–511. https://doi.org/10.1016/j.ccr.2011.03.004.Non-Receptor

Haan, S., Knotholes, M., Behrmann, I., Müller-Esterl, W., Heinrich, P. C., & Schaper, F. (2000). Cytoplasmic STAT proteins associate prior to activation. *Biochemical Journal*, *345*(3), 417–421. https://doi.org/10.1042/0264-6021:3450417

Hahn, Y.-I., Kim, S.-J., Choi, B.-Y., Cho, K.-C., Bandu, R., Kim, K. P., … Surh, Y.-J. (2018). Curcumin interacts directly with the Cysteine 259 residue of STAT3 and induces apoptosis in H-Ras transformed human mammary epithelial cells. *Scientific Reports*, *8*(1), 6409. https://doi.org/10.1038/s41598-018-23840-2

Han, Z.-J., Feng, Y.-H., Gu, B.-H., Li, Y.-M., & Chen, H. (2018). The post-translational modification, SUMOylation, and cancer. *International Journal of Oncology*, *52*(4), 1081–1094. https://doi.org/10.3892/ijo.2018.4280

Harris, T. J., Grosso, J. F., Yen, H.-R., Xin, H., Kortylewski, M., Albesiano, E., … Drake, C. G. (2007). Cutting edge: An in vivo requirement for STAT3 signaling in TH17 development and TH17-dependent autoimmunity. *Journal of Immunology (Baltimore, Md. : 1950)*, *179*(7), 4313–4317. https://doi.org/10.4049/jimmunol.179.7.4313

Hazan-Halevy, I., Harris, D., Liu, Z., Liu, J., Li, P., Chen, X., … Estrov, Z. (2010a). STAT3 is constitutively phosphorylated on serine 727 residues, binds DNA, and activates transcription in CLL cells. *Blood*, *115*(14), 2852–2863. https://doi.org/10.1182/blood-2009-10-230060

Hazan-Halevy, I., Harris, D., Liu, Z., Liu, J., Li, P., Chen, X., … Estrov, Z. (2010b). STAT3 is constitutively phosphorylated on serine 727 residues, binds DNA, and activates transcription in CLL cells. *Blood*, *115*(14), 2852–2863. https://doi.org/10.1182/blood-2009-10-230060

Heidelberger, S., Zinzalla, G., Antonow, D., Essex, S., Piku Basu, B., Palmer, J., … Thurston, D. E. (2013). Investigation of the protein alkylation sites of the STAT3:STAT3 inhibitor Stattic by mass spectrometry. *Bioorganic & Medicinal Chemistry Letters*, *23*(16), 4719–4722. https://doi.org/https://doi.org/10.1016/j.bmcl.2013.05.066

Herrera, F., Chen, Q., & Schubert, D. (2010). Synergistic effect of retinoic acid and cytokines on the regulation of glial fibrillary acidic protein expression. *The Journal of Biological Chemistry*, *285*(50), 38915–38922. https://doi.org/10.1074/jbc.M110.170274

Herrera, F., & Fleming, T. (2011). a -Synuclein modifies huntingtin aggregation in living cells. *FEBS LETTERS*. https://doi.org/10.1016/j.febslet.2011.11.019

Herrera, F., Gonçalves, S., & Outeiro, T. F. (2012a). Imaging protein oligomerization in neurodegeneration using bimolecular fluorescence complementation. *Methods in Enzymology*, *506*, 157–174. https://doi.org/10.1016/B978-0-12-391856-7.00033-0

Herrera, F., Gonçalves, S., & Outeiro, T. F. (2012b). Imaging Protein Oligomerization in Neurodegeneration Using Bimolecular Fluorescence Complementation, *506*, 157–174. https://doi.org/10.1016/B978-0-12-391856-7.00033-0

Herrmann, A., Vogt, M., Mönnigmann, M., Clahsen, T., Sommer, U., Haan, S., … Müller-Newen, G. (2007). Nucleocytoplasmic shuttling of persistently activated STAT3. *Journal of Cell Science*, *120*(18), 3249–3261. https://doi.org/10.1242/jcs.03482

Herrmann, J. E., Imura, T., Song, B., Qi, J., Ao, Y., Nguyen, T. K., … Sofroniew, M. V. (2008). STAT3 is a critical regulator of astrogliosis and scar formation after spinal cord injury. *Journal of Neuroscience*, *28*(28), 7231–7243. https://doi.org/10.1523/JNEUROSCI.1709-08.2008

Hevehan, D. L., Miller, W. M., & Papoutsakis, E. T. (2002). Differential expression and phosphorylation of distinct STAT3 proteins during granulocytic differentiation. *Blood*, *99*(5), 1627–1637. https://doi.org/10.1182/blood.v99.5.1627

Hiller, M., Huse, K., Szafranski, K., Rosenstiel, P., Schreiber, S., Backofen, R., & Platzer, M. (2006). Phylogenetically widespread alternative splicing at unusual GYNGYN donors. *Genome Biology*, *7*(7), 1–16. https://doi.org/10.1186/gb-2006-7-7-r65

Hirano, T., Nakajima, K., & Hibi, M. (1997). Signaling mechanisms through gp130: A model of the cytokine system. *Cytokine and Growth Factor Reviews*, *8*(4), 241–252. https://doi.org/10.1016/S1359-6101(98)80005-1

Hol, E. M., & Pekny, M. (2015). Glial fibrillary acidic protein (GFAP) and the astrocyte intermediate filament system in diseases of the central nervous system. *Current Opinion in Cell Biology*, *32*, 121–130. https://doi.org/10.1016/j.ceb.2015.02.004

Hou, T., Ray, S., Lee, C., & Brasier, A. R. (2008). The STAT3 NH 2 -terminal Domain Stabilizes Enhanceosome Assembly by Interacting with the p300 Bromodomain *, *283*(45), 30725–30734. https://doi.org/10.1074/jbc.M805941200

Hsia, H.-C., Hutti, J. E., & Baldwin, A. S. (2017). Cytosolic DNA Promotes Signal Transducer and Activator of Transcription 3 (STAT3) Phosphorylation by TANK-binding Kinase 1 (TBK1) to Restrain STAT3 Activity. *The Journal of Biological Chemistry*, *292*(13), 5405–5417. https://doi.org/10.1074/jbc.M116.771964

Hu, C.-D., Chinenov, Y., & Kerppola, T. K. (2002). Visualization of interactions among bZIP and Rel family proteins in living cells using bimolecular fluorescence complementation. *Molecular Cell*, *9*(4), 789–798. https://doi.org/10.1016/s1097-2765(02)00496-3

Hu, C.-D., & Kerppola, T. K. (2003). Simultaneous visualization of multiple protein interactions in living cells using multicolor fluorescence complementation analysis. *Nature Biotechnology*, *21*(5), 539–545. https://doi.org/10.1038/nbt816

Huang, C., Zhang, Z., Chen, L., Lee, H. W., Ayrapetov, M. K., Zhao, T. C., … Eugene Chin, Y. (2018). Acetylation within the N- and C-terminal domains of src regulates distinct roles of STAT3-mediated tumorigenesis. *Cancer Research*, *78*(11), 2825–2838. https://doi.org/10.1158/0008-5472.CAN-17-2314

Huang, Guanyi, Yan, H., Ye, S., Tong, C., & Ying, Q.-L. (2014). STAT3 phosphorylation at tyrosine 705 and serine 727 differentially regulates mouse ESC fates. *Stem Cells (Dayton, Ohio)*, *32*(5), 1149–1160. https://doi.org/10.1002/stem.1609

Huang, Guochang, Lu, H., Hao, A., Ng, D. C. H., Ponniah, S., Guo, K., … Cao, X. (2004). GRIM-19, a Cell Death Regulatory Protein, Is Essential for Assembly and Function of Mitochondrial Complex I. *Molecular and Cellular Biology*, *24*(19), 8447–8456. https://doi.org/10.1128/mcb.24.19.8447-8456.2004

Hynes, T. R., Yost, E., Mervine, S., & Berlot, C. H. (2008). Multicolor BiFC analysis of competition among G protein beta and gamma subunit interactions. *Methods (San Diego, Calif.)*, *45*(3), 207–213. https://doi.org/10.1016/j.ymeth.2008.06.008

Ihle, J. N. (2001). The Stat family in cytokine signaling. *Current Opinion in Cell Biology*, *13*(2), 211–217. https://doi.org/10.1016/S0955-0674(00)00199-X

Inagaki, M., Gonda, Y., Nishizawa, K., Kitamura, S., Sato, C., Ando, S., … Nishi, Y. (1990). Phosphorylation sites linked to glial filament disassembly in vitro locate in a non-??-helical head domain. *Journal of Biological Chemistry*, *265*(8), 4722–4729.

Inagaki, M., Matsuoka, Y., Tsujimura, K., Ando, S., Tokui, T., Takahashi, T., & Inagaki, N. (1996). Dynamic property of intermediate filaments: regulation by phosphorylation. *Bioessays*, *18*, 481–487.

Isaacs, A., Baker, M., Wavrant-De Vrièze, F., & Hutton, M. (1998). Determination of the gene structure of human GFAP and absence of coding region mutations associated with frontotemporal dementia with parkinsonism linked to chromosome 17. *Genomics*, *51*(1), 152–154. https://doi.org/10.1006/geno.1998.5360

Jany, P. L., Hagemann, T. L., & Messing, A. (2013). GFAP expression as an indicator of disease severity in mouse models of Alexander disease. *ASN Neuro*, *5*(1), e00109. https://doi.org/10.1042/AN20130003

Johnson, A. B. (2002). Alexander disease: a review and the gene. International Journal of Developmental Neuroscience : The Official Journal of the International Society for Developmental Neuroscience, 20(3–5), 391–394. https://doi.org/10.1016/s0736-5748(02)00045-x

Johnsson, N., & Varshavsky, A. (1994). Split ubiquitin as a sensor of protein interactions in vivo. *Proceedings of the National Academy of Sciences of the United States of America*, *91*(22), 10340–10344. https://doi.org/10.1073/pnas.91.22.10340

Johnston, P. A., & Grandis, J. R. (2011). STAT3 signaling: Anticancer strategies and challenges. *Molecular Interventions*, *11*(1), 18–26. https://doi.org/10.1124/mi.11.1.4

Jones, S. A., & Jenkins, B. J. (2018). Recent insights into targeting the IL-6 cytokine family in inflammatory diseases and cancer. *Nature Reviews Immunology*, *18*(12), 773–789. https://doi.org/10.1038/s41577-018-0066-7

Kalakonda, S., Nallar, S. C., Lindner, D. J., Hu, J., Reddy, S. P., & Kalvakolanu, D. V. (2007). Tumor-suppressive activity of the cell death activator GRIM-19 on a constitutively active signal transducer and activator of transcription 3. *Cancer Research*, *67*(13), 6212–6220. https://doi.org/10.1158/0008-5472.CAN-07-0031

Kamphuis, W., Mamber, C., Moeton, M., Kooijman, L., Sluijs, J. A., Jansen, A. H. P., … Hol, E. M. (2012). GFAP Isoforms in Adult Mouse Brain with a Focus on Neurogenic Astrocytes and Reactive Astrogliosis in Mouse Models of Alzheimer Disease. *PLoS ONE*, *7*(8), e42823. https://doi.org/10.1371/journal.pone.0042823

Kato, H., Yamamoto, T., Yamamoto, H., Ohi, R., So, N., & Iwasaki, Y. (1990). Immunocytochemical characterization of supporting cells in the enteric nervous system in Hirschsprung's disease. *Journal of Pediatric Surgery*, *25*(5), 514–519. https://doi.org/10.1016/0022-3468(90)90563-O

Kenworthy, A. K. (2001). Imaging protein-protein interactions using fluorescence resonance energy transfer microscopy. *Methods (San Diego, Calif.)*, *24*(3), 289–296. https://doi.org/10.1006/meth.2001.1189

Kerppola, T. K. (2008a). BIMOLECULAR FLUORESCENCE COMPLEMENTATION (BiFC) ANALYSIS AS A PROBE OF PROTEIN INTERACTIONS

IN LIVING CELLS. *Annu. Rev. Biophys*, *37*, 465–487. https://doi.org/10.1146/annurev.biophys.37.032807.125842.BIMOLECULAR

Kerppola, T. K. (2008b). Design and implementation of bimolecular fluorescence complementation (BiFC) assays for the visualization of protein interactions in living cells. *Nature Protocols*, *1*(3), 1278–1286. https://doi.org/10.1038/nprot.2006.201

Kerppola, T. K. (2010). Visualization of Molecular Interactions Using Analysis : Characteristics of Protein Fragment. *October*, *38*(10), 2876–2886. https://doi.org/10.1039/b909638h.VISUALIZATION

Kim, B., Kim, S., & Jin, M. S. (2018). Crystal structure of the human glial fibrillary acidic protein 1B domain. *Biochemical and Biophysical Research Communications*, *503*(4), 2899–2905. https://doi.org/10.1016/j.bbrc.2018.08.066

Kim, E., Kim, M., Woo, D.-H., Shin, Y., Shin, J., Chang, N., … Lee, J. (2013). Phosphorylation of EZH2 activates STAT3 signaling via STAT3 methylation and promotes tumorigenicity of glioblastoma stem-like cells. *Cancer Cell*, *23*(6), 839–852. https://doi.org/10.1016/j.ccr.2013.04.008

Kodama, Y., & Hu, C. D. (2012). Bimolecular fluorescence complementation (BiFC): A 5-year update and future perspectives. *BioTechniques*, *53*(5), 285–298. https://doi.org/10.2144/000113943

Kodama, Y., & Wada, M. (2009). Simultaneous visualization of two protein complexes in a single plant cell using multicolor fluorescence complementation analysis. *Plant Molecular Biology*, *70*(1–2), 211–217. https://doi.org/10.1007/s11103-009-9467-0

Kretzschmar, A. K., Dinger, M. C., Henze, C., Brocke-Heidrich, K., & Horn, F. (2004). Analysis of Stat3 (signal transducer and activator of transcription 3) dimerization by fluorescence resonance energy transfer in living cells. *Biochemical Journal*, *377*(2), 289–297. https://doi.org/10.1042/BJ20030708

Kumanishi, T., Usui, H., Ichikawa, T., Nishiyama, A., Katagirp, T., Abe, S., … Shimizu, N. (1992). Human glial fibrillary acidic protein (GFAP): molecular cloning of the complete cDNA sequence and chromosomal localization (chromosome 17) of the GFAP gene. *Acta Neuropathologica*, *83*, 569–578.

Lee, J. L., Wang, M. J., & Chen, J. Y. (2009). Acetylation and activation of STAT3 mediated by nuclear translocation of CD44. *Journal of Cell Biology*, *185*(6), 949–957. https://doi.org/10.1083/jcb.200812060

Lee, S.-C., Min, H.-Y., Jung, H. J., Park, K. H., Hyun, S. Y., Cho, J., … Lee, H.-Y. (2019). Essential role of insulin-like growth factor 2 in resistance to histone deacetylase inhibitors. *Physiology & Behavior*, *176*(3), 139–148. https://doi.org/10.1038/onc.2016.92.Essential

Li, L., Cheung, S. H., Evans, E. L., & Shaw, P. E. (2010). Modulation of gene expression and tumor cell growth by redox modification of STAT3. *Cancer Research*, *70*(20). https://doi.org/10.1158/0008-5472.CAN-10-0894

Li, R., Johnson, A. B., Salomons, G., Goldman, J. E., Naidu, S., Quinlan, R., … Brenner, M. (2005). Glial fibrillary acidic protein mutations in infantile, juvenile, and adult forms of Alexander disease. *Annals of Neurology*, *57*(3), 310–326. https://doi.org/10.1002/ana.20406

Li, R., Messing, A., Goldman, J. E., & Brenner, M. (2002). GFAP mutations in Alexander disease, *20*, 259–268.

Li, X., Zhang, Z., Li, L., Gong, W., Lazenby, A. J., Swanson, B. J., … Wen, H. (2017). Myeloid-derived cullin 3 promotes STAT3 phosphorylation by inhibiting OGT expression and protects against intestinal inflammation. *Journal of Experimental Medicine*, *214*(4). https://doi.org/10.1084/jem.20161105

Lim, C. P., & Cao, X. (2006). Structure, function, and regulation of STAT proteins. *Molecular BioSystems*, *2*(11), 536–550. https://doi.org/10.1039/b606246f

Lin, G.-S., Chen, Y.-P., Lin, Z.-X., Wang, X.-F., Zheng, Z.-Q., & Chen, L. (2014). STAT3 serine 727 phosphorylation influences clinical outcome in glioblastoma. *International Journal of Clinical and Experimental Pathology*, *7*(6), 3141—3149. Retrieved from https://europepmc.org/articles/PMC4097241

Lin, J.-S., & Lai, E.-M. (2017). Protein-Protein Interactions: Co-Immunoprecipitation. *Methods in Molecular Biology (Clifton, N.J.)*, *1615*, 211–219. https://doi.org/10.1007/978-1-4939-7033-9_17

Liu, B. A., Engelmann, B. W., & Nash, P. D. (2012). The language of SH2 domain interactions defines phosphotyrosine-mediated signal transduction. *FEBS Letters*, *586*(17), 2597–2605. https://doi.org/https://doi.org/10.1016/j.febslet.2012.04.054

Louis, D. N., Perry, A., Reifenberger, G., von Deimling, A., Figarella-Branger, D., Cavenee, W. K., … Ellison, D. W. (2016). The 2016 World Health Organization Classification of Tumors of the Central Nervous System: a summary. *Acta Neuropathologica*, *131*(6), 803–820. https://doi.org/10.1007/s00401-016-1545-1

Lufei, C., Ma, J., Huang, G., Zhang, T., Novotny-Diermayr, V., Ong, C. T., & Cao, X. (2003). GRIM-19, a death-regulatory gene product, suppresses Stat3 activity via functional interaction. *EMBO Journal*, *22*(6), 1325–1335. https://doi.org/10.1093/emboj/cdg135

Ma, L., Huang, C., Wang, X.-J., Xin, D. E., Wang, L.-S., Zou, Q. C., … Chin, Y. E. (2017). Lysyl Oxidase 3 Is a Dual-Specificity Enzyme Involved in STAT3 Deacetylation

and Deacetylimination Modulation. *Molecular Cell*, *65*(2), 296–309. https://doi.org/10.1016/j.molcel.2016.12.002

Maria Goreti usboko. (2018). MOLECULAR SIGNALING MECHANISMS AT THE μ-OPIOID RECEPTOR. Gastrointestinal Endoscopy, 10(1), 279–288. Retrieved from http://dx.doi.org/10.1053/j.gastro.2014.05.023%0Ahttps://doi.org/10.1016/j.gie.2018.04.013%0Ahttp://www.ncbi.nlm.nih.gov/pubmed/29451164%0Ahttp://www.pubmedcentral.nih.gov/articlerender.fcgi?artid=PMC5838726%250Ahttp://dx.doi.org/10.1016/j.gie.2013.07.022

Maritano, D., Sugrue, M. L., Tininini, S., Dewilde, S., Strobl, B., Fu, X., … Poli, V. (2004). The STAT3 isoforms alpha and beta have unique and specific functions. *Nature Immunology*, *5*(4), 401–409. https://doi.org/10.1038/ni1052

McCall, M. a, Gregg, R. G., Behringer, R. R., Brenner, M., Delaney, C. L., Galbreath, E. J., … Messing, a. (1996). Targeted deletion in astrocyte intermediate filament (Gfap) alters neuronal physiology. *Proceedings of the National Academy of Sciences of the United States of America*, *93*(June 1996), 6361–6366. https://doi.org/10.1073/pnas.93.13.6361

McLachlan, M. J., Katzenellenbogen, J. A., & Zhao, H. (2011). A new fluorescence complementation biosensor for detection of estrogenic compounds. *Biotechnology and Bioengineering*, *108*(12), 2794–2803. https://doi.org/10.1002/bit.23254

Mehta, A., Ramachandra, C. J. A., Chitre, A., Singh, P., Lua, C. H., & Shim, W. (2017). Acetylated Signal Transducer and Activator of Transcription 3 Functions as Molecular Adaptor Independent of Transcriptional Activity During Human Cardiogenesis. *Stem Cells (Dayton, Ohio)*, *35*(10), 2129–2137. https://doi.org/10.1002/stem.2665

Messing, a, Head, M. W., Galles, K., Galbreath, E. J., Goldman, J. E., & Brenner, M. (1998). Fatal encephalopathy with astrocyte inclusions in GFAP transgenic mice. *The American Journal of Pathology*, *152*(2), 391–398.

Messing, A., Brenner, M., Feany, M. B., Nedergaard, M., & Goldman, J. E. (2012). Alexander Disease. *J Cell Sci*, *32*(15), 5017–5023. https://doi.org/10.1016/j.micinf.2011.07.011.Innate

Meyer, T., & Vinkemeier, U. (2004). Nucleocytoplasmic shuttling of STAT transcription factors. *European Journal of Biochemistry*, *271*(23–24), 4606–4612. https://doi.org/10.1111/j.1432-1033.2004.04423.x

Michnick, S. W. (2003). Protein fragment complementation strategies for biochemical network mapping. *Current Opinion in Biotechnology*, *14*(6), 610–617. https://doi.org/10.1016/j.copbio.2003.10.014

Middeldorp, J., & Hol, E. M. (2011). GFAP in health and disease. *Progress in Neurobiology*, *93*(3), 421–443. https://doi.org/10.1016/j.pneurobio.2011.01.005

Miller, K. E., Kim, Y., Huh, W., Park, H., Developmental, C., & Program, B. (2016). BiFC analysis: advances and recent applications for genome-wide interaction studies. *Journal of Molecular Biology*, *427*(11), 2039–2055. https://doi.org/10.1016/j.jmb.2015.03.005.Bimolecular

Min, H.-Y., Lee, S.-C., Woo, J. K., Jung, H. J., Park, K. H., Jeong, H. M., … Lee, H.-Y. (2018). Essential role of DNA methyltransferase 1-mediated transcription of insulin-like Growth Factor 2 in Resistance to Histone Deacetylase Inhibitors. *2015 IEEE Summer Topicals Meeting Series, SUM 2015*, *10*(1), 1–13. https://doi.org/10.1158/1078-0432.CCR-16-0534.Essential

Morell, M., Espargaro, A., Aviles, F. X., & Ventura, S. (2008). Study and selection of in vivo protein interactions by coupling bimolecular fluorescence complementation and flow cytometry. *Nature Protocols*, *3*(1), 22–33. https://doi.org/10.1038/nprot.2007.496

Mori, R., Wauman, J., Icardi, L., Van der Heyden, J., De Cauwer, L., Peelman, F., … Tavernier, J. (2017). TYK2-induced phosphorylation of Y640 suppresses STAT3 transcriptional activity. *Scientific Reports*, *7*(1), 15919. https://doi.org/10.1038/s41598-017-15912-6

Nakagawa, C., Inahata, K., Nishimura, S., & Sugimoto, K. (2011). Improvement of a Venus-based bimolecular fluorescence complementation assay to visualize bFos-bJun interaction in living cells. *Bioscience, Biotechnology, and Biochemistry*, *75*(7), 1399–1401. https://doi.org/10.1271/bbb.110189

Nallar, S. C., & Kalvakolanu, D. V. (2017). GRIM-19: A master regulator of cytokine induced tumor suppression, metastasis and energy metabolism. *Cytokine & Growth Factor Reviews*, (33), 1–18. https://doi.org/10.1016/j.cytogfr.2016.09.001.GRIM-19

Namanja, A. T., Wang, J., Buettner, R., Colson, L., & Chen, Y. (2016). Allosteric communication across STAT3 domain associated with STAT3. *Journal of Molecular Biology*, *428*(3), 579–589. https://doi.org/10.1016/j.jmb.2016.01.003.Allosteric

Nawashiro, H., Messing, A., Azzam, N., & Brenner, M. (1998). Mice lacking GFAP are hypersensitive to traumatic cerebrospinal injury. *Neuroreport*, *9*(8), 1691–1696.

Niwa, H., Burdon, T., Chambers, I., & Smith, A. (1998). Self-renewal of pluripotent embryonic stem cells is mediated via activation of STAT3. *Genes and Development*, *12*(13), 2048–2060. https://doi.org/10.1101/gad.12.13.2048

Nkansah, E., Shah, R., Collie, G. W., Parkinson, G. N., Palmer, J., Rahman, K. M., … Wilderspin, A. F. (2013). Observation of unphosphorylated STAT3 core protein

binding to target dsDNA by PEMSA and X-ray crystallography. *FEBS Letters*, *587*(7), 833–839. https://doi.org/10.1016/j.febslet.2013.01.065

Nobuta, H., Ghiani, C. A., Paez, P. M., Spreuer, V., Dong, H., Korsak, R. A., … Waschek, J. A. (2012). STAT3-Mediated astrogliosis protects myelin development in neonatal brain injury. *Annals of Neurology*, *72*(5), 750–765. https://doi.org/https://doi.org/10.1002/ana.23670

Nooren, I. M. A., & Thornton, J. M. (2003). Diversity of protein-protein interactions. *EMBO Journal*, *22*(14), 3486–3492. https://doi.org/10.1093/emboj/cdg359

O'Callaghan, J. P., Kelly, K. A., VanGilder, R. L., Sofroniew, M. V., & Miller, D. B. (2014). Early activation of STAT3 regulates reactive astrogliosis induced by diverse forms of neurotoxicity. *PLoS ONE*, *9*(7). https://doi.org/10.1371/journal.pone.0102003

Oda, A., Wakao, H., & Fujita, H. (2002). Calpain is a signal transducer and activator of transcription (STAT) 3 and STAT5 protease. *Blood*, *99*(5), 1850–1852. https://doi.org/10.1182/blood.v99.5.1850

Ohashi, K., Kiuchi, T., Shoji, K., Sampei, K., & Mizuno, K. (2012). Visualization of cofilin-actin and Ras-Raf interactions by bimolecular fluorescence complementation assays using a new pair of split Venus fragments. *BioTechniques*, *52*(1). https://doi.org/10.2144/000113777

Ohbayashi, N., Ikeda, O., Taira, N., Yamamoto, Y., Muromoto, R., Sekine, Y., … Matsuda, T. (2007). LIF- and IL-6-induced acetylation of STAT3 at Lys-685 through PI3K/Akt activation. *Biological and Pharmaceutical Bulletin*, *30*(10), 1860–1864. https://doi.org/10.1248/bpb.30.1860

Okada, Y., Watanabe, T., Shoji, T., Taguchi, K., Ogo, N., & Asai, A. (2018). Visualization and quantification of dynamic STAT3 homodimerization in living cells using homoFluoppi. *Scientific Reports*, *8*(1), 1–13. https://doi.org/10.1038/s41598-018-20234-2

Okamoto, T., Inozume, T., Mitsui, H., Kanzaki, M., Harada, K., Shibagaki, N., & Shimada, S. (2010). Overexpression of GRIM-19 in Cancer Cells Suppresses STAT3-Mediated Signal Transduction and Cancer Growth. *Molecular Cancer Therapeutics*, *9*(8), 2333–2343. https://doi.org/10.1158/1535-7163.mct-09-1147

Parpura, V., Heneka, M. T., Montana, V., Oliet, S. H. R., Schousboe, A., Haydon, P. G., … Verkhratsky, A. (2012). Glial cells in (patho)physiology. *Journal of Neurochemistry*, *121*(1), 4–27. https://doi.org/10.1111/j.1471-4159.2012.07664.x

Pekny, M., Levéen, P., Pekna, M., Eliasson, C., Berthold, C. H., Westermark, B., & Betsholtz, C. (1995). Mice lacking glial fibrillary acidic protein display astrocytes devoid of intermediate filaments but develop and reproduce normally. *The EMBO Journal*, *14*(8), 1590–1598.

Pelletier, J. N., Campbell-Valois, F.-X., & Michnick, S. W. (1998). Oligomerization domain-directed reassembly of active dihydrofolate reductase from rationally designed fragments. *Proceedings of the National Academy of Sciences*, *95*(21), 12141–12146. https://doi.org/10.1073/pnas.95.21.12141

Pfleger, K. D. G., & Eidne, K. A. (2005). Monitoring the formation of dynamic G-protein-coupled receptor-protein complexes in living cells. *The Biochemical Journal*, *385*(Pt 3), 625–637. https://doi.org/10.1042/BJ20041361

Pfleger, K. D. G., & Eidne, K. A. (2006). Illuminating insights into protein-protein interactions using bioluminescence resonance energy transfer (BRET). *Nature Methods*, *3*(3), 165–174. https://doi.org/10.1038/nmeth841

Pilati, C., Amessou, M., Bihl, M. P., Balabaud, C., Van Nhieu, J. T., Paradis, V., … Zucman-Rossi, J. (2011a). Somatic mutations activating STAT3 in human inflammatory hepatocellular adenomas. *Journal of Experimental Medicine*, *208*(7), 1359–1366. https://doi.org/10.1084/jem.20110283

Pilati, C., Amessou, M., Bihl, M. P., Balabaud, C., Van Nhieu, J. T., Paradis, V., … Zucman-Rossi, J. (2011b). Somatic mutations activating STAT3 in human inflammatory hepatocellular adenomas. *The Journal of Experimental Medicine*, *208*(7), 1359–1366. https://doi.org/10.1084/jem.20110283

Pranada, A. L., Metz, S., Herrmann, A., Heinrich, P. C., & Müller-Newen, G. (2004). Real Time Analysis of STAT3 Nucleocytoplasmic Shuttling. *Journal of Biological Chemistry*, *279*(15), 15114–15123. https://doi.org/10.1074/jbc.M312530200

Prust, M., Wang, J., Morizono, H., Messing, a, Brenner, M., Gordon, E., … Vanderver, a. (2011). GFAP mutations, age at onset, and clinical subtypes in Alexander disease. *Neurology*, *77*(13), 1287–1294. https://doi.org/10.1212/WNL.0b013e3182309f72

Qi, Y. B., Garren, E. J., Shu, X., Tsien, R. Y., & Jin, Y. (2012). Photo-inducible cell ablation in Caenorhabditis elegans using the genetically encoded singlet oxygen generating protein miniSOG, (15). https://doi.org/10.1073/pnas.1204096109

Quinlan, R. a, Brenner, M., Goldman, J. E., & Messing, A. (2007). GFAP and its role in Alexander disease. *Experimental Cell Research*, *313*(10), 2077–2087. https://doi.org/10.1016/j.yexcr.2007.04.004

Raaijmakers, J. A. M., Solari, R., Koenderman, L., Lammers, J.-W. J., de Groot, R. P., Armstrong, J., … van Dijk, T. B. (2017). STAT3β, a Splice Variant of Transcription Factor STAT3, Is a Dominant Negative Regulator of Transcription. *Journal of Biological Chemistry*, *271*(22), 13221–13227. https://doi.org/10.1074/jbc.271.22.13221

Ray, S., Boldogh, I., & Brasier, A. R. (2005). STAT3 NH 2 -Terminal Acetylation Is Activated by the Hepatic Acute-Phase Response and Required for IL-6 Induction of

Angiotensinogen. *Gastroenterology*, *129*, 1616–1632. https://doi.org/10.1053/j.gastro.2005.07.055

Ray, S., Zhao, Y., Jamaluddin, M., Edeh, C. B., Lee, C., & Brasier, A. R. (2014). Inducible STAT3 NH2 terminal mono-ubiquitination promotes BRD4 complex formation to regulate apoptosis. *Cellular Signalling*, *26*(7), 1445–1455. https://doi.org/10.1016/j.cellsig.2014.03.007

Reeves, S. a, Helman, L. J., Allison, a, & Israel, M. a. (1989). Molecular cloning and primary structure of human glial fibrillary acidic protein. *Proceedings of the National Academy of Sciences of the United States of America*, *86*(13), 5178–5182.

Remy, I., & Michnick, S. W. (2007). Application of protein-fragment complementation assays in cell biology. *BioTechniques*, *42*(2), 137–145. https://doi.org/10.2144/000112396

Ren, Z., Mao, X., Mertens, C., Krishnaraj, R., Qin, J., Mandal, P. K., … Chen, X. (2008). Crystal structure of unphosphorylated STAT3 core fragment. *Biochemical and Biophysical Research Communications*, *374*(1), 1–5. https://doi.org/10.1016/j.bbrc.2008.04.049

Renner, E. D., Rylaarsdam, S., Aňover-sombke, S., Rack, A. L., Reichenbach, J., Carey, J. C., … Ochs, H. D. (2008). Novel STAT3 mutations, reduced TH17 cell numbers, and variably defective STAT3 phosphorylation in Hyper-IgE syndrome. *J Allergy Clin Immunol*, *122*(1), 181–187. https://doi.org/10.1016/j.jaci.2008.04.037.Novel

Richards, F. M. (1958). ON THE ENZYMIC ACTIVITY OF SUBTILISIN-MODIFIED RIBONUCLEASE. Proceedings of the National Academy of Sciences, 44(2), 162–166. https://doi.org/10.1073/pnas.44.2.162

Riol, H., Tardy, M., Rolland, B., Lévesque, G., & Murthy, M. R. (1997). Detection of the peripheral nervous system (PNS)-type glial fibrillary acidic protein (GFAP) and its mRNA in human lymphocytes. *Journal of Neuroscience Research*, *48*(1), 53–62. https://doi.org/10.1002/(SICI)1097-4547(19970401)48:1<53::AID-JNR5>3.0.CO;2-D

Robida, A. and Kerppola, T. (2009). BIMOLECULAR FLUORESCENCE COMPLEMENTATION ANALYSIS OF INDUCIBLE PROTEIN INTERACTIONS: EFFECTS OF FACTORS AFFECTING PROTEIN FOLDING ON FLUORESCENT PROTEIN FRAGMENT ASSOCIATION. *Journal of Molecular Biology*, *394*(3), 391–409. https://doi.org/10.1016/j.jmb.2009.08.069.BIMOLECULAR

Rodrigues, B. R., Queiroz-Hazarbassanov, N., Lopes, M. H., Bleggi-Torres, L. F., Suzuki, S., Cunha, I. W., … Martins, V. R. (2016). Nuclear unphosphorylated STAT3 correlates with a worse prognosis in human glioblastoma. *Pathology - Research and Practice*, *212*(6), 517–523. https://doi.org/https://doi.org/10.1016/j.prp.2016.03.001

Rossi, F., Charlton, C. A., & Blau, H. M. (1997). Monitoring protein-protein interactions in intact eukaryotic cells by β-galactosidase complementation. *Proceedings of the National Academy of Sciences of the United States of America*, *94*(16), 8405–8410. https://doi.org/10.1073/pnas.94.16.8405

Russo, L. S. J., Aron, A., & Anderson, P. J. (1976). Alexander's disease: a report and reappraisal. *Neurology*, *26*(7), 607–614.

Saka, Y., Hagemann, A. I., & Smith, J. C. (2008). Visualizing protein interactions by bimolecular fluorescence complementation in Xenopus. *Methods*, *45*, 192–195. https://doi.org/10.1016/j.ymeth.2008.06.005

Sakaguchi, M., Oka, M., Iwasaki, T., Fukami, Y., & Nishigori, C. (2012). Role and regulation of STAT3 phosphorylation at Ser727 in melanocytes and melanoma cells. *The Journal of Investigative Dermatology*, *132*(7), 1877–1885. https://doi.org/10.1038/jid.2012.45

Sasse, J., Hemmann, U., Schwartz, C., Schniertshauer, U., Heesel, B., Landgraf, C., … Horn, F. (1997). Mutational analysis of acute-phase response factor/Stat3 activation and dimerization. *Molecular and Cellular Biology*, *17*(8), 4677–4686. https://doi.org/10.1128/mcb.17.8.4677

Schaefer, T. S., Sanders, L. K., & Nathans, D. (1995). Cooperative transcriptional activity of Jun and Stat3f3 , a short form of Stat3, *92*(September), 9097–9101.

Schlecht, U., Miranda, M., Suresh, S., Davis, R. W., & St Onge, R. P. (2012). Multiplex assay for condition-dependent changes in protein-protein interactions. *Proceedings of the National Academy of Sciences of the United States of America*, *109*(23), 9213–9218. https://doi.org/10.1073/pnas.1204952109

Schuringa, J. J., Schepers, H., Vellenga, E., & Kruijer, W. (2001). Ser727-dependent transcriptional activation by association of p300 with STAT3 upon IL-6 stimulation. *FEBS Letters*, *495*(1–2), 71–76. https://doi.org/10.1016/S0014-5793(01)02354-7

Seifert, G., Schilling, K., & Steinhäuser, C. (2006). Astrocyte dysfunction in neurological disorders: a molecular perspective. *Nature Reviews. Neuroscience*, *7*(3), 194–206. https://doi.org/10.1038/nrn1870

Seri, B., García-Verdugo, J. M., McEwen, B. S., & Alvarez-Buylla, A. (2001). Astrocytes give rise to new neurons in the adult mammalian hippocampus. *The Journal of Neuroscience*, *21*(18), 7153–7160.

Sestito, R., Madonna, S., Scarponi, C., Cianfarani, F., Failla, C. M., Cavani, A., … Albanesi, C. (2011). STAT3-dependent effects of IL-22 in human keratinocytes are

counterregulated by sirtuin 1 through a direct inhibition of STAT3 acetylation. *The FASEB Journal*, *25*(3), 916–927. https://doi.org/10.1096/fj.10-172288

Sgrignani, J., Garofalo, M., Matkovic, M., Merulla, J., Catapano, C. V., & Cavalli, A. (2018). Structural biology of STAT3 and its implications for anticancer therapies development. *International Journal of Molecular Sciences*, *19*(6). https://doi.org/10.3390/ijms19061591

Sheridan, D. L., Berlot, C. H., Robert, A., Inglis, F. M., Jakobsdottir, K. B., Howe, J. R., & Hughes, T. E. (2002). A new way to rapidly create functional, fluorescent fusion proteins: random insertion of GFP with an in vitro transposition reaction. *BMC Neuroscience*, *3*(1), 7. https://doi.org/10.1186/1471-2202-3-7

Shu, X., Lev-Ram, V., Deerinck, T. J., Qi, Y., Ramko, E. B., Davidson, M. W., … Tsien, R. Y. (2011). A genetically encoded tag for correlated light and electron microscopy of intact cells, tissues, and organisms. *PLoS Biology*, *9*(4). https://doi.org/10.1371/journal.pbio.1001041

Shyu, J. Y., Liu, H., Deng, X., & Hu, C.-D. (2006). Identification of new fluorescent protein fragments for bimolecular fluorescence complementation analysis under physiological conditions. *BioTechniques*, *40*, 61–66.

Sihag, R. K., Inagaki, M., Yamaguchi, T., Shea, T. B., & Pant, H. C. (2007). Role of phosphorylation on the structural dynamics and function of types III and IV intermediate filaments. *Experimental Cell Research*, *313*(10), 2098–2109. https://doi.org/10.1016/j.yexcr.2007.04.010

Simon, A. R., Rai, U., Fanburg, B. L., & Cochran, B. H. (1998). Activation of the JAK-STAT pathway by reactive oxygen species. *The American Journal of Physiology*, *275*(6), C1640-52. https://doi.org/10.1152/ajpcell.1998.275.6.C1640

Sofroniew, M. V., & Vinters, H. V. (2010). Astrocytes: biology and pathology. *Acta Neuropathologica*, *119*(1), 7–35. https://doi.org/10.1007/s00401-009-0619-8

Sosunov, A. A., McKhann, G. M., & Goldman, J. E. (2017). The origin of Rosenthal fibers and their contributions to astrocyte pathology in Alexander disease. *Acta Neuropathologica Communications*, *5*(1), 27. https://doi.org/10.1186/s40478-017-0425-9

Sosunov, A., Olabarria, M., & Goldman, J. E. (2018). Alexander disease: an astrocytopathy that produces a leukodystrophy. *Brain Pathology*, *28*(3), 388–398. https://doi.org/https://doi.org/10.1111/bpa.12601

Srivastava, J., & DiGiovanni, J. (2016). Non-canonical Stat3 signaling in cancer. *Molecular Carcinogenesis*, *55*(12), 1889–1898. https://doi.org/10.1002/mc.22438

Stark, G. R., & Darnell, J. E. (2012). The JAK-STAT Pathway at Twenty. *Immunity*, *36*(4), 503–514. https://doi.org/10.1016/j.immuni.2012.03.013

Stark, G. R., Wang, Y., & Lu, T. (2011). Lysine methylation of promoter-bound transcription factors and relevance to cancer. *Cell Research*, *21*(3), 375–380. https://doi.org/10.1038/cr.2010.174

Struk, S., Jacobs, A., Sánchez Martín-Fontecha, E., Gevaert, K., Cubas, P., & Goormachtig, S. (2019). Exploring the protein-protein interaction landscape in plants. *Plant, Cell & Environment*, *42*(2), 387–409. https://doi.org/10.1111/pce.13433

Su, Y., Huang, X., Huang, Z., Huang, T., Xu, Y., & Yi, C. (2020). STAT3 Localizes in Mitochondria-Associated ER Membranes Instead of in Mitochondria. *Frontiers in Cell and Developmental Biology*, *8*(April), 1–10. https://doi.org/10.3389/fcell.2020.00274

Sun, D. A., Yu, H., Spooner, J., Tatsas, A. D., Davis, T., Abel, T. W., … Konrad, P. E. (2008). Postmortem analysis following 71 months of deep brain stimulation of the subthalamic nucleus for Parkinson disease. *Journal of Neurosurgery*, *109*(2), 325–329. https://doi.org/10.3171/JNS/2008/109/8/0325

Tammineni, P., Anugula, C., Mohammed, F., Anjaneyulu, M., Larner, A. C., & Sepuri, N. B. V. (2013). The import of the transcription factor STAT3 into mitochondria depends on GRIM-19, a component of the electron transport chain. *Journal of Biological Chemistry*, *288*(7), 4723–4732. https://doi.org/10.1074/jbc.M112.378984

Tang, G., Perng, M. D., Wilk, S., Quinlan, R., & Goldman, J. E. (2010). Oligomers of mutant glial fibrillary acidic protein (GFAP) Inhibit the proteasome system in alexander disease astrocytes, and the small heat shock protein alphaB-crystallin reverses the inhibition. *The Journal of Biological Chemistry*, *285*(14), 10527–10537. https://doi.org/10.1074/jbc.M109.067975

Tomokane, N., Iwaki, T., Tateishi, J., Iwaki, A., & Goldman, J. E. (1991). Rosenthal fibers share epitopes with alpha B-crystallin, glial fibrillary acidic protein, and ubiquitin, but not with vimentin. Immunoelectron microscopy with colloidal gold. *The American Journal of Pathology*, *138*(4), 875–885.

Truong, K., & Ikura, M. (2001). The use of FRET imaging microscopy to detect protein-protein interactions and protein conformational changes in vivo. *Current Opinion in Structural Biology*, *11*(5), 573–578. https://doi.org/10.1016/S0959-440X(00)00249-9

Tsuda, M., Kohro, Y., Yano, T., Tsujikawa, T., Kitano, J., Tozaki-Saitoh, H., … Inoue, K. (2011). JAK-STAT3 pathway regulates spinal astrocyte proliferation and neuropathic pain maintenance in rats. *Brain*, *134*(4), 1127–1139. https://doi.org/10.1093/brain/awr025

Turton, K. B., Annis, D. S., Rui, L., Esnault, S., & Mosher, D. F. (2015). Ratios of four STAT3 splice variants in human eosinophils and diffuse large B cell lymphoma cells. *PLoS ONE*, *10*(5), 1–15. https://doi.org/10.1371/journal.pone.0127243

Vidi, P.-A., Chemel, B. R., Hu, C.-D., & Watts, V. J. (2008). Ligand-dependent oligomerization of dopamine D(2) and adenosine A(2A) receptors in living neuronal cells. *Molecular Pharmacology*, *74*(3), 544–551. https://doi.org/10.1124/mol.108.047472

Villalobos, V., Naik, S., & Piwnica-Worms, D. (2007). Current state of imaging protein-protein interactions in vivo with genetically encoded reporters. *Annual Review of Biomedical Engineering*, *9*, 321–349. https://doi.org/10.1146/annurev.bioeng.9.060906.152044

Villarino, A. V, Kanno, Y., Ferdinand, J. R., & O'Shea, J. J. (2015). Mechanisms of Jak/STAT signaling in immunity and disease. *Journal of Immunology (Baltimore, Md. : 1950)*, *194*(1), 21–27. https://doi.org/10.4049/jimmunol.1401867

Vogt, M., Domoszlai, T., Kleshchanok, D., Lehmann, S., Schmitt, A., Poli, V., … Muller-Newen, G. (2011). The role of the N-terminal domain in dimerization and nucleocytoplasmic shuttling of latent STAT3. *Journal of Cell Science*, *124*(6), 900–909. https://doi.org/10.1242/jcs.072520

Waadt, R., Schmidt, L. K., Lohse, M., Hashimoto, K., Bock, R., & Kudla, J. (2008). Multicolor bimolecular fluorescence complementation reveals simultaneous formation of alternative CBL/CIPK complexes in planta. *The Plant Journal : For Cell and Molecular Biology*, *56*(3), 505–516. https://doi.org/10.1111/j.1365-313X.2008.03612.x

Waitkus, M. S., Chandrasekharan, U. M., Willard, B., Tee, T. L., Hsieh, J. K., Przybycin, C. G., … DiCorleto, P. E. (2014). Signal Integration and Gene Induction by a Functionally Distinct STAT3 Phosphoform. *Molecular and Cellular Biology*, *34*(10), 1800–1811. https://doi.org/10.1128/mcb.00034-14

Walter, M., Chaban, C., Schütze, K., Batistic, O., Weckermann, K., Näke, C., … Kudla, J. (2004). Visualization of protein interactions in living plant cells using bimolecular fluorescence complementation. *The Plant Journal : For Cell and Molecular Biology*, *40*(3), 428–438. https://doi.org/10.1111/j.1365-313X.2004.02219.x

Wang, R., Cherukuri, P., & Luo, J. (2005). Activation of Stat3 sequence-specific DNA binding and transcription by p300/CREB-binding protein-mediated acetylation. *Journal of Biological Chemistry*, *280*(12), 11528–11534. https://doi.org/10.1074/jbc.M413930200

Waris, G., Huh, K. W., & Siddiqui, A. (2001). Mitochondrially associated hepatitis B virus X protein constitutively activates transcription factors STAT-3 and NF-kappa B via oxidative stress. *Molecular and Cellular Biology*, *21*(22), 7721–7730. https://doi.org/10.1128/MCB.21.22.7721-7730.2001

Wegrzyn, J., Potla, R., Chwae, Y. J., Sepuri, N. B. V., Zhang, Q., Koeck, T., … Larner, A. C. (2009). Function of mitochondrial Stat3 in cellular respiration. *Science*, *323*(5915), 793–797. https://doi.org/10.1126/science.1164551

Wegrzyn, J., Potla, R., Chwae, Y., Sepuri, N. B. V, Koeck, T., Derecka, M., … Fawcett, P. (2009). Function of Mitochondrial Stat3 in Cellular Respiration. *Science*, *323*(5915), 793–797. https://doi.org/10.1126/science.1164551.Function

Wehr, M. C., Reinecke, L., Botvinnik, A., & Rossner, M. J. (2008). Analysis of transient phosphorylation-dependent protein-protein interactions in living mammalian cells using split-TEV. *BMC Biotechnology*, *8*, 1–15. https://doi.org/10.1186/1472-6750-8-55

Wen, Z., & Darnell, J. E. (1997). Mapping of Stat3 serine phosphorylation to a single residue (727) and evidence that serine phosphorylation has no influence on DNA binding of Stat1 and Stat3. *Nucleic Acids Research*, *25*(11), 2062–2067. https://doi.org/10.1093/nar/25.11.2062

Wen, Z., Zhong, Z., & Darnell, J. E. (1995). Maximal activation of transcription by statl and stat3 requires both tyrosine and serine phosphorylation. *Cell*, *82*(2), 241–250. https://doi.org/10.1016/0092-8674(95)90311-9

Wetie, A. G. N., Sokolowska, I., Woods, A. G., Roy, U., Loo, J. A., & Darie, C. C. (2013). Investigation of stable and transient protein-protein interactions: past, present and future. *Bone*, *13*(0), 1–7. https://doi.org/10.1002/pmic.201200328.Investigation

Weydt, P., & La Spada, A. R. (2006). Targeting protein aggregation in neurodegeneration – lessons from polyglutamine disorders. *Expert Opinion on Therapeutic Targets*, *10*(4), 505–513. https://doi.org/10.1517/14728222.10.4.505

Wu, P., & Brand, L. (1994). Resonance energy transfer: methods and applications. *Analytical Biochemistry*, *218*(1), 1–13. https://doi.org/10.1006/abio.1994.1134

Xiong, A., Yang, Z., Shen, Y., Zhou, J., & Shen, Q. (2014). Transcription factor STAT3 as a novel molecular target for cancer prevention. *Cancers*, *6*(2), 926–957. https://doi.org/10.3390/cancers6020926

Xu, Z., Xue, T., Zhang, Z., Wang, X., Xu, P., Zhang, J., … Chen, Y. (2011). Role of signal transducer and activator of transcription-3 in up-regulation of GFAP after epilepsy. *Neurochemical Research*, *36*(12), 2208–2215. https://doi.org/10.1007/s11064-011-0576-1

Yang, J., Chatterjee-Kishore, M., Staugaitis, S. M., Nguyen, H., Schlessinger, K., Levy, D. E., & Stark, G. R. (2005). Novel roles of unphosphorylated STAT3 in oncogenesis and transcriptional regulation. *Cancer Research*, *65*(3), 939–947.

Yang, J., Huang, J., Dasgupta, M., Sears, N., Miyagi, M., Wang, B., … Stark, G. R. (2010). Reversible methylation of promoter-bound STAT3 by histone-modifying enzymes. *Proceedings of the National Academy of Sciences of the United States of America*, *107*(50), 21499–21504. https://doi.org/10.1073/pnas.1016147107

Yang, J., & Stark, G. R. (2008). Roles of unphosphorylated STATs in signaling. *Cell Research*, *18*(4), 443–451. https://doi.org/10.1038/cr.2008.41

Yang, R., & Rincon, M. (2016). Mitochondrial Stat3, the need for design thinking. *International Journal of Biological Sciences*, *12*(5), 532–544. https://doi.org/10.7150/ijbs.15153

Yoshida, T., Sasaki, M., Yoshida, M., Namekawa, M., Okamoto, Y., Tsujino, S., … Nakagawa, M. (2011). Nationwide survey of Alexander disease in Japan and proposed new guidelines for diagnosis. *J Neurol*, *258*(11), 1998–2008. https://doi.org/10.1007/s00415-011-6056-3

Yuan, Z. L., Guan, Y. J., Chatterjee, D., & Chin, Y. E. (2005). Stat3 dimerization regulated by reversible acetylation of a single lysine residue. *Science*, *307*(5707), 269–273. https://doi.org/10.1126/science.1105166

Yue, H., Li, W., Desnoyer, R., & Karnik, S. S. (2010). Role of nuclear unphosphorylated STAT3 in angiotensin II type 1 receptor-induced cardiac hypertrophy. *Cardiovascular Research*, *85*(1), 90–99. https://doi.org/10.1093/cvr/cvp285

Yue, L., Li, L., Li, D., Yang, Z., Han, S., Chen, M., … Hui, L. (2017). High-throughput screening for Survivin and Borealin interaction inhibitors in hepatocellular carcinoma. *Biochemical and Biophysical Research Communications*, *484*(3), 642–647. https://doi.org/10.1016/j.bbrc.2017.01.160

Zammarchi, F., De Stanchina, E., Bournazou, E., Supakorndej, T., Martires, K., Riedel, E., … Cartegni, L. (2011). Antitumorigenic potential of STAT3 alternative splicing modulation. *Proceedings of the National Academy of Sciences of the United States of America*, *108*(43), 17779–17784. https://doi.org/10.1073/pnas.1108482108

Zamo, A., Chiarle, R., Piva, R., Howes, J., Fan, Y., Chilosi, M., … Inghirami, G. (2002). Anaplastic lymphoma kinase (ALK) activates Stat3 and protects hematopoietic cells from cell death. *Oncogene*, *21*(7), 1038–1047. https://doi.org/10.1038/sj.onc.1205152

Zhang, J. J., Zhao, Y., Chait, B. T., Lathem, W. W., Ritzi, M., Knippers, R., & Darnell, J. E. (1998). Ser727-dependent recruitment of MCM5 by Stat1α in IFN-γ-induced transcriptional activation. *EMBO Journal*, *17*(23), 6963–6971. https://doi.org/10.1093/emboj/17.23.6963

Zhang, J., Yang, J., Roy, S. K., Tininini, S., Hu, J., Bromberg, J. F., … Kalvakolanu, D. V. (2003). The cell death regulator GRIM-19 is an inhibitor of signal transducer and activator of transcription 3. *Proceedings of the National Academy of Sciences*, *100*(16), 9342–9347. https://doi.org/10.1073/pnas.1633516100

Zhang, Q., Raje, V., Yakovlev, V. A., Yacoub, A., Szczepanek, K., Meier, J., … Larner, A. C. (2013). Mitochondrial localized Stat3 promotes breast cancer growth via phosphorylation of serine 727. *Journal of Biological Chemistry*, *288*(43), 31280–31288. https://doi.org/10.1074/jbc.M113.505057

Zhang, S., Li, W., Wang, W., Zhang, S. S., Huang, P., & Zhang, C. (2013). Expression and Activation of STAT3 in the Astrocytes of Optic Nerve in a Rat Model of Transient Intraocular Hypertension. *PLOS ONE*, *8*(1), 1–10. https://doi.org/10.1371/journal.pone.0055683

Zhang, W., Du, Y., Jiang, T., Geng, W., Yuan, J., & Zhang, D. (2015). Upregulation of GRIM-19 inhibits the growth and invasion of human breast cancer cells. *Mol Med Rep*, *12*(2), 2919–2925. https://doi.org/10.3892/mmr.2015.3757

Zheng, M., Turton, K. B., Zhu, F., Li, Y., Grindle, K. M., Annis, D. S., … Rui, L. (2016). A mix of S and ΔS variants of STAT3 enable survival of activated B-cell-like diffuse large B-cell lymphoma cells in culture. *Oncogenesis*, *5*(1), e184–e184. https://doi.org/10.1038/oncsis.2015.44

Apoio financeiro da FCT e do FSE no âmbito do Quadro Comunitário de Apoio,

Bolsa nº PD/BD/128163/2016

ITQB-UNL | Av. da República, 2780-157 Oeiras, Portugal
Tel (+351) 214 469 100 | Fax (+351) 214 411 277

www.itqb.unl.pt